

AN OUNCE OF PREVENTION:
PROBABILISTIC LOSS ESTIMATION FOR
PERFORMANCE-BASED EARTHQUAKE ENGINEERING

Thesis by

Judith Mitrani-Reiser

In Partial Fulfillment of the Requirements for the

Degree of

Doctor of Philosophy

CALIFORNIA INSTITUTE OF TECHNOLOGY

Pasadena, California

2007

(Defended January 8, 2007)

© 2007

Judith Mitrani-Reiser

All Rights Reserved

I dedicate this to Adina and Amira Marroquin, my two beautiful nieces.

Acknowledgements

I would like to thank my advisor, James Beck for sharing his wisdom with me so patiently throughout the years. I am extremely appreciative for his careful and thoughtful mentoring, for his unwavering support of my work, and for never cutting a meeting short. He has taught me to be a thorough scientist, and I would be fortunate to count him as a collaborator in years to come.

Thanks also to my committee members, for their insightful discussions and recommendations. Special thanks to Keith Porter, whose expertise has helped guide my work for the past four years. Thanks to Mary Comerio, whose passion for seismic risk management gives meaning to my work. Thank you also to John Hall and Tom Heaton for impromptu discussions that ground my work.

This work has been possible thanks to funding from the George Housner Fellowship and from grants provided by the Pacific Earthquake Engineering Research (PEER) Center. A special thank you to my PEER collaborators: Howard Blecher, Gregory Deierlein, Christine Goulet, Curt Haselton, and Jonathan Stewart. Thank you to Gee Hecksher, Vivian Gonzales, Charles Scawthorn, and Fire Captain Danny DeAngelis for consulting and assisting on my project.

I would like to thank all the wonderful friends and colleagues at UC Berkeley and Caltech, who helped support my caffeine habit and who made the long hours of graduate school pass so quickly: Sarah Bergbreiter, Isaac Chenchiah, Jianye Ching, Javier de Vicente Buendia, Jan Goethals, Veronica Grasso, Nick Hudson, Dimitrios Konstantinidis, Babak Jamshidi, Connie Lu, Jeff Moore, Juan Morla, Matt Muto, Prashant Purohit, Alfonso

Ramos, Andreas Schellenberg, Jeff Scruggs, Alex Taflanidis, and Albert To, among many others. Thank you also to the Dickinson Lab for making me an honorary member; a special thank you to Phoebe Dickinson, Usha McFarling, and Fatimah Johnson for being such caring friends.

I wish to acknowledge the tireless work of the Caltech staff that make the work environment such a pleasure; in particular Brandi Jones, Perendah Kia, Martha Oropesa, Carolina Oseguera, Elvira Serpe, and Ernie, whose daily lunch specials I will miss.

I am grateful to my in-laws, Sammy and Barbara Reiser for raising a *mench*, and I thank them and the extended Reiser family for unselfishly sharing their love with me. I warmly thank my California-based cousins, the Ramirez, Maya, Suissa and Stigmon families, who have opened their homes and hearts so graciously during our stay in California.

I would like to especially thank my parents, Julio and Elisa Mitrani, for their unconditional love and support throughout the years. I am so grateful for the sacrifices they made in their own lives to seek a better life for their children in America. I am blessed to have them as role models; I will never stop learning from them. I would also like to thank my second set of parents, my grandparents Fortuna and Victor Mitrani, who keep me well fed, love me, and continue to nurture me. I would like to thank my loving sister, Susana, who has always been my confidant and protector; our relationship is strengthened with each new stage of life. Thank you also to my dear brother-in-law, Albert Marroquin who has brought so much happiness to our family and who can appreciate good college football (Go Gators!).

My deepest gratitude goes to my best friend, my husband Michael Reiser, who is my rock. You have been beside me throughout every step of my career and have always held my hand through the happy and the trying times. Your intelligence motivates me, your compassion inspires me, and your love elates me. Every moment together is divine and wherever you are is *home*. The past eight years have been a great adventure; I can't wait to see what's next!

Abstract

Performance-based earthquake engineering (PBEE) is a methodology that incorporates desired performance levels into the design process. *Performance* in PBEE can be expressed in economic terms, or as elapsed downtime, or in terms of life and building safety objectives. These performance objectives are relevant to various types of stakeholders. They should be addressed in building loss estimation procedures because after an earthquake, the repair cost will not be the only “loss” suffered by building stakeholders. In a sizeable earthquake, there will likely also be some losses due to business interruption during the repair effort, building closure taken as a post-earthquake safety precaution, and human casualties caused by building failures during the seismic event.

An analytical approach for PBEE is developed and implemented to evaluate the performance of a new reinforced-concrete moment-frame office building. The PBEE approach used is consistent with the Pacific Earthquake Engineering Research (PEER) center’s modular framework, which is divided into four core analytical stages: hazard analysis, structural analysis, damage analysis, and loss analysis. Future losses of the building are uncertain because they depend on uncertain quantities, such as the shaking intensity of the earthquake, the mechanical properties of the facility, and the uncertain damageability and unit repair costs of the facility. An analytical approach is developed to propagate these uncertainties. This work presents the mathematical foundation for the damage and loss analyses, and a description of its implementation into software. The results from running this software on multiple design variants of the building are presented,

including seismic vulnerabilities as a function of shaking intensity and corresponding expected annual losses.

The methodology developed and implemented in this work estimates the direct economic losses due to repair costs as well as two types of indirect economic losses, those produced by building downtime and by human fatalities. A procedure for a virtual inspection is used to assess the safety of buildings, based on current damage assessment guidelines. Additionally, a model is established to estimate human fatalities caused by the partial and global collapse of buildings, using probabilities of fatality based on relevant empirical data and the results of the virtual inspection process. A simplified methodology is presented for estimating building downtime after seismic events, including mobilization delays before construction begins and the elapsed time needed to repair damaged building components. The losses due to downtime and human fatalities are then added to the building repair cost in order to estimate the total building loss, which is then used to perform a benefit-cost analysis of the benchmark building. The work presented, is to our knowledge, the most faithful attempt to estimate the main decision variables (termed the *3 Ds*—dollars, deaths, and downtime), proposed by PEER and the ATC-58 Project for performance assessment of structures.

Contents

Acknowledgements	v
Abstract	vii
Contents	ix
List of Figures	xiii
List of Tables	xvii
Introduction	1
1.1 Earlier work in performance-based earthquake engineering	2
1.2 Beyond Vision 2000	5
1.3 PEER	8
1.4 ATC-58	9
1.5 Plan for thesis	11
Performance-Based Earthquake Engineering Framework	13
2.1 PEER’s PBEE methodology	13
2.2 Introduction to PEER benchmark study	16
2.2.1 PEER benchmark building and site	17
2.2.2 Damageable structural components	18
2.2.3 Damageable nonstructural components	23

2.2.4	Table of considered damageable building components	24
2.3	PEER benchmark PSHA	25
2.4	PEER benchmark structural analysis	28
2.4.1	Three-dimensional considerations	30
2.5	MDLA toolbox	33
2.5.1	MDLA input: Table of damageable assemblies	34
2.5.2	MDLA input: Table of fragility and cost distribution functions	35
2.5.3	MDLA input: Structural analysis results	35
2.5.4	Program architecture	37
2.5.5	Program output	38
	Damage Estimation	41
3.1	Procedure for damage analysis	41
3.2	Fragility functions for benchmark study	42
3.2.1	Beams and columns	43
3.2.2	Column-slab connections	47
3.2.3	Drywall partitions and finish	48
3.2.4	Interior paint	49
3.2.5	Exterior glazing	51
3.2.6	Ceiling	52
3.2.7	Sprinklers	53
3.2.8	Elevators	54
3.3	Damage results for benchmark study	56
	Building and Life Safety	67
4.1	Building safety	67
4.1.1	ATC 20	68
4.1.2	Virtual inspector	69
4.1.3	Building safety results for benchmark study	72
4.2	Life safety	78
4.2.1	History of fatality modeling	78
4.2.2	Methodology and example of fatality estimation	84
	Estimation of Direct Losses	93

5.1 Procedure for establishing vulnerability functions	93
5.2 Component cost distribution for benchmark study	94
5.3 Results of vulnerability functions for benchmark study	100
5.3.1 Results for design comparisons	100
5.3.2 Results for modeling comparisons	103
5.4 Calculation of expected annual loss due to repairs	106
5.4.1 Disaggregation of EAL	107
5.4.2 Discussion of results	109
Estimation of Indirect Losses and Benefit-Cost Analysis	111
6.1 Building downtime	112
6.1.1 Rational components of downtime	112
6.1.2 Irrational components of downtime	114
6.1.3 Methodology and example of downtime losses	116
6.1.4 Downtime loss results for benchmark building	121
6.1.5 Comparison of downtime results with university studies	124
6.2 Expected annual losses due to fatalities	126
6.2.1 Human loss results for benchmark building	127
6.3 Total expected annual losses for benchmark building	128
6.4 Illustrative benefit-cost analysis	129
Concluding Remarks	133
7.1 Significant results and major contributions	133
7.1.1 Chapter 2: Performance-based earthquake engineering framework	133
7.1.2 Chapter 3: Damage estimation	134
7.1.3 Chapter 4: Building and life safety	135
7.1.4 Chapter 5: Estimation of direct losses	136
7.1.5 Chapter 6: Estimation of indirect losses and benefit-cost analysis	137
7.2 Limitations of research	138
7.3 Future directions	140
References	143

List of Figures

Figure 1.1. Recommended seismic performance objectives for buildings. The mean recurrence intervals of 43 years, 72 years, 475 years, and 949 years correspond to Poisson arrival events with 50% probability of exceedance in 30 yrs, 50% in 50 yrs, 10% in 50 yrs and 10% in 100 years, respectively (after SEAOC 1995).	4
Figure 2.1 Schematic of PEER methodology (Porter 2003).	16
Figure 2.2 Plan and elevation views of the perimeter-frame benchmark building (reproduced from Haselton et al. 2007).	20
Figure 2.3 Floor plan of ground floor.	21
Figure 2.4 Floor plan of floors 2–4.	21
Figure 2.5 Automatic sprinkler piping system of ground floor.	22
Figure 2.6 Automatic sprinkler piping system of floors 2–4.	22
Figure 2.7 Mean uniform hazard spectra (5% damping) for the LA Bulk Mail site for seven hazard levels (reproduced from Goulet et al., 2006). The spectral acceleration at $T=1$ sec is used for the benchmark study, so the hazard levels shown in this plot correspond to $S_a(T=1 \text{ sec}) = 0.10 \text{ g}, 0.19 \text{ g}, 0.26 \text{ g}, 0.30 \text{ g}, 0.44 \text{ g}, 0.55 \text{ g}, 0.82 \text{ g}$.	28
Figure 2.8 Static pushover curves for the fiber and lumped-plasticity models of one design variant (Design A) of the benchmark building, reproduced from Goulet et al. (2007).	30
Figure 2.9 <i>EDP</i> numbering for structural components in the N-S and E-W directions.	31
Figure 2.10 Combinations for <i>DDI</i> for biaxially loaded columns.	32
Figure 2.11 Biaxial moment relationship for columns (reproduced from ACI 1990).	33
Figure 2.12 Input and output parameters for the MDLA toolbox.	34
Figure 2.13 Fitted and empirical cumulative distribution functions of peak roof drift ratio (EW-dir) results for four levels of <i>IM</i> .	37
Figure 2.14 Schematic of MDLA toolbox.	39
Figure 3.1 Fragility functions for RC moment-frame members.	46
Figure 3.2 Fragility functions for column-slab connections.	48
Figure 3.3 Fragility functions for the wallboard partitions.	49
Figure 3.4 Fragility function for interior paint.	51

Figure 3.5	Fragility functions for exterior glazing.	52
Figure 3.6	Fragility function for acoustical ceiling.	53
Figure 3.7	Fragility function for braced automatic sprinklers.	54
Figure 3.8	Fragility function for hydraulic elevators.	55
Figure 3.9	Average probabilities of damage per story level for variant #1.	59
Figure 3.10	Average probabilities of damage per story level for variant #2.	60
Figure 3.11	Average probabilities of damage per story level for variant #3.	60
Figure 3.12	Average probabilities of damage per story level for variant #6.	61
Figure 3.13	Average probabilities of damage per story level for variant #9.	61
Figure 3.14	Average probabilities of damage per story level for variant #11.	62
Figure 3.15	Average probabilities of damage per story level for variant #12.	62
Figure 3.16	Average probabilities of damage per story level for variant #13.	63
Figure 3.17	Average probabilities of damage per story level for variant #14.	63
Figure 3.18	Average probabilities of damage per story level for variant #15.	64
Figure 3.19	Comparison of the average probabilities of column damage per story level of design variants #1, #2, #9, and #6 (from left to right).	64
Figure 3.20	Comparison of the average probabilities of beam damage per story level of design variants #1, #2, #9, and #6 (from left to right).	65
Figure 3.21	Comparison of the average probabilities of beam damage per story level of design variants #1, #2, #9, and #6 (from left to right).	65
Figure 4.1	Event tree model for building safety evaluation based on ATC-20's (1985, 1995, 1996a) (a) rapid evaluation, and (b) detailed evaluation procedures.	72
Figure 4.2	A comparison of the probabilities of building safety tagging between a design that includes the SCWB provision (VID #2) and one that does not (VID #9). The solid lines represent tagging after a rapid evaluation and the dashed lines represent tagging after a detailed evaluation; the color of the lines correspond to ATC-20's (1996a) red ("UNSAFE"), yellow ("LIMITED ENTRY"), and green ("INSPECTED") tags.	75
Figure 4.3	Fractional office building occupancy throughout the day, modeled after Coburn et al. (1992). The dashed version is the modified pattern used here to account for weekend and holiday occupancy.	88
Figure 4.4	Event tree model for fatality estimation of a specific building, considering the probabilities of local and global collapse at every hazard level.	92
Figure 5.1	Contributions to mean total repair cost for (a) variant #1,	96
Figure 5.2	Contributions to mean total repair cost for (a) variant #3,	96
Figure 5.3	Contributions to mean total repair cost for (a) variant #9,	97
Figure 5.4	Contributions to mean total repair cost for (a) variant #12,	97
Figure 5.5	Contributions to mean total repair cost for (a) variant #14,	98

Figure 5.6 Design comparisons of mean repair costs for (a) all structural components, and (b) all nonstructural components.	99
Figure 5.7 (a) Vulnerability functions for variants #1 and #2,	102
Figure 5.8 (a) Vulnerability functions for variants #1 and #6,	103
Figure 5.9 (a) Vulnerability curves for variants #1 and #11,	105
Figure 5.10 Vulnerability curves for variants #1, #13, #14 and #15.	106
Figure 5.11 A disaggregation of the expected annual loss for Design A (VID #1).	107
Figure 6.1 Gantt chart for fast-track repair scheme applied to an example 3-story steel frame building (reproduced from Beck et al. 1999).	117
Figure 6.2 Gantt chart showing fast-track repair scheme at two hazard levels for Design A (VID #1).	122
Figure 6.3 A comparison of the total downtime and the irrational and rational components of downtime for the baseline perimeter-frame (Design A, VID #1) and space-frame (Design E, VID #6) designs.	125

List of Tables

Table 1.1. Target Building Performance Levels, reproduced from Table C1-2 in FEMA 356 (FEMA 2000), describing the range of damage of structural and nonstructural components for various target building performance levels.	7
Table 1.2. Criteria for assigning structural performance level to concrete frame members, reproduced from Table C1-3 in FEMA 356 (FEMA 2000).	8
Table 1.3. Criteria for assigning nonstructural performance level to concrete frame members, reproduced from Table C1-5 in FEMA 356 (FEMA 2000).	11
Table 2.1 Damageable structural components in the benchmark building.	19
Table 2.2 Damageable nonstructural components in the benchmark building.	24
Table 2.3 Table of damageable assemblies for perimeter-frame design.	24
Table 2.4 Table of damageable assemblies for space-frame design.	25
Table 2.5 Summary of assembly fragility and cost distribution parameters.	36
Table 3.1 Williams et al. (1997) damage states and consequences for concrete columns.	43
Table 3.2 Stone and Taylor (1993) damage states and consequences for concrete columns.	45
Table 3.3 Summary of benchmark building designs and structural models.	56
Table 4.1 Summary of virtual inspector results of various benchmark building designs for three largest hazard levels.	77
Table 4.2 Death and injury ratios from some major U.S. earthquakes. All entries, but the last, are from NOAA (1972).	80
Table 4.3 Comparison of fatality models that is disaggregated by building type and damage quantity (modified from Table 19 in Shoaf and Seligson, 2005).	83
Table 4.4 Mean and variance of fatality models for local collapse and global collapse of the building, calculated with equation (4.6).	89
Table 4.5 Design variant descriptions and corresponding EANF results.	91
Table 5.1 Design variant descriptions and corresponding EAL results.	108

Table 6.1	Summary of damage states and associated repair-time parameters for benchmark building's damageable assemblies (Hecksler 2006).	114
Table 6.2	Design variant descriptions, corresponding downtime (irrational, rational and total downtimes) results at each hazard level, and EALD results.	123
Table 6.3	Expert-based estimates of downtime for the U.C. Berkeley campus based on building type and size, and extent of damage (reproduced from Comerio 2006).	126
Table 6.4	Design variant descriptions and corresponding expected annual number of fatalities (EANF) and the expected annual loss due to fatalities (EALF).	128
Table 6.5	Summary of expected annual losses for the three decision variables and five designs of the benchmark building.	132

CHAPTER 1

Introduction

Performance-based earthquake engineering can be defined as the assessment of expected system-level performance of a structure subjected to seismic excitation, as well as the detailed design of its structural and nonstructural features to achieve prescribed performance goals. These performance goals may be described at various levels: performance of structural members (e.g., probability of minor cracking of reinforced concrete members), performance of nonstructural elements (e.g., probability of functionality of essential utilities), global performance (e.g., probability of collapse), building safety (e.g., probability of red tagging), life safety (e.g., probability of number of lives lost), and equivalent economic performance metrics (e.g., exceedance probabilities for levels of repair cost).

The economic repercussions of U.S. earthquakes cannot be understated—massive losses can be attributed to several earthquakes of the last four decades alone, including the 1994 Northridge earthquake (\$17–\$26 billion), the 1989 Loma Prieta earthquake (\$11 billion), the 1964 Anchorage earthquake (\$3.2 billion), and the 1971 San Fernando earthquake (\$2.7 billion).¹ Considering the substantial economic impact of earthquakes, the adoption of performance-based earthquake engineering methods by the professional civil engineering

¹ These figures are in 2005 \$USD from the Insurance Information Institute (2006).

community will result in the prevention of unnecessary future losses. Hence the title of this dissertation, excerpted from Benjamin Franklin's well-known advice: "An ounce of prevention is worth a pound of cure."²

1.1 Earlier work in performance-based earthquake engineering

In a broad sense, performance-based earthquake engineering has its origins in the early 20th century: seismic design provisions of early U.S. building codes, beginning with the 1927 Uniform Building Code (PCBO 1927), sought to "permit structures to withstand earthquakes without collapse or endangerment of life safety" (Hamburger and Moehle 2000). In the 1970s, code requirements were added to enhance damage control for important facilities. Modern building codes (e.g., ICC 2003; ASCE 2006) provide design guidelines intended to achieve a specific performance objective (life safety and some degree of damage control), given a particular hazard (e.g., FEMA (2000)) specifies effects that are 2/3 those of the maximum considered earthquake, defined as an event producing a ground motion intensity with a 2% exceedance probability in 50 years).

New documents have been published in recent years that attempt to provide for more-robust performance-based seismic design. The first of these was Vision 2000 (SEAOC 1995), written by practicing engineers and scholars in an attempt to "embrace a broader scope of design and construction quality assurance issues and...yield more predictable seismic performance over a range of earthquake demands." Vision 2000 describes various hazard levels: the *frequent* intensity level with a 50% exceedance probability in 30 years hazard level, the *occasional* intensity level with a 50% exceedance probability in 50 years, the *rare* intensity level with a 10% exceedance probability in 50 years, and the *very rare* intensity level with a 10% exceedance probability in 100 years. Vision 2000 also defines various structural performance levels: *fully operational*, *operational*, *life safe*, and *near collapse* in terms of damage to structural and nonstructural components and in terms of

² Benjamin Franklin coined this phrase as a way to convince Philadelphians of the need to support the nation's first fire department to lessen irreversible economic losses, as fires were a considerable threat to 18th century America (Wikipedia 2006).

consequences to the occupants and functions carried on within the facility. Vision 2000 offers relationships between these hazard and performance levels for various building categories. This relationship is shown graphically in Figure 1.1, which shows the performance level that should be satisfied for the given hazard level and the type of structure. The diagonal lines representing different “objectives” in this figure correspond to different facility types (e.g., a facility with large quantities of toxic material that has a large impact if damaged is categorized as a safety critical objective; a hospital or police station is considered an essential objective; a facility with hazardous materials that has limited impact if damaged is considered a hazardous objective; residential and most commercial buildings are categorized as basic objective).

In 1996, the Applied Technology Council (ATC 1996b) published *Seismic Evaluation and Retrofit of Concrete Buildings* (ATC-40). In 1997, the Federal Emergency Management Agency (FEMA 1997a, b) published the *National Earthquake Hazards Reduction Program (NEHRP) Guidelines for the Seismic Rehabilitation of Buildings* and associated *Commentary* documents (FEMA 273 and 274, 1997). These documents, prepared by the Building Seismic Safety Council, addressed the rehabilitation of existing structures, and led to the most comprehensive guidelines for PBEE to date: the *Prestandard and Commentary for the Seismic Rehabilitation of Buildings* (FEMA 356, 2000).

The FEMA 356 report was intended to encourage wider use of FEMA 273 by converting it into mandatory language, and to provide a basis for a future, nationally recognized, ANSI-approved standard that incorporates its approaches and technology into mainstream design and construction practice. FEMA 356 was written to provide professional engineers nationwide a tool for designing seismic rehabilitation measures for existing structures. The document defines various target building performance levels and earthquake hazard levels similar to those presented in Vision 2000. A target building performance for a specific earthquake hazard is selected by the designer and the client together, and the building is designed according to the specifications of this standard. Performance levels are defined for structural and nonstructural systems, whose damage is described approximately. The

performance levels and descriptions of corresponding physical damage are shown in Table 1.1.

There are many tables in FEMA-356 for specific performance levels for various structural systems (e.g., for concrete frames, braced steel frames, metal deck diaphragms) and for nonstructural systems (e.g., for glazing, piping, cladding). These tables also include some engineering limit states (e.g., drift values) believed to correspond to the various performance levels for a particular component. These limit states are not intended to be used as acceptance criteria or in the postearthquake evaluation of damage, but are instead indicative of the range that exists for the limit states that typical structures undergo.

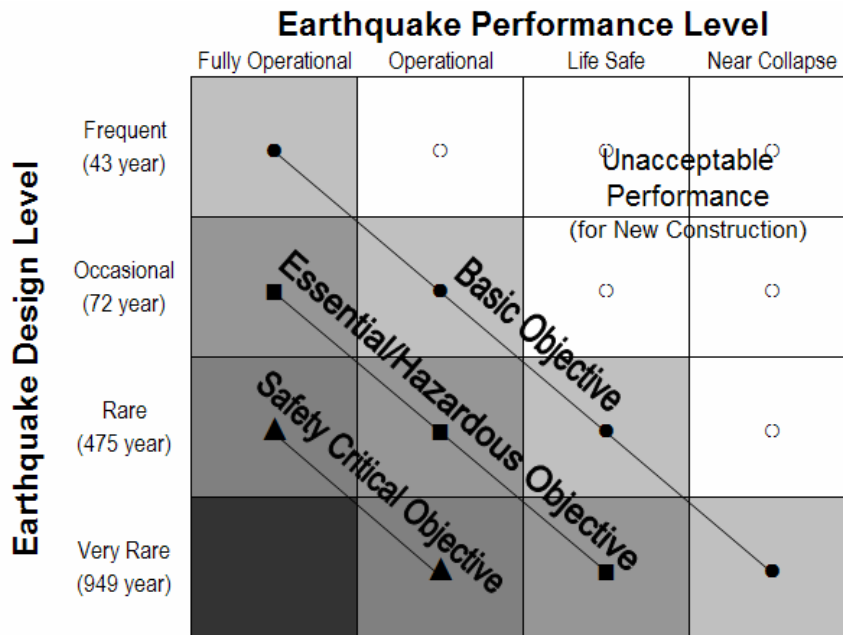


Figure 1.1. Recommended seismic performance objectives for buildings. The mean recurrence intervals of 43 years, 72 years, 475 years, and 949 years correspond to Poisson arrival events with 50% probability of exceedance in 30 yrs, 50% in 50 yrs, 10% in 50 yrs and 10% in 100 years, respectively (after SEAOC 1995).

1.2 Beyond Vision 2000

Although the development of PBEE has been progressing in recent years, current methods have several limitations, such as a lack of a consistent procedure for ground motion selection corresponding to a given hazard level and the analysis of structural elements. Perhaps the most notable limitation of existing methods is the use of component-level acceptance criteria, as opposed to probabilistic system-level performance criteria. In FEMA 356, any combination of repaired elements, undamaged existing elements, and new elements is modeled using specified procedures and compared against performance-level acceptance criteria; the ultimate goal is to pass the criteria agreed upon by the stakeholder and structural engineer. By contrast, the goal of the methodology used in the present study is to quantify performance using probabilistic measures on quantities that are of direct interest to building stakeholders, namely: repair costs, life safety, and postearthquake operability (“dollars, deaths, and downtime”).

Although FEMA 356 does not attempt to quantify the probability of achieving a given performance level or to quantify repair costs, number or likelihood of fatalities, or loss-of-use duration, it does address component-level and system-level damage states and relates them to life safety and postearthquake operability, as shown in Table 1.1. However, it can be difficult to use these relationships to quantify dollars, deaths, and downtime. The damage states given in FEMA 356 tend to be qualitative and open to multiple interpretations. Tables 1.2 and 1.3, reproduced from FEMA 356, give various examples of the qualitative language used to describe damage states for concrete frame systems, cladding, glazing, partitions, and ceilings. Some examples of this language are: *minor*, *distributed*, *some*, *many*, *extensive*, and *most*. Such qualitative language is difficult to employ in a quantitative, probabilistic model of damage and loss, especially considering that some of the categories of building components addressed in the tables are quite broad.

It is necessary to better define and quantify these component damage states; in this thesis, fragility functions are used to estimate the probabilities of being in these damage states

(Chapter 3). These fragility functions are used to establish correspondence between the values of structural response and specific damage states in a probabilistic way. As used in this thesis, a fragility function quantifies the probability that a particular type of component will reach or exceed a clearly defined damage state as a function of the structural response to which it is subjected. These resulting probabilities of damage for building components are used to estimate losses from future seismic events (i.e., repair costs, fatalities, and downtime).

Another limitation of damage and loss assessment in current PBEE procedures is the lack of a standard methodology and consistent data for the development of new fragility functions. A clear definition of the damage states and the corresponding fragility functions are necessary for every damageable building component considered in the damage assessment. Similarly, clear definitions of the repair efforts and the probabilistic repair costs associated with the damage states are required for all damageable components. In the last few years, there has been much advancement in the development of fragility and cost distribution functions for damageable building components, but much work is still needed in this area to cover the wide range of damageable components present in real buildings. To overcome this paucity of data, some researchers have suggested the use of a lumping scheme of nonstructural components to create *story fragility functions*. The use of these story fragility functions is a good solution if performing approximate damage assessment in the absence of empirical damage data, but not when component-specific fragility functions are available that allow a more detailed understanding of the building's performance to be obtained.

It is important to gather the data available for fragility function development in a single location to ease information dissemination to practitioners and researchers. It is also important to standardize the development of these functions; the researchers who are performing experiments should report damage in a systematic way so that it may be useful for loss estimators. There have been suggestions made for government entities, such as the National Institute of Standards and Technology (NIST 2006), to maintain a database of fragility functions; this much-needed step has not yet been realized.

Table 1.1. Target Building Performance Levels, reproduced from Table C1-2 in FEMA 356 (FEMA 2000), describing the range of damage of structural and nonstructural components for various target building performance levels.

Damage Control and Building Performance Levels				
	Target Building Performance Levels			
	Collapse Prevention Level (5-E)	Life Safety Level (3-C)	Immediate Occupancy Level (1-B)	Operational Level (1-A)
Overall Damage	Severe	Moderate	Light	Very Light
General	Little residual stiffness and strength, but load-bearing columns and walls function. Large permanent drifts. Some exits blocked. Infills and unbraced parapets failed or at incipient failure. Building is near collapse.	Some residual strength and stiffness left in all stories. Gravity-load-bearing elements function. No out-of-plane failure of walls or tipping parapets. Some permanent drift. Damage to partitions. Building may be beyond economical repair.	No permanent drift. Structure substantially retains original strength and stiffness. Minor cracking of facades, partitions, and ceilings as well as structural elements. Elevators can be restarted. Fire protection operable.	No permanent drift. Structure substantially retains original strength and stiffness. Minor cracking of facades, partitions, and ceilings as well as structural elements. All systems important to normal operation are functional.
Nonstructural components	Extensive damage.	Falling hazards mitigated but many architectural, mechanical, and electrical systems are damaged.	Equipment and contents are generally secure, but may not operate due to mechanical failure or lack of utilities.	Negligible damage occurs. Power and other utilities are available, possibly from standby sources.
Comparison w/ NEHRP provisions for the Design Earthquake	Significantly more damage and greater risk.	Somewhat more damage and slightly higher risk.	Less damage and lower risk.	Much less damage and lower risk.

Table 1.2. Criteria for assigning structural performance level to concrete frame members, reproduced from Table C1-3 in FEMA 356 (FEMA 2000).

Table C1-3 Structural Performance Levels and Damage 1, 2, 3—Vertical Elements				
Structural Performance Levels				
Elements	Type	Collapse Prevention (S-5)	Life Safety (S-3)	Immediate Occupancy (S-1)
Concrete Frames	Primary	Extensive cracking and hinge formation in ductile elements. Limited cracking and/or splice failure in some nonductile columns. Severe damage in short columns.	Extensive damage to beams. Spalling of cover and shear cracking (<1/8" width) for ductile columns. Minor spalling in nonductile columns. Joint cracks <1/8" wide.	Minor hairline cracking. Limited yielding possible at a few locations. No crushing (strains below 0.003).
	Secondary	Extensive spalling in columns (limited shortening) and beams. Severe joint damage. Some reinforcing buckled.	Extensive cracking and hinge formation in ductile elements. Limited cracking and/or splice failure in some nonductile columns. Severe damage in short columns.	Minor spalling in a few places in ductile columns and beams. Flexural cracking in beams and columns. Shear cracking in joints <1/16" width.
	Drift	4% transient or permanent.	2% transient; 1% permanent.	1% transient; negligible permanent.

1.3 PEER

The Pacific Earthquake Engineering Research Center, also known as PEER, is a multi-campus and multidisciplinary 10-year program (funded by the National Science Foundation) that has focused on developing a complete methodology for performance-based earthquake engineering within a probabilistic framework. This methodology is intended to be a more robust framework than the ones provided by the first-generation performance-based earthquake engineering procedures described above. The methodology proposed by PEER, which forms the basis for the research presented in this dissertation, is described in detail in Chapter 2. In addition to the development of a probabilistic performance assessment framework for seismic design, other contributions by the PEER research center include:

- PEER Strong Motion Database: a compilation of over 1,500 records from 143 different earthquakes in a web-accessible format, including more accurate characterizations of site conditions at various strong motion stations (Moehle and Deierlein 2004; PEER 2005a). <http://peer.berkeley.edu/smcat/>
- OpenSees Software: the Open System for Earthquake Engineering Simulation is an open-source computational platform for structural and geotechnical analyses that includes improved models for reinforced-concrete structures, shallow and deep foundations, and liquefiable soils (Moehle and Deierlein 2004; OpenSees 2006). <http://opensees.berkeley.edu/>
- Structural Performance Database: a compilation of over 400 cyclic, lateral-load tests of various types of reinforced concrete columns, e.g., columns with rectangular, circular, and octagonal cross sections (PEER 2005b). <http://nisee.berkeley.edu/spd/>

1.4 ATC-58

A new project is underway by the Applied Technology Council (ATC) to develop the next-generation guidelines for performance-based earthquake engineering design. This project is sponsored by FEMA and is known as ATC-58; it has an advisory committee composed of experts from various fields including engineers, architects, government officials, social scientists, and researchers. Although FEMA-356 addresses component-level and system-level damage states and relates them to various qualitative performance levels in guidelines for the rehabilitation of existing structures (which rely heavily on the designing engineer's opinion), it is not an ANSI³-approved standard for performance-based seismic design of new buildings. The goal of ATC-58 (Whittaker et al. 2004) is to create a standard for the design of new structures and the upgrade of existing ones that incorporates the building performance level desired by the stakeholders into the design process, using clear and quantitative definitions for building performance (i.e., life safety, building operability, and economic losses). The project is divided into two parts, and the ATC-58 committee is currently working on the first phase, which is to develop the "performance verification procedure." This procedure is what engineers will use to evaluate whether the building design meets the prescribed objectives set by stakeholders. The second phase of the project

³ ANSI (American National Standards Institute) is a private nonprofit organization that oversees the development of standards for products and services in the United States (ANSI 2006).

will be to develop the design guidelines for engineers and to generate the building performance guidelines to help direct stakeholders; the second phase will likely begin in a few years.

Although the first phase of ATC-58 is not yet complete, an interim report is currently available (representing 25% of the planned document) that outlines the framework for performance assessment (ATC 2005). This report gives two levels for assessment that are appropriate for different steps of the design process (i.e., if the design process is in its early stages, the details of the building will not be known and gross estimates must be made to determine building performance and estimate future losses). Also, ATC-58 provides the following assessment types: intensity based, scenario based, and time based. The intensity-based assessment determines the probability of loss for a given hazard level; the scenario-based assessment determines the probability of loss for a specified seismic event; the time-based assessment addresses the probability of loss over a given time period, such as the design life of the structure. Each of these assessments addresses different concerns that stakeholders are likely to have.

The ATC-58 report gives some guidance on how to sort the damageable components of a building into what are termed “performance groups.” A performance group is defined (ATC 2005) by the type of building component (e.g., wallboard partitions) that experience similar demands (e.g., peak interstory drifts) and will have similar damage patterns. These guidelines also propose three ways to assess building performance: direct economic losses (e.g., repair costs), downtime (e.g., interruption of building functions), and casualties (e.g. number of deaths or serious injuries). Of these three performance evaluation metrics, only the first, the direct economic losses, has so far been addressed significantly; modeling for downtime and casualties are yet to be developed by the authors of ATC-58. The results from PEER research have been used in the development of the ATC-58 guidelines.

Table 1.3. Criteria for assigning nonstructural performance level to concrete frame members, reproduced from Table C1-5 in FEMA 356 (FEMA 2000).

Nonstructural Performance Levels and Damage ¹ —Architectural Components				
Nonstructural Performance Levels				
Component	Hazards Reduced N-D	Life Safety N-C	Immediate Occupancy N-B	Operational N-A
Cladding	Severe distortion in connections. Distributed cracking, bending, crushing, and spalling of cladding elements. Some fracturing of cladding, but panels do not fall in areas of public assembly.	Severe distortion in connections. Distributed cracking, bending, crushing, and spalling of cladding elements. Some fracturing of cladding, but panels do not fall.	Connections yield; minor cracks (<1/16" width) or bending in cladding.	Connections yield; minor cracks (<1/16" width) or bending in cladding.
Glazing	General shattered glass and distorted frames in unoccupied areas. Extensive cracked glass; little broken glass in occupied areas.	Extensive cracked glass; little broken glass.	Some cracked panes; none broken.	Some cracked panes; none broken.
Partitions	Distributed damage; some severe cracking, crushing, and racking in some areas.	Distributed damage; some severe cracking, crushing, and racking in some areas.	Cracking to about 1/16" width at openings. Minor crushing and cracking at corners.	Cracking to about 1/16" width at openings. Minor crushing and cracking at corners.
Ceilings	Extensive damage. Dropped suspended ceiling tiles. Moderate cracking in hard ceilings.	Extensive damage. Dropped suspended ceiling tiles. Moderate cracking in hard ceilings.	Minor damage. Some suspended ceiling tiles disrupted. A few panels dropped. Minor cracking in hard ceilings.	Generally negligible damage. Isolated suspended panel dislocations, or cracks in hard ceilings.

1.5 Plan for thesis

This thesis presents the damage and loss analysis procedures developed under funding from the PEER Center and recently implemented as part of a benchmark study of the

performance of new reinforced-concrete moment-frame buildings (Haselton et al. 2007). Given the recent advances in the integration of PBEE into design standards, the work presented in this dissertation has been mindful of the progress and challenges toward this end. Chapter 2 of this dissertation outlines the PEER methodology for performance-based earthquake engineering, describes the benchmark study undertaken to assess the performance of reinforced-concrete buildings designed with current building codes, and summarizes the development of the MDLA (MATLAB Damage and Loss Analysis) toolbox implemented in this study to perform the damage and loss analyses. The results of these analyses are presented in Chapter 3 through Chapter 6. Specifically, Chapter 3 introduces the methodology and the fragility functions needed to complete this damage analysis. The results of the damage analysis are then used in Chapter 4; the *virtual inspector* is introduced as a methodology to determine the probability of red and green safety tags for the building at various hazard levels and to estimate the number of fatalities caused by building failures. The damage analysis results are also used in Chapter 5 to calculate the direct economic losses associated with the repair effort needed to return the building to its undamaged state. The results of safety tagging affects the total downtime of a structure after a seismic event, and so they are used in a methodology for calculating indirect losses associated with building downtime that is given in Chapter 6. In addition, the calculation of indirect losses associated with human fatalities is also presented in this chapter. Finally, this chapter incorporates all the losses into a benefit-cost analysis that may be used by building owners together with structural engineers in the design process as a preventative measure. The thesis concludes with a summary of the work presented here and suggestions for future work in Chapter 7.

CHAPTER 2

Performance-Based Earthquake Engineering Framework

The PEER framework for performance-based earthquake engineering (PBEE) has been developed to estimate the performance of structures in seismic-prone regions. The methodology for implementing this modular framework is described in detail in this chapter. Also, this chapter introduces a recent benchmark study that applies the methodology to determine the performance of several designs of a new reinforced-concrete moment-frame commercial building, and clearly states the assumptions made for this implementation. In addition, the software developed for the purpose of estimating the damage and losses for the benchmark study, the MDLA toolbox, is described in some detail.

2.1 PEER's PBEE methodology

Among other things, the PBEE methodology can be used to estimate the mean annual frequency with which a particular performance metric will exceed various levels for a given location (Porter 2003; Moehle and Deierlein 2004; Mitrani-Reiser et al. 2006; Goulet et al. 2007; Haselton et al. 2007). The four main steps are presented in Figure 2.1: hazard analysis, structural analysis, damage analysis, and loss analysis. The methodology is expressed mathematically in Equation (2.1). In both the figure and the equation, $p[X|Y]$ denotes the probability density of X conditioned on Y , $\lambda[X|Y]$ denotes the mean occurrence

rate of X given Y , IM denotes an intensity measure (e.g., $S_a(T_1)$), EDP denotes engineering demand parameters (e.g., drift and plastic rotations), DM denotes damage measures (e.g., spalled concrete, collapse), and DV denotes decision variables (e.g., repair costs, fatalities).

The first step in this approach is the hazard analysis, which evaluates the seismic hazard for a particular facility, considering nearby faults, site distance, source-to-site conditions, facility location, facility design, etc. Probabilistic seismic hazard analysis (PSHA) is used to evaluate the mean occurrence rate (mean frequency) of events having an intensity measure (IM) greater than a threshold value, im , for a specific site of interest (e.g., Cornell 1968, Kramer 1996, Field 2005). PSHA requires the use of seismic-hazard source models and ground-motion attenuation models. The ground shaking at the site is parameterized via an intensity measure. The hazard curve, $\lambda[IM|D]dIM$, is the mean arrival rate of events in $[IM, IM + dIM]$. Some traditional intensity measures are peak ground acceleration and spectral acceleration at chosen periods (e.g., $S_a(T_1)$, the damped elastic spectral acceleration at the small-amplitude fundamental period of the structure). The latter measure is used in this work.

The second step is the structural analysis, in which the engineer creates a structural model of the facility in order to estimate the uncertain structural response. The PEER PBEE methodology does not prescribe the type of model that should be used. In the PEER benchmark project described later, an open-source software program (sponsored by PEER and NSF) known as OpenSees (2006) was used to develop and analyze structural models of a building. This software contains a library of elements, materials, and section types to facilitate the building of a structural model. Also, the computational resources in OpenSees include linear-equation solvers, time-integration schemes, and solution algorithms. A non-linear dynamic analysis is used to estimate structural response for the benchmark study. The response is measured in terms of a vector of engineering demand parameters ($EDPs$), conditioned on the intensity measure IM and design. Some examples of $EDPs$ are: directional peak transient interstory drift, directional peak diaphragm acceleration, peak plastic hinge rotation, and peak positive curvature in the beams. The structural model should accurately capture the behavior of the building for low-intensity and high-intensity

seismic events, since damage at all levels of ground motion contribute to total losses. Note that the methodology allows for uncertainty in the structural models.

The third step of this methodology is the damage analysis. This step involves using fragility functions that express the probability that a facility component (e.g., beam, column, wall partition, etc.) is in or exceeds a particular damage state as a function of an *EDP*. The methodology does not specify how to aggregate the damageable building components and extensive research has been and continues to be conducted for damageable components at many levels; some researchers lump all components that are susceptible to the same EDP and will have similar damage patterns into one damageable “group,” while other researchers consider each component separately. In this study, we lump all like components on the same floor that are sensitive to the same EDP into one damage group. The different damage states for each damageable group are indicative of the corresponding repair efforts needed to restore that component type to an undamaged state. The fragility functions, compiled based on laboratory experiments, analytical investigation, expert opinion, or some combination, are used to create a probabilistic array of damage measures, *DM*.

The *DMs* calculated in the damage analysis are used in the final step of the PEER methodology, the loss analysis. This analysis is the probabilistic estimation of structural performance conditioned on the damage state of all components. Currently, the PEER methodology does not prescribe exactly which decision variables should be chosen in the loss analysis. However, performance metrics that have been previously considered include repair cost, repair duration, and loss of life. All three of these metrics are evaluated in this work. In addition to these, building safety tagging is also considered. Each metric provides unique and valuable information for stakeholders. This final step of the methodology gives estimates of the mean annual frequency with which various levels of *DV* are exceeded; these can be used to inform a variety of risk-management decisions. Note that PEER does not sponsor particular software programs for the hazard, damage, and loss analyses. A program, the MATLAB Damage and Loss Analysis (MDLA) toolbox, was developed as part of this work to integrate the hazard and structural analysis results and perform the

damage and loss analyses (Mitrani-Reiser et al. 2006); details of the MDLA program are presented in Section 2.5.

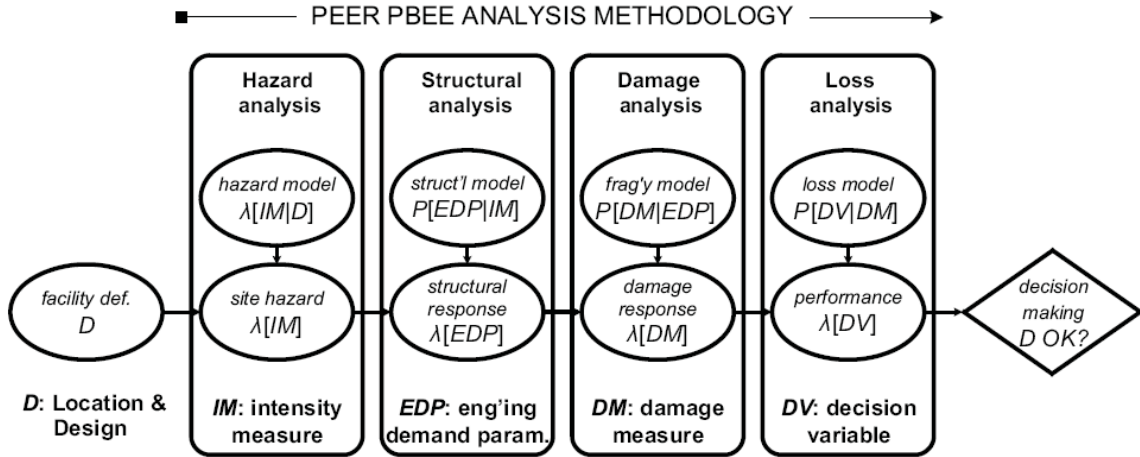


Figure 2.1 Schematic of PEER methodology (Porter 2003).

$$\lambda[DV | D] = \iiint p[DV | DM, D] p[DM | EDP, D] p[EDP | IM, D] \lambda[IM | D] dIM dEDP dDM \quad (2.1)$$

2.2 Introduction to PEER benchmark study

The benchmark study presented here is a collaborative effort between UCLA, Stanford and Caltech; each university was responsible for a different module of the PEER methodology (Figure 2.1), with UCLA performing the hazard analysis, Stanford the structural analysis and Caltech the damage and loss analyses. Each module's output feeds into the following analysis step and is thus limited or enhanced by the capabilities of the previous step. The purpose of this study was to implement PEER's PBEE methodology on various designs and models of a new four-story reinforced-concrete moment-frame office building for various hazard levels, and to probabilistically evaluate the performance of the structure in terms of the following decision variables: direct losses (i.e., repair cost), indirect losses (i.e., economic loss due to business interruption), building safety and corresponding downtime (i.e., safety tagging), and life safety (i.e., number of fatalities). The performance

is evaluated for various structural realizations, and the results are compared in Chapter 4-Chapter 6.

2.2.1 PEER benchmark building and site

The site for the benchmark building was selected to represent a typical urban location in a highly seismic region of California where near-fault motions are not of concern; the chosen site is the LA Bulk Mail Facility in Bell, CA (coordinates 33.996° N, 118.162° W), located approximately 7 miles southeast of downtown Los Angeles. The site was chosen such that specific features of the region (e.g., basin edge effects) would not dominate the ground motions; this site met the benchmark selection criteria and also had the advantage of available high quality geotechnical data from the Resolution of Site Response Issues from the Northridge Earthquake program (ROSRINE 2005). The site is located on deep sediments that are mostly Quaternary alluvial deposits, and the upper 30 meters consist of sands and silts with traces of clay and cobbles that correspond to an average shear wave velocity $V_{s-30} = 285$ m/s (NEHRP soil category D) (Goulet et al. 2006). Further details of the site hazard characterization may be found in Haselton, et al. (2007).

The benchmark structure, a 4-story, reinforced-concrete moment-frame office building, is a hypothetical structure that was designed specifically for this study according to IBC-2003, ASCE7-02, and ACI 318-02. Several designs were created for the benchmark study to represent the variability of design for different engineers using the same building code, including perimeter-frame and space-frame variants.⁴ These design variants are described in detail in Haselton et al. (2007), and briefly summarized here:

Design A: This is the baseline perimeter-frame design that reflects current practice, including above-code beam flexural strength and strong-column weak-beam (SCWB) ratios.

⁴ The space-frame design has a similar layout to the perimeter-frame design (i.e., same number of bays in both directions and same number of floors), except that the gravity system is ignored.

Design B: This design, although code conforming, is less conservative than Design A, with code-minimum force requirements, beam flexural strength, and SCWB ratios.

Design C: This design is intended to be easy to construct since the specified member dimensions, reinforcing schedule, and material properties of the second floor beams and first story columns are repeated in the upper-story beams and columns.

Design D: This design is the same as Design C, except that the SCWB provision is not enforced. Therefore, this design is non-code-conforming and was included in the study to demonstrate the importance of enforcing the SCWB provision in building designs.

Design E: This is the baseline space-frame design that reflects current practice, based on the provisions of the 2003 IBC (ICC 2003) and ACI 318-02 (ACI 2002).

The plan and elevation views of the building are given in Figure 2.2. The sizes of the moment-frame columns for the code-conforming designs range from 24"×28" to 30"×40"; the moment-frame beams sizes are between 24"×24" and 24"×40". The gravity frame in the perimeter-frame designs are composed of 18"-square reinforced concrete columns and an 8" post-tensioned two-way slab. Further details on member dimensions, reinforcing schedules, and material properties are available in Haselton et al. (2007). Some architectural features were assumed for the hypothetical benchmark building to later include in the loss analysis; the details for these are presented in Section 2.2.3. The floor plans showing these architectural finishes throughout the height of the building are given in Figure 2.3–Figure 2.6.

2.2.2 Damageable structural components

To estimate the performance of code-conforming reinforced-concrete SMRFs in general, one would need to assess the performance of many buildings of different heights and configurations while considering the effects of design uncertainty for each building. While this would be valuable, the benchmark study's focus was on a single four-story RC SMRF office building at a single site. Various structural designs were considered in order to investigate the variability in performance that results from various design decisions. The intent of the benchmark design was to emulate current practice as closely as possible, and to that end the designs of two practitioner-designed RC SMRF buildings were reviewed

and the corresponding structural engineers were interviewed to better understand the controlling factors of their designs. The structural components from the benchmark building that were considered for the probabilistic loss analysis are: moment-frame beams and columns, moment-frame beam-column joints, gravity columns, and slab-columns joints. Those actually used in the damage and loss analysis of the benchmark study are summarized along with their associated *EDP* and fragility function reference in .

The beam-column joints and gravity-frame columns were not considered in the present study because they are not expected to make a significant difference in the loss results. With strong-column weak-beam provision of current design standards, one can assume that the damage to the joint is equal to or less than the damage to the beam. Repair costs for the damage states and the corresponding detailed outline of the repair effort for each damage state, provided by a professional cost estimator (Beck et al. 2002), show that the cost to include the joint in the repair is small. Therefore, it is assumed that whatever minor costs ignored from the beam-column joints in the moment frames is accounted for in the uncertainty of the repair cost for the adjacent beams. A static pushover analysis of the baseline perimeter-frame design shows that the plastic rotation demands for the gravity columns are at least an order of magnitude smaller than their capacities; and thus will likely contribute a modest amount to the total repair costs. These reasons justify ignoring the beam-column joint and the gravity-frame column in the damage and loss analysis.

Table 2.1 Damageable structural components in the benchmark building.

Components	EDP	Reference
RC SMRF beams	Displacement Damage Index (DDI)	Williams et al. (1997)
RC SMRF columns	Displacement Damage Index (DDI)	Williams et al. (1997)
Gravity Frame: Slab-Column Joints	Peak Transient Drift Ratio (PTDR)	Aslani (2005)

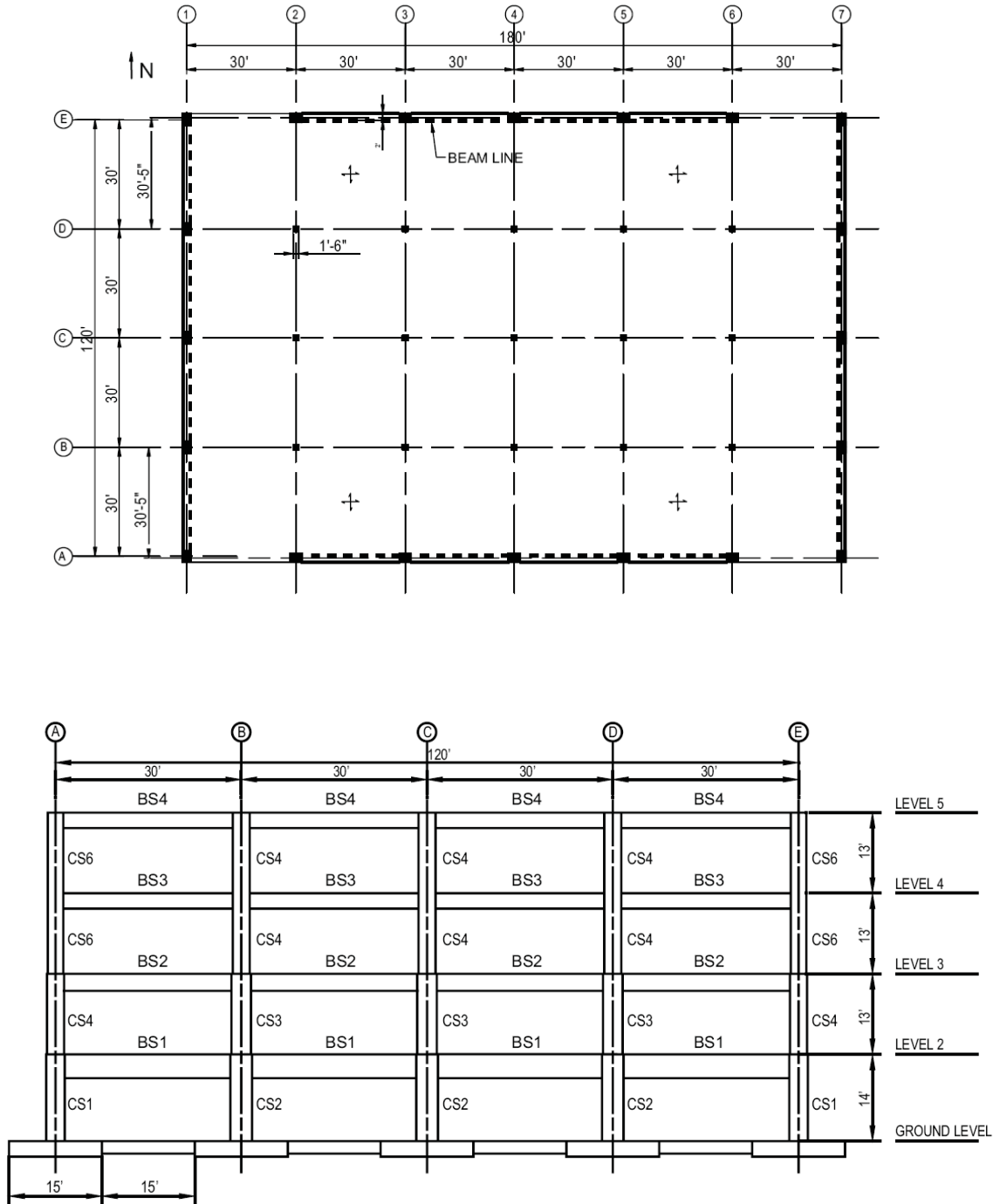


Figure 2.2 Plan and elevation views of the perimeter-frame benchmark building (reproduced from Haselton et al. 2007).

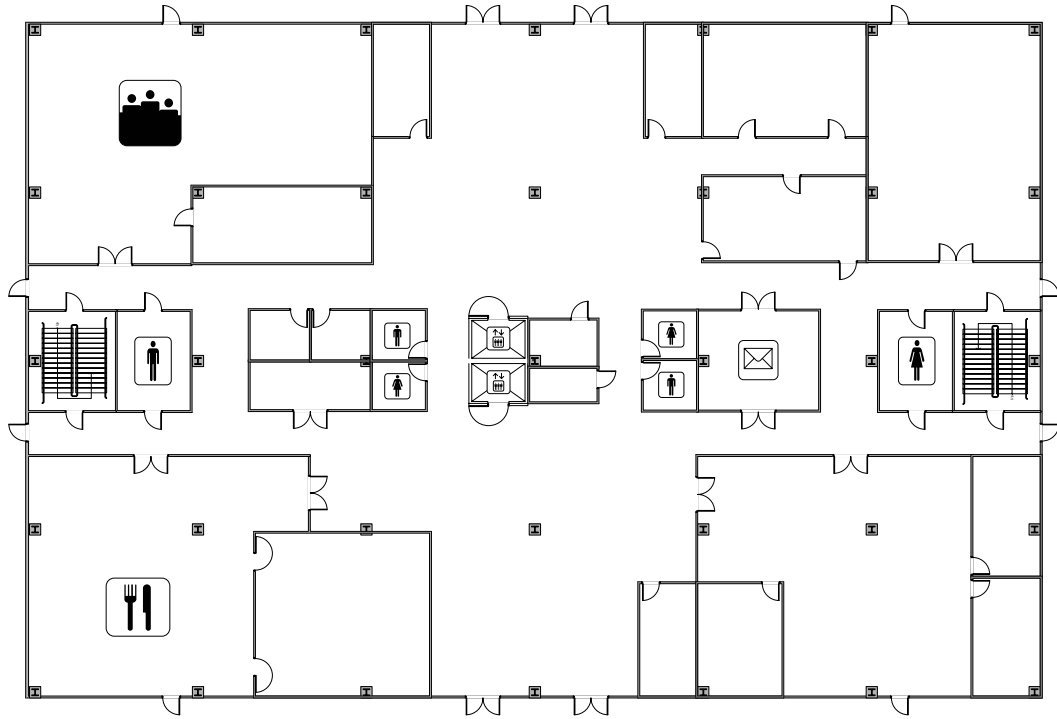


Figure 2.3 Floor plan of ground floor.

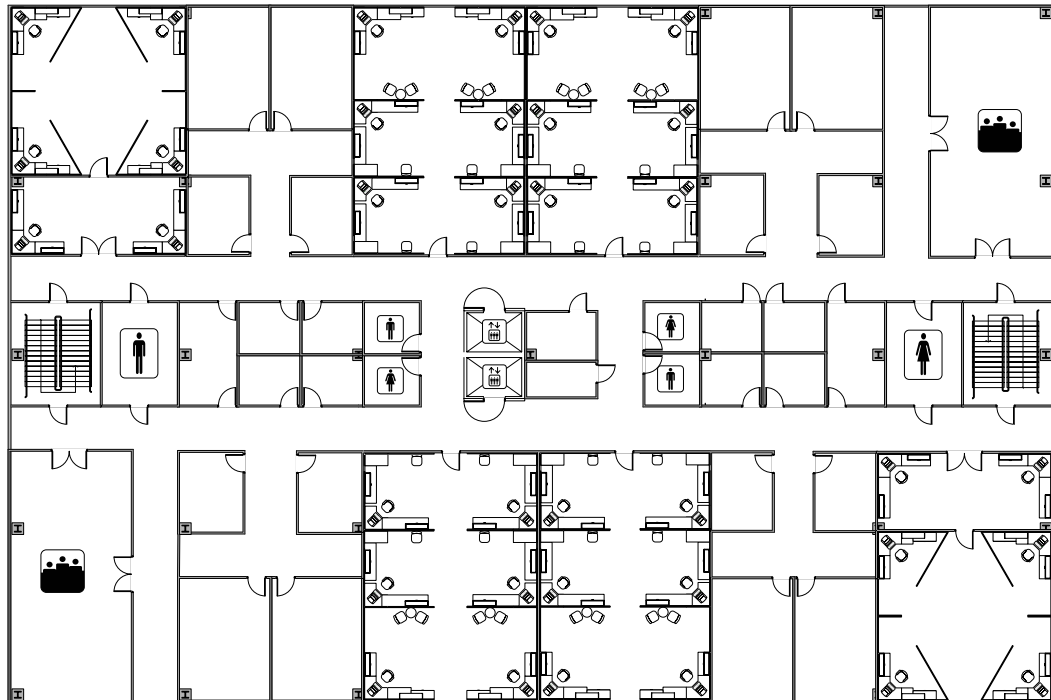


Figure 2.4 Floor plan of floors 2-4.

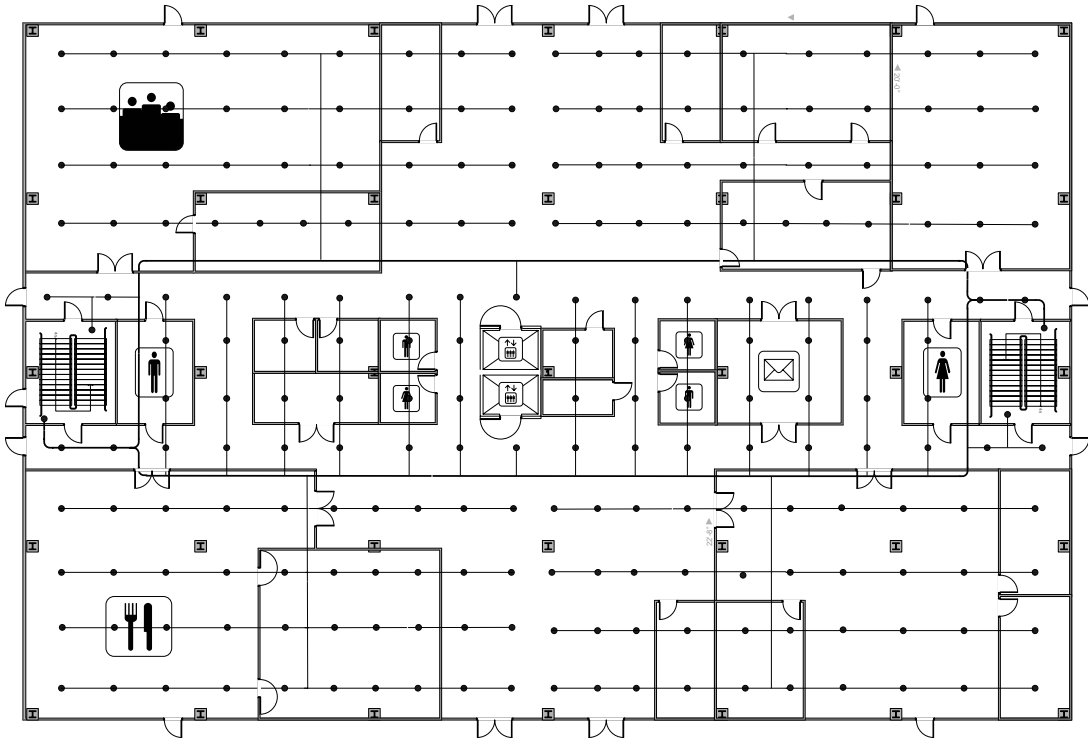


Figure 2.5 Automatic sprinkler piping system of ground floor.

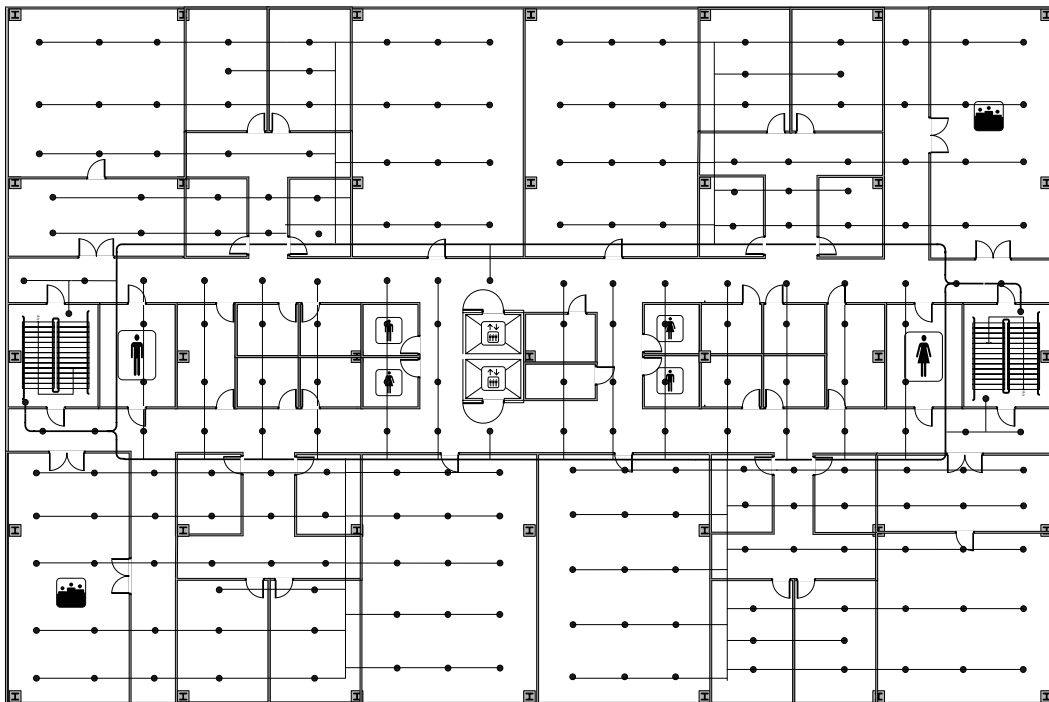


Figure 2.6 Automatic sprinkler piping system of floors 2-4.

2.2.3 *Damageable nonstructural components*

The structural and nonstructural components of a real, constructed building can be determined from the as-built drawings, supplemented perhaps by site investigations. The benchmark building examined here is *not* a real facility, so the design of its structural and nonstructural components was constrained only by the code and common practice. The building was designed for an “office” occupancy type, and the rendered realistic architectural plans are shown in Figure 2.3-Figure 2.6 in Section 2.2.1. These drawings are used to quantify the nonstructural components of the building—the exterior closure, interior finishes, and selected mechanical, electrical, and plumbing features that would most likely account for most of the repair cost. Loss analysis results from other PBEE studies (e.g., Beck et al. 2002) have suggested that the building components for this facility that would contribute the most to repair cost are its structural members, drywall partitions and interior paint. Thus, this benchmark study focuses on these, and additional components with fragility functions that are readily available. Mechanical equipment, such as that involved in the heating, ventilation and air-conditioning systems, are damaged in earthquakes because they are not bolted down to floors; since the building is designed as “new” construction, it is assumed that the mechanical equipment would be properly bolted down for seismic precautions and can thus be considered rugged. The building nonstructural components considered for the damage and loss analyses, along with their associated *EDP*’s and fragility function references are summarized in Table 2.2.

Table 2.2 Damageable nonstructural components in the benchmark building.

Components	EDP	Reference
Exterior Walls	Peak Transient Drift Ratio (PTDR)	Behr and Worrell (1998); Porter et al. (2001)
Interior Partitions	Peak Transient Drift Ratio (PTDR)	Porter et al. (2001); Rihal (1982)
Conveying Systems ¹	Peak Ground Acceleration (PGA)	Benuska (1990); Finley et al. (1996); Porter (2007)
Plumbing ² and Fire Protection ³	Peak Diaphragm Acceleration (PDA)	Porter et al. (2001); Sprinkler Fitters U.A. (1989)
Ceiling Systems	Peak Diaphragm Acceleration (PDA)	Porter et al. (2001)
¹ Elevators and escalators. ² Domestic water distribution, sanitary waste system, and specialty plumbing. ³ Sprinkler systems and standpipes.		

2.2.4 Table of considered damageable building components

A table of the itemized components considered in the damage and loss analyses, including brief descriptions and quantities, is given below in Table 2.3 for the perimeter-frame designs and in Table 2.4 for the space-frame designs. Assembly types follow the numbering system of Porter (2000), which is based on that of RSMeans Corp. (2001).

Table 2.3 Table of damageable assemblies for perimeter-frame design.

Assembly Type	Assembly Description	Unit	Quantity
3.5.190.1102.01	Ductile cast-in-place reinforced concrete beams	ea	64
3.5.180.1101.01	Ductile cast-in-place reinforced concrete columns	ea	80
B1045.003	Column-slab connections	ea	80
6.1.500.0001.01	Drywall partition, 5/8", 1 side, on metal stud	64 sf	1,293
6.1.500.0002.01	Drywall finish, 5/8", 1 side, on metal stud	64 sf	1,293
4.7.100.0001.01	Exterior glazing, 5' × 6' pane Al frame	pane	1,060
6.7.100.5800.01- 6.7.100.5800.31	Acoustical ceiling, 2' × 4' light Al grid attached	sf	81,000
8.2.110.0000.02	Automatic sprinklers, braced	12 lf	793
7.1.100.0000.01	Hydraulic elevators	ea	2

Table 2.4 Table of damageable assemblies for space-frame design.

Assembly Type	Assembly Description	Unit	Quantity
3.5.190.1102.01	Ductile cast-in-place reinforced concrete beams	ea	232
3.5.180.1101.01	Ductile cast-in-place reinforced concrete columns	ea	140
6.1.500.0001.01	Drywall partition, 5/8", 1 side, on metal stud	64 sf	1,293
6.1.500.0002.01	Drywall finish, 5/8", 1 side, on metal stud	64 sf	1,293
4.7.100.0001.01	Exterior glazing, 5' × 6' pane Al frame	pane	1,060
6.7.100.5800.01- 6.7.100.5800.31	Acoustical ceiling, 2' × 4' light Al grid attached	sf	81,000
8.2.110.0000.02	Automatic sprinklers, braced	12 lf	793
7.1.100.0000.01	Hydraulic elevators	ea	2

2.3 PEER benchmark PSHA

In the probabilistic seismic hazard analysis (PSHA), the seismic source model identifies the faults in the region of the site posing a significant threat from ground shaking. Seismic events of interest on a fault segment may be characterized by their possible values of magnitude and the mean rate at which such events occur. A Poisson process is commonly adopted for seismic recurrence models in seismic engineering (Cornell 1968, 1986). The ground-motion attenuation model gives IM at the site as a function of magnitude and location of the event, taking into account soil conditions at the site and source faulting types. The seismic-hazard source model and the ground-motion attenuation model are used to create the probability distributions of magnitude and distance, and of IM , respectively. These distributions are used in combination with the rate of seismic activity on each of the N_S regional faults to calculate the mean total rate of seismic events of interest giving $IM \geq im$:

$$\begin{aligned}
 \lambda_{IM}(im) &= \sum_{i=1}^{N_S} \lambda_i P[IM \geq im \mid \text{event of interest on the } i\text{th fault}] \\
 &= \sum_{i=1}^{N_S} \lambda_i \iint P[IM \geq im \mid M_i, R_i] p(M_i, R_i) dM_i dR_i
 \end{aligned} \tag{2.2}$$

where λ_i is the mean rate of occurrence of events of interest on the i th fault; $p(M_i, R_i)$ is the joint probability density function of magnitude M_i and source-to-site distance R_i given that an event of interest has occurred on the i th fault; and $P[IM \geq im | M_i, R_i]$ is the complementary cumulative distribution function of IM , conditioned on M_i and R_i for an event on the i th fault, which is given by the ground-motion attenuation model.

The function $\lambda_{IM}(im)$ when plotted against im is usually referred to as the *hazard rate function* or just *hazard function* (e.g. Benjamin and Cornell 1970, Ang and Tang 1975, Andrews and Moss 1993). This is consistent with the terminology in reliability theory where the hazard function for a Poisson process is the mean occurrence rate of failures, or, more generally, of some event of concern (Andrews and Moss 1993). For seismic hazards, the mean occurrence rate λ_{IM} is usually specified in units of per year and is often called simply the *annual frequency* of the events of interest, although strictly speaking it is the *mean annual frequency*. It is perhaps preferable to use the terminology *mean annual rate* since frequency is used with other meanings in earthquake engineering and seismology.

In seismic hazard analysis, the probability of IM exceeding a threshold im over a specified time period is of particular interest. This is usually derived based on a Poisson model (Cornell 1986; Kramer 1996):

$$P[N = n | t] = \frac{(\lambda t)^n e^{-\lambda t}}{n!}, \quad (2.3)$$

where N represents the uncertain number of occurrences of a specified type of event during a specified time duration, t , and λ represents the mean rate of occurrence of such events. The probability that at least one such event will occur over time t is given by:

$$\begin{aligned} P[N \geq 1 | t] &= 1 - P[N = 0 | t] \\ &= 1 - e^{-\lambda t}. \end{aligned} \quad (2.4)$$

The probability that at least one seismic event of interest will occur over time t which has $IM \geq im$ is therefore:

$$\begin{aligned} H_{IM}(im | t) &= P[IM \geq im | t] \\ &= 1 - e^{-\nu_{IM}(im)t} \\ &\approx \nu_{IM}(im)t, \text{ for small } \nu_{IM}(im)t, \end{aligned} \quad (2.5)$$

which is often called the *hazard curve* for the time duration, t (Cornell 1996). However, in the literature on seismic hazard, the same terminology is also often applied to the hazard (rate) function in Equation (2.2), sometimes being used for the two different concepts in the same publication, especially when $t=1$ in Equation (2.5). This sloppiness in the terminology is presumably encouraged by the result that the annual probability of exceedance as a function of IM is well approximated by the mean rate of exceedance as a function of IM for all but very low values of IM , as shown by Equation (2.5) with $t=1$ and ν_{IM} small.

The probabilistic seismic hazard analysis in the PEER benchmark project was conducted for seven hazard levels, considering several sources of modeling uncertainty (details of this are given in Haselton et al., 2007). The mean hazard spectra for these seven levels are given in Figure 2.7. The IM chosen for the benchmark study is the 5% damped spectral acceleration at the building's first mode period, $S_a(T_1=1 \text{ sec})$.⁵ When selecting appropriate ground-motion records for each hazard level, the parameter ε ("epsilon") is considered, which is a period-dependent quantity that measures the normalized offset of spectral acceleration at a given period from the median that is expected from ground-motion prediction equations (Goulet et al. 2006). Baker and Cornell (2005) have shown that ε can have a great effect on structural response because it is a measure of spectral shape; these authors also show that ε has a greater effect on structural response than distance or magnitude. Additionally, Goulet et al. (2006) have shown that the building's collapse capacity is sensitive to ε . Therefore, representative suites of ground motions were selected to match target values of magnitude and distance that had appropriate values of ε for each

⁵ The computed fundamental periods of the seven designs range from 0.53 sec to 1.25 sec (Goulet et al., 2007).

hazard level. The records were selected based on the geometric mean of the two horizontal components, and so that they require a scale factor of 5.0 or less to match the target value of $S_a(T_1=1\text{sec})$. Further details of the probabilistic seismic hazard analysis and of the ground-motion record-selection procedure are available in Goulet et al. (2007).

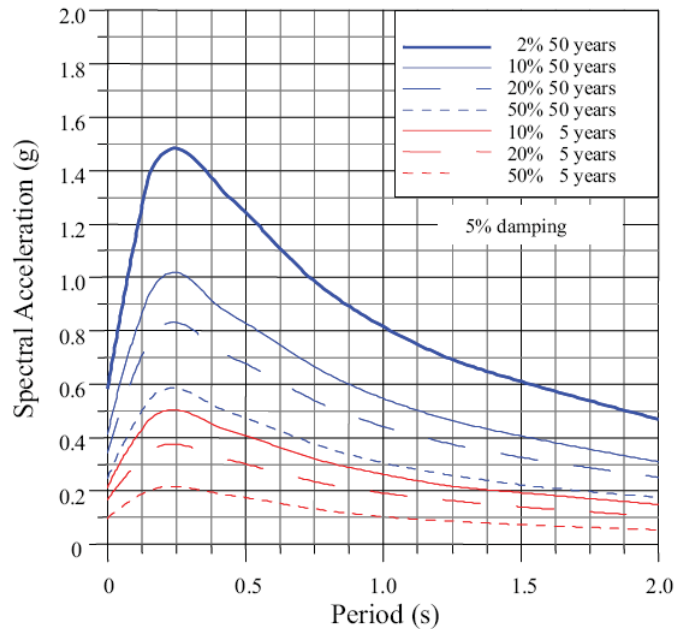


Figure 2.7 Mean uniform hazard spectra (5% damping) for the LA Bulk Mail site for seven hazard levels (reproduced from Goulet et al., 2006). The spectral acceleration at $T=1$ sec is used for the benchmark study, so the hazard levels shown in this plot correspond to $S_a(T=1 \text{ sec}) = 0.10 \text{ g}, 0.19 \text{ g}, 0.26 \text{ g}, 0.30 \text{ g}, 0.44 \text{ g}, 0.55 \text{ g}, 0.82 \text{ g}$.

2.4 PEER benchmark structural analysis

It is imperative that the structural model is accurate for low- and high-level ground motions. As mentioned earlier, the damage that occurs in low-level ground motions that are more frequent, will substantially contribute to losses (Mitrani-Reiser et al., 2006). Also, the high-level ground motions that are less frequent are of concern for the building's probability of collapse and the overall safety of its occupants (Goulet et al., 2007). There are currently no models that accurately represent structural behavior for the range of hazards considered in the study. Thus, two types of models are used: a fiber model is used

for low intensity levels to capture initial yielding, and a lumped-plasticity model is used for high intensity levels to depict strength and stiffness deterioration and collapse (Haselton et al., 2007). Incremental dynamic analysis, IDA (Vamvatsikos and Cornell 2002), was used to estimate sidesway collapse.

Nonlinear dynamic analyses of the benchmark building were carried out using the OpenSees software described in Section 2.1. A two-dimensional model of a four-bay frame was created for each design variant and analyzed for each horizontal component of ground motion, which is appropriate for the perimeter-frame designs since the orthogonal sets of planar frames are separate from one another (Hall 2003). The structural model for the perimeter-frame designs includes a parallel gravity frame to represent the additional contribution to stiffness and strength from the gravity system. Additionally, a “leaning column” is included in these models to account for the P-Delta effects that come from the gravity loads tributary to the gravity system (Haselton et al., 2007). This two-dimensional model ignores the biaxial behavior of the columns in the space-frame designs, and so they were designed only for flexural demands in one direction. The following section describes the combination strategy of the structural responses for both directions that is later used in the damage analysis.

Additionally, static pushover analyses were performed to examine the general load-deflection relationship for the benchmark building. This was used to compare the results of various models (i.e., the fiber lumped-plasticity models). Figure 2.8 shows the results of the static pushover of three models for the baseline perimeter-frame design (Design A). The pushover curves in this figure illustrate that the fiber model is less numerically stable than the lumped-plasticity models, and it stops converging at 3% roof drift. Also, the lumped-plasticity models are capable of capturing the strain softening behavior that the fiber model can not.

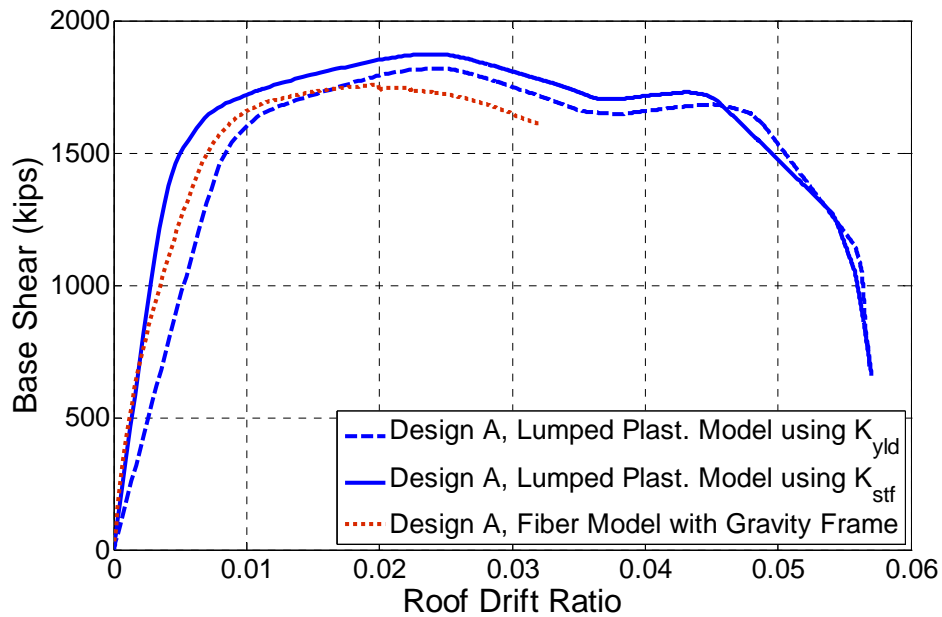


Figure 2.8 Static pushover curves for the fiber and lumped-plasticity models of one design variant (Design A) of the benchmark building, reproduced from Goulet et al. (2007).

2.4.1 Three-dimensional considerations

Although the perimeter-frame and space-frame designs both have 4 bays in the N-S and 6 bays in the E-W directions, the space-frame design has additional moment-frame structural members to consider in the loss analysis. These members include the beams in the exterior bays in the E-W direction and all the interior beams and columns of the building. For simplicity, the benchmark building was designed only in the N-S direction and similar structural behavior is assumed in the E-W direction (i.e., it is assumed to have similar strength and stiffness as the N-S direction). This is a realistic assumption for strength since practitioners would likely reduce element strengths in the E-W direction to benefit from the additional bays; the assumption for stiffness is acceptable as well since the building-code stiffness requirements do not control the design.

Using the above assumptions, the same four-bay frame model is used to represent the behavior in both the N-S and E-W directions for both the perimeter-frame and space-frame designs. The behavior of the extra members in the 6-bay E-W space frame is extrapolated from the structural analysis of the 4-bay N-S frame. We assume that the interior beams and columns adjacent to one another will have similar levels of damage. Thus the *EDPs* for interior beams and columns from the four-bay structural model are replicated for the additional bays, as shown below in Figure 2.9.

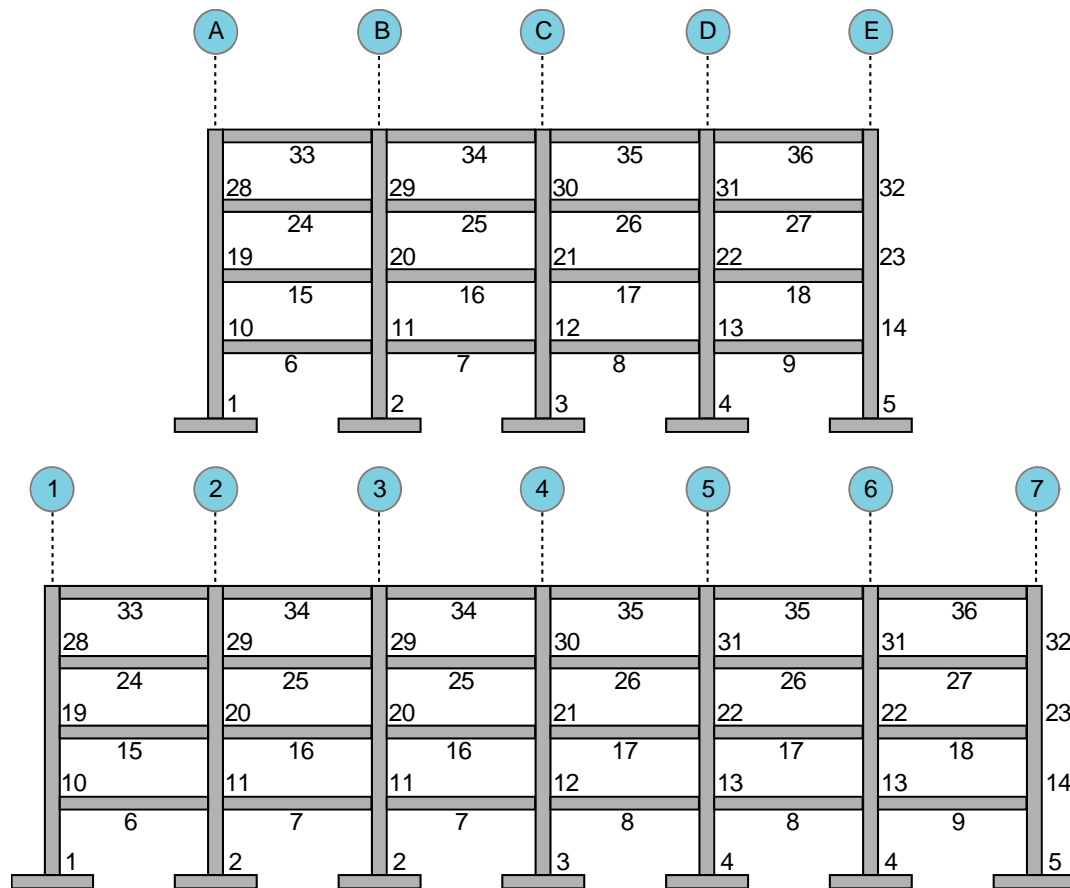


Figure 2.9 *EDP* numbering for structural components in the N-S and E-W directions.

The column members in the space-frame design are common to the lateral resisting frames in the N-S and E-W directions. The question arises then, if the fragility function is expressed in terms of DDI in Equation (3.2) for one direction, how should one combine DDIs corresponding to the same column but in two perpendicular directions? Three possible combinations were considered: simple maximum (DDI is taken as the larger of the

two directions), absolute sum (DDI is taken as the sum of the DDIs from the two directions), and square root of the sum of the squares (SRSS). These are shown graphically in Figure 2.10 and are given by:

$$\begin{aligned} DDI_{SM} &= \max(DDI_i, DDI_j) , \\ DDI_{AS} &= DDI_i + DDI_j , \\ DDI_{SRSS} &= \sqrt{(DDI_i^2 + DDI_j^2)} . \end{aligned} \quad (2.6)$$

In the figure, points along each line have the same combined DDI=1.

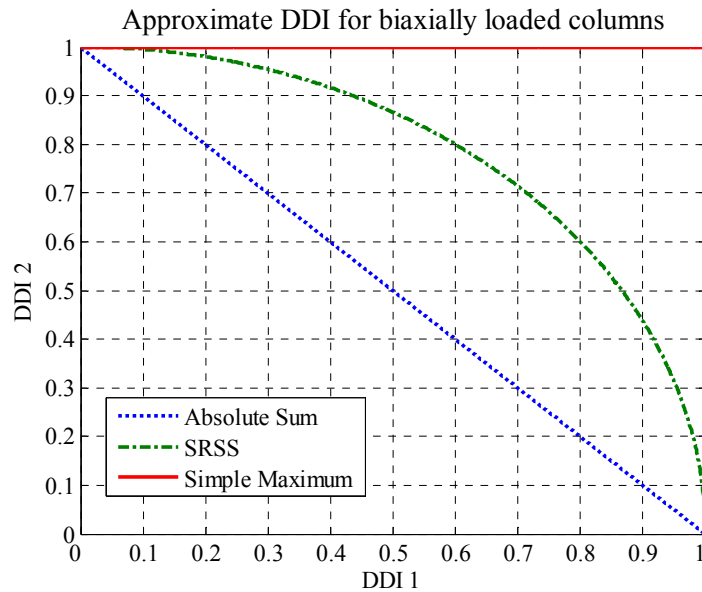


Figure 2.10 Combinations for *DDI* for biaxially loaded columns.

The ACI Design Handbook for columns was consulted to determine which combination of DDI would be most appropriate to estimate the damage of the columns (ACI 1990). Figure 2.11 is from the ACI Handbook and shows the biaxial moment relationship for a number of values of the biaxial bending constant. The biaxial bending design constant, $\beta = 0.5$, $\beta = 0.7071$, and $\beta = 1.0$ respectively correspond to the absolute sum, the SRSS and the simple maximum curves of Figure 2.10. The value of β depends on the design and nominal axial loads, the material and the geometric properties of the columns. Based on these criteria, the values of β range from 0.58 to 0.73 for the columns of the benchmark building. Thus,

SRSS is a reasonable method to combine the *DDI* values of the N-S and E-W directions of the columns and was used in this study.

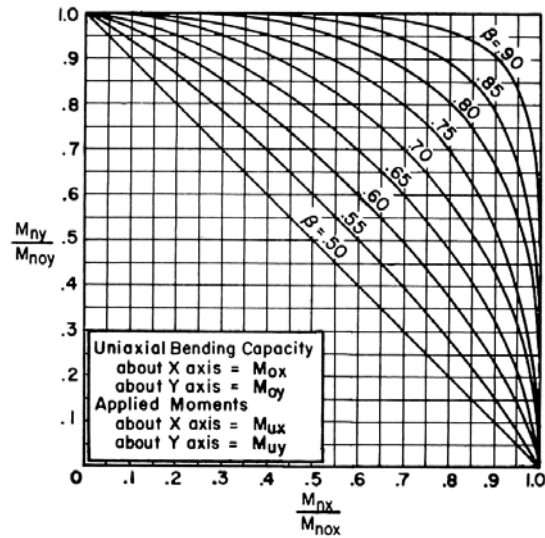


Figure 2.11 Biaxial moment relationship for columns (reproduced from ACI 1990).

2.5 MDLA toolbox

The modular framework of the PEER methodology allows for straightforward software development. The MATLAB damage and loss analysis toolbox (MDLA) was created as part of the PEER benchmark study, as an implementation of the damage and loss analyses portions of the PEER methodology. The input and output parameters for the program are shown graphically in Figure 2.12. The inputs for the toolbox are: a database of fragility and cost distribution functions, a table of the damageable components of the benchmark building, and the hazard and structural analysis results. The outputs of the toolbox are the probability of exceedance of damage states for all damageable components in the structure and the *DVs* for the PEER methodology. The *DVs* considered in this study are the repair costs to restore the building to an undamaged state, collapse probabilities, building safety tagging, and losses due to downtime and fatalities.

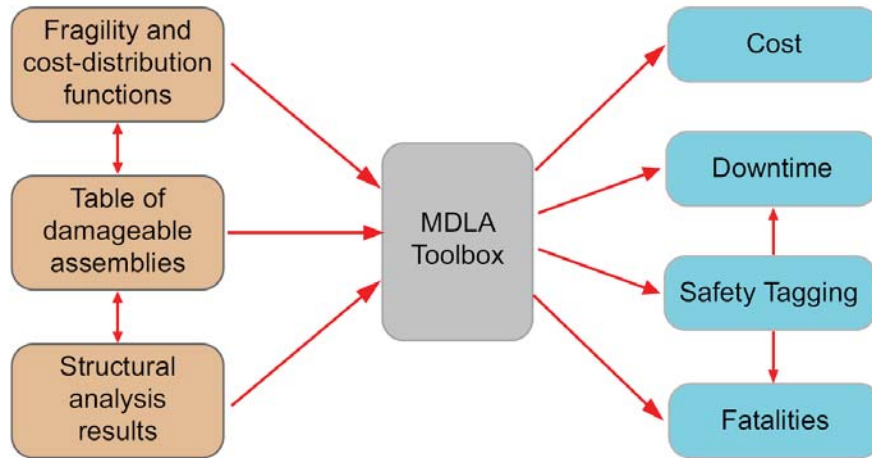


Figure 2.12 Input and output parameters for the MDLA toolbox.

2.5.1 MDLA input: Table of damageable assemblies

The table of damageable assemblies is created by itemizing the components in a building that may contribute to earthquake losses. These tables are given in Section 2.2.4 (Table 2.3 and Table 2.4) for the perimeter-frame and space-frame benchmark designs. The building's damageable components are described using five categories: assembly type, assembly description, location, unit, and quantity. The assembly type is a unique identifying number for each component type. The taxonomy of building components used in this study was introduced by Porter (2000) and is based on the RS Means numbering format (RS Means, Corp., 2001). The assembly description simply describes each unique damageable component in the building. The location number indicates the floor or story level where the components are located in the building. The unit of a damageable building component varies with assembly type and depends on the component's fragility function used in the damage analysis. Finally, the quantity of components is used for bookkeeping purposes in the damage and loss analyses, to account for damage to all components of the same type.

2.5.2 MDLA input: Table of fragility and cost distribution functions

The table of damageable assemblies is used by the MDLA toolbox to select the fragility and cost-distribution functions from a library of available functions, for use in the damage and loss analyses. This library of functions is internal to the toolbox, but can be edited as new ones become available. The parameters of the fragility and the unit-repair-cost functions that are used in this study are summarized in Table 2.5. Since these functions are implemented as lognormal distributions, the required parameters are the median (x_m) and the logarithmic standard deviation (β).

2.5.3 MDLA input: Structural analysis results

The structural analysis step of the PEER PBEE methodology results in structural responses, or *EDPs*. The lognormal distribution is often used by researchers (e.g., Miranda and Aslani 2003) to fit structural analysis data. Figure 2.13 shows the empirical cumulative distribution functions (*cdf*) from the raw data for peak roof acceleration of Design A in the EW-direction for four *IM* levels, and the corresponding fitted lognormal *cdf*s. The fit of the lognormal *cdf* to the empirical *cdf* is very good considering that only two parameters have been adjusted based on the data. The lognormal fits performed by the MDLA toolbox pass the Kolomogorov-Smirnov and Lilliefors goodness-of-fit tests (Massey 1951; Miller 1956; Lilliefors 1967) at the 1% level of significance.

There are 60 *EDPs* of interest identified for the perimeter-frame structural model based on the table of damageable assemblies in and Table 2.2. These include 4 peak diaphragm accelerations (one per floor), 20 peak transient drifts (one per story and column line), and 36 deformation damage indices (one per structural member). There are 84 *EDPs* of interest identified for the space-frame structural model. These include 4 peak diaphragm accelerations (one per floor), 28 peak transient drifts (one per story and column line), and 52 deformation damage indices (one per structural member).

Table 2.5 Summary of assembly fragility and cost distribution parameters.

Assembly Description	Unit	Damage State	Fragility Parameters		Repair Cost Parameters	
			x_m	β	x_m (\$)	β
Ductile CIP RC beams	ea	Light	0.08	1.36	8,000	0.42
Ductile CIP RC beams	ea	Moderate	0.31	0.89	22,500	0.40
Ductile CIP RC beams	ea	Severe	0.71	0.80	34,300	0.37
Ductile CIP RC beams	ea	Collapse	1.28	0.74	34,300	0.37
Ductile CIP RC columns	ea	Light	0.08	1.36	8,000	0.42
Ductile CIP RC columns	ea	Moderate	0.31	0.89	22,500	0.40
Ductile CIP RC columns	ea	Severe	0.71	0.80	34,300	0.37
Ductile CIP RC columns	ea	Collapse	1.28	0.74	34,300	0.37
Column-slab connections	ea	Light cracking	0.0030	0.40	35	0.20
Column-slab connections	ea	Severe cracking	0.0100	0.30	435	0.20
Column-slab connections	ea	Punching shear failure	0.0045	0.60	3,273	0.20
Drywall partition	64 ft ²	Visible	0.0039	0.17	88	0.20
Drywall partition	64 ft ²	Significant	0.0085	0.23	525	0.20
Drywall finish	64 ft ²	Visible	0.0039	0.17	88	0.20
Drywall finish	64 ft ²	Significant	0.0085	0.23	253	0.20
Exterior glazing	pane	Crack	0.040	0.36	439	0.26
Exterior glazing	pane	Fallout	0.046	0.33	439	0.26
Acoustical ceiling	ft ²	Collapse	$92/(l+w)$	0.81	2.21*A	0.50
Automatic sprinklers	12 ft	Fracture	32	1.40	900	0.50
Hydraulic elevators	ea	Failure	0.41	0.28	5,000	1.00

l = room length; w = room width; A = room area

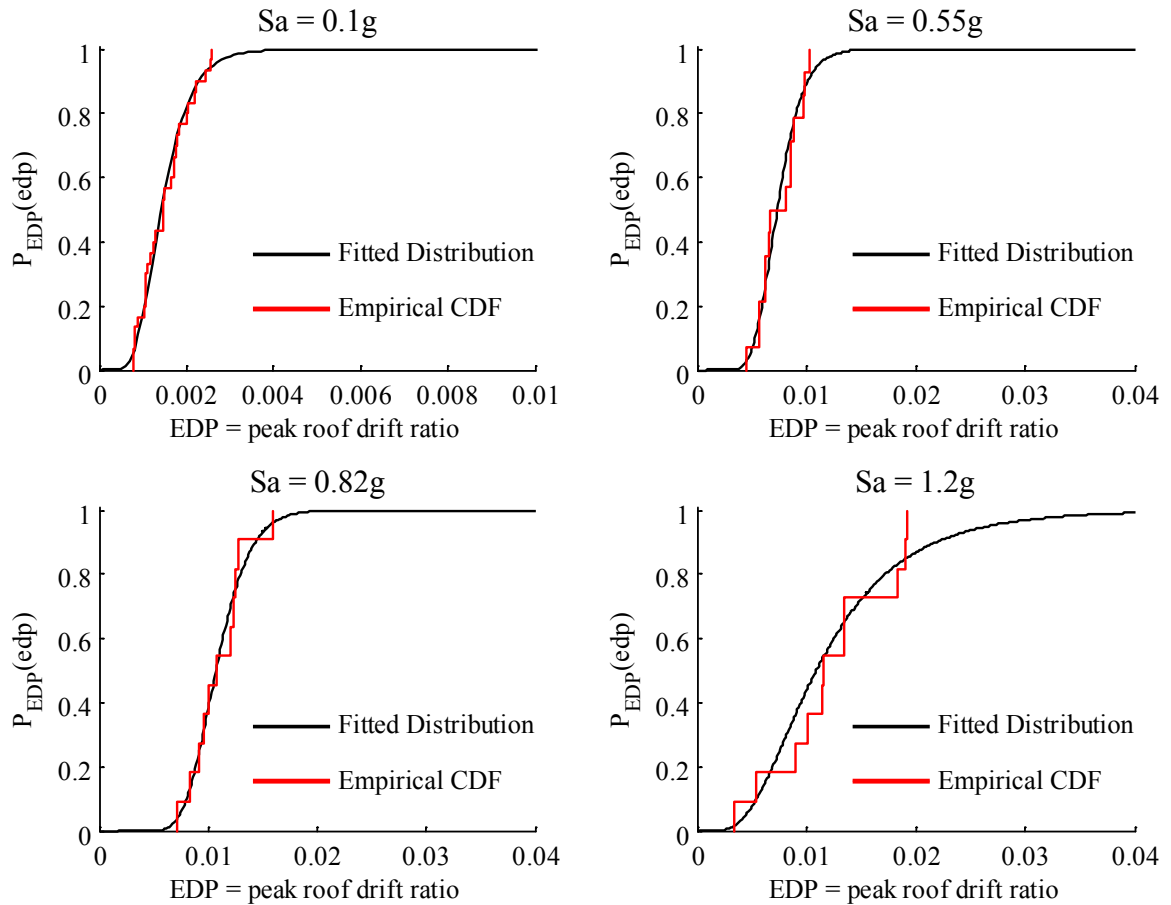


Figure 2.13 Fitted and empirical cumulative distribution functions of peak roof drift ratio (EW-dir) results for four levels of IM .

2.5.4 Program architecture

The flowchart for the MATLAB Damage and Loss Analysis (MDLA) toolbox is shown in Figure 2.14, which identifies the key modules of the software and the connections between these modules. The modularity of this program reflects the modularity of the PEER PBEE methodology. The umbrella module, “ANL_main” organizes the structural analysis results, extracts the fragility and cost-distribution function parameters of interest, fits the lognormal distributions to the calculated EDP data, calls the damage and loss analysis module, and calculates the repair costs moments. The “extract_EDP_matrix” module formats the structural responses and extracts vectors of EDP data for each structural simulation. The “generate_frag_cost_params” module chooses fragility and cost-distribution function

parameters of interest from an internal library. The “Loss_Analysis” module performs the damage and loss analyses, as outlined in Chapter 3, Chapter 5 and Chapter 6; results from this module are also found in these chapters. The “rc_moments” module computes the first four non-central moments of unit repair cost. The “generate_logn_pdf_params” module fits lognormal distributions to the raw *EDP* data. The “Loss_Analysis” module calls two other functions: “failure_prob” and “discrete_simpson.” The “failure_prob” module determines the failure probability, or the probability that the i^{th} assembly is in damage state j . The “discrete_simpson” module performs numerical integration, using Simpson’s method.

2.5.5 Program output

Results of the damage and loss analyses for the PEER benchmark study are presented in Chapter 3 through Chapter 6. These results include the average probability of damage for the mean design variants, the mean and variance of repair costs at each hazard level, the repair-cost vulnerability functions, the expected annual losses, the probability of safety tagging and associated downtime for damage assessments and repairs, the probability of fatalities and the mean losses associated with these deaths, and some modeling and design comparisons of the various design and modeling variants of the benchmark building.

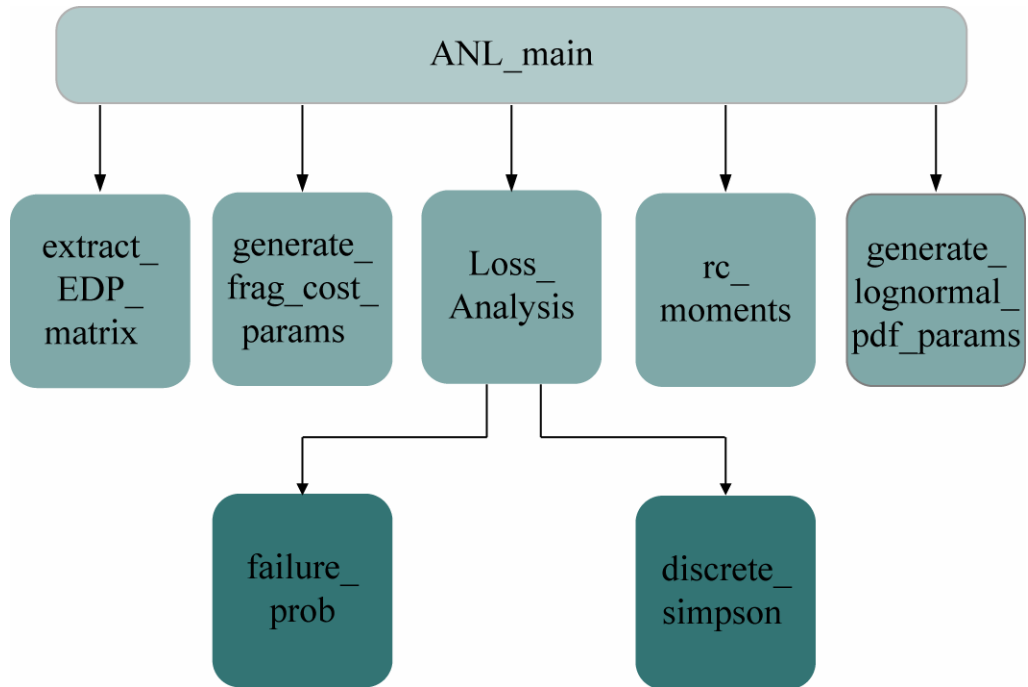


Figure 2.14 Schematic of MDLA toolbox.

CHAPTER 3

Damage Estimation

The probability of damage for each damageable component in the benchmark building is estimated using the MDLA toolbox; this is the intermediate analytical step necessary for subsequent determination of building losses given the structural analysis results. This chapter describes the methodology used for damage analysis of the structural and nonstructural building components considered to significantly contribute to overall building losses. The engineering demand parameters (EDPs) used for each of these components is identified, along with the considered damage states and associated repair efforts. The fragility functions used in the damage estimation, which describe the probability of the components being in or exceeding the described damage states, are mostly taken from Porter's comprehensive work on the assembly-based vulnerability methodology (2000). The per-story average probabilities of damage for the moment-frame elements and the wallboard partitions in all the benchmark building variants are presented at the conclusion of the chapter.

3.1 Procedure for damage analysis

The structural analysis results are input to component fragility functions to compute the probability of reaching or exceeding damage state j , for a component of type i , conditioned on the structure not collapsing and on IM :

$$P[DM_{ij} | NC, im] = \int_{edp_i} P[DM_{ij} | edp_i] p(edp_i | NC, im) dedp_i \quad (3.1)$$

The first component of the integrand, $P[DM_{ij} | edp_i]$, is the probability of reaching or exceeding the damage state j for a given building component, conditioned on $EDP i$ appropriate for component of type i (this probability comes directly from the corresponding fragility function). The second component of the integrand, $p(edp_i | NC, im)$, is the probability density of $EDP i$, conditioned on the structure not collapsing (NC) and on a given IM level. To evaluate this component, a lognormal distribution is fit to the structural response data, as is done by other researchers (e.g., Miranda and Aslani 2003). The probability of collapse given IM is also estimated as part of the structural analysis results by taking the fraction of structural analyses for that IM that give excessive sidesway motions.

3.2 Fragility functions for benchmark study

Fragility and cost distribution functions are created using experimental data, earthquake experience, analysis, expert opinion, or some combination of these. A review of loss estimation research shows that lognormal distributions are commonly used for fragility functions (e.g., Kennedy and Ravindra 1984, Beck et al 2002, Aslani and Miranda 2004) and are reasonable to use for repair-cost distribution functions (e.g., Porter 2000). To fully describe a lognormal distribution, the median and logarithmic standard deviation are needed. Therefore, the median capacity and logarithmic standard deviations of capacity (defined as the EDP value that causes an assembly to reach or exceed a given damage state) are used to create the fragility functions, and then to estimate damage. Also, the corresponding median unit repair costs and logarithmic standard deviations of cost are used to create the cost distribution functions, to estimate the repair cost.

3.2.1 Beams and columns

Various damage indices are used to quantify damage of reinforced-concrete (RC) structural members. Williams et al. (1997) studied eight damage indices for concrete elements, using data from cyclic tests of beams and beam-column joints under combined shear and flexure. These authors introduce five damage states, shown in Table 7.1. They demonstrate that three indices: a modified Park-Ang Damage Index (*PADI*), ductility, and modified stiffness ratio, are consistently reliable indicators of severe damage to the beam and joint. They also show that the damage indices that most accurately represent the development of damage throughout the experiments are a modified PADI, ductility, a modified stiffness ratio, and an index calculated from increments in the plastic displacement. They conclude that the more sophisticated indices that take into account the damage caused by repeated cycling gave no more reliable information of damage than the simpler indices such as ductility and stiffness degradation.

Table 3.1 Williams et al. (1997) damage states and consequences for concrete columns.

Damage State	Visible Damage	Likely Consequences
None	None or small number of light cracks, either flexural (90°) or shear (45°).	No loss of use or structural repair needed.
Light	Widespread light cracking; or a few cracks > 1mm; or light shear cracks tending to flatten toward 30°.	Only minimal loss of use, possible some minor repair needed to restore structure to its design strength.
Moderate	Significant cracking, e.g. 90° cracks > 2mm; 45° cracks > 2mm; 30° cracks > 1mm.	Structure closed for several weeks for major repairs.
Severe	Very large flexure or shear cracks, usually accompanied by limited spalling of cover concrete.	Structure damaged beyond repair and must be demolished.
Collapse	Very severe cracking and spalling of concrete; buckling, kinking or fracture of rebar.	Structure has completely or partially collapsed.

The modified PADI was first introduced with the release of IDARC Version 3.0, a computer program created for the inelastic damage analysis of reinforced concrete structures (Kunnath et al. 1992):

$$PADI = \frac{\Phi_m - \Phi_r}{\Phi_u - \Phi_r} + \beta \left(\frac{A_t}{\Phi_u M_y} \right) \quad (3.1)$$

where

Φ_m = maximum curvature attained during seismic loading,

Φ_u = curvature associated with nominal ultimate moment capacity of the section,

Φ_r = recoverable curvature at unloading,

β = strength deterioration parameter,

A_t = total area contained in M- Φ loops,

M_y = yield moment of section.

This version of the software was heavily modified for a NIST study on the seismic performance of circular bridge columns designed in accordance with AASHTO/CALTRANS standards (Stone and Taylor 1993). Stone and Taylor (1993) examined 82 spiral-reinforced bridge piers to estimate the threshold damage indices for yield, ultimate, and failure damage states. These damage states are described in more detail in Table 3.2. These authors suggest that because the modified PADI is in non-dimensional format, comparisons may be made between columns of different sizes and of different loading histories.

Table 3.2 Stone and Taylor (1993) damage states and consequences for concrete columns.

Damage State	Likely Consequences
None	Light cracking may have occurred without compromising serviceability.
Repairable	Member has yielded and extensive spalling may have occurred. Inherent stiffness remains and member will likely need repair, not replacement.
Demolish	Member loaded beyond ultimate load, and will likely fail in another severe seismic event.
Collapse	Member has completely failed, implying additional collapse in structural system.

The above-mentioned studies (Williams et al. 1997; Stone and Taylor 1993), and the a study by Williams and Sexsmith (1997) give clear definitions of damage states for reinforced concrete flexural members and appropriate empirical data to develop fragility functions (Beck et al. 2002). The fragility functions shown in Figure 3.1 were developed by Beck et al. (2002), and are used here to relate *EDP* values from the structural analysis to probabilities of exceeding each level of damage. These authors chose to use the deformation damage index (*DDI*) portion of the modified *PADI* in Equation (3.1) ($\beta = 0$), as the *EDP* for the fragility functions. Because rotation was a more readily available *EDP* from the present structural analyses, we assume that curvature is constant over the plastic hinge length, and use *DDI* in terms of chord rotations:

$$DDI = \frac{\Phi_m - \Phi_r}{\Phi_u - \Phi_r} = \frac{(\theta_m - \theta_r)/L_p}{(\theta_u - \theta_r)/L_p} = \frac{\theta_{p_transient}}{\theta_u - \theta_r}, \quad (3.2)$$

where

θ_m = maximum hinge rotation attained during seismic loading,

θ_u = ultimate hinge rotation that is limited by hoop fracture or rebar buckling, and calculated from Fardis (2003),

θ_r = recoverable rotation at unloading,

L_p = plastic hinge length,

$\theta_{p_transient} (\theta_m - \theta_r)$ = peak transient plastic hinge rotation.

Beck et al. (2002) note that there is no consensus among researchers about the value for β in the energy term of $PADI$, and that in some cases this term might even have negative values. This and the lack of consistent data motivated us to use the fragility functions developed in Beck et al. (2002). Since the initiation of this study, the PEER Structural Performance Database of over 400 cyclic, lateral-load tests of reinforced concrete columns has been made available to researchers via the World Wide Web (Berry et al. 2004). It would be beneficial in future work to create fragility functions from this database, and compare the loss results to those presented here.

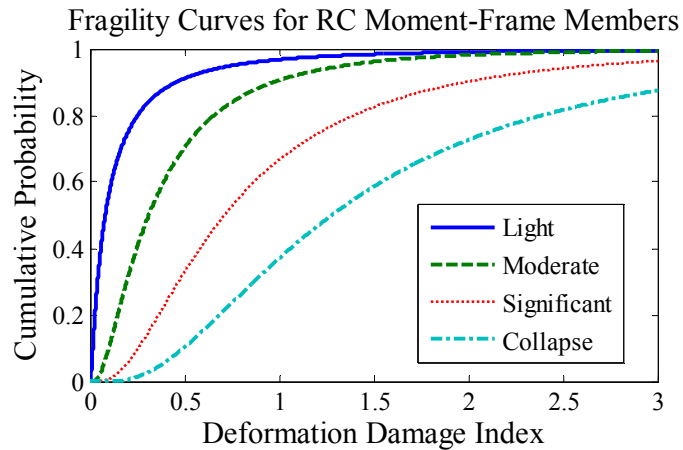


Figure 3.1 Fragility functions for RC moment-frame members.

Each level of damage in Figure 3.1 corresponds to a specific repair effort. Beck et al. (2002) considered a variety of repair methods available to restore damaged concrete elements to an undamaged state: epoxy injection, replacement of damaged concrete, interior reinforcing, exterior reinforcing by reinforced-concrete jacketing, exterior reinforcing by steel jacketing, exterior reinforcing by steel bracing, combined methods, fiber-reinforced polymers jacketing, and infill walls and wing walls. Based on their review of the use of these repair methods in industry, Beck et al. (2002) proposed the following repair efforts for the damage states considered in their fragility curves: the light damage state is repaired by epoxy injection; the moderate damage state corresponds to a jacketed repair; and the severe and collapse damage states correspond to replacement of the member. Note that no damage is also a damage state, known as “none”. These researchers

used professional cost estimators to calculate repair costs. The details of this evaluation are available in their report (Beck et al. 2002); the results used in this study are summarized in Table 2.5. Note that a few years have passed since the repair costs were estimated, and inflation is taken into account through the an inflation factor, C_i .

3.2.2 Column-slab connections

The fragility and repair of slab-column connections may depend on a number of parameters. Experimental results of column-slab damage reported by researchers (Aslani 2005, Kang et al., 2006) were used to develop the fragility functions for this study, shown in Figure 3.2. The associated repair cost distributions were developed based on the recommendations of a professional cost estimator. The fragility functions relate the peak interstory drift ratio (but calculated as the average of peak transient interstory drift ratio in stories above and below the slab) to the probabilities of reaching or exceeding the following three damage states: (1) a “light cracking” damage state that is repaired using a surface coating of the affected area, (2) a “severe cracking” damage state that corresponds to epoxy injection repair of the affected area, and (3) a “punching shear (without collapse)” damage state that corresponds to replacing the concrete in the slab surface. The maximum value of IDR in either orthogonal direction (i.e., from the governing ground motion component) is the EDP chosen to estimate the damage of the column-slab connections. The details of the development of these fragility and cost distribution functions is given in Haselton et al. (2007) and summarized in Table 2.5.

Beam-column joint fragility is not included in the present study, but the omission is not judged to make a material difference in the loss estimate for this building because the structural analyses showed that the rotations in the joints are very small. This is consistent with modern capacity design requirements that force damage to occur in adjacent columns and beams rather than in the joints. Furthermore, even if there is some damage in the joints, it is reasonable to expect that this damage would be less severe than that of the adjacent beam. Additionally, Brown and Lowes (2007) compiled results from 45 conforming beam-

column connection tests and found that none exhibited damage requiring joint replacement. This suggests that the damage will be relatively greater in the adjacent columns and beams, as compared to the joint itself.

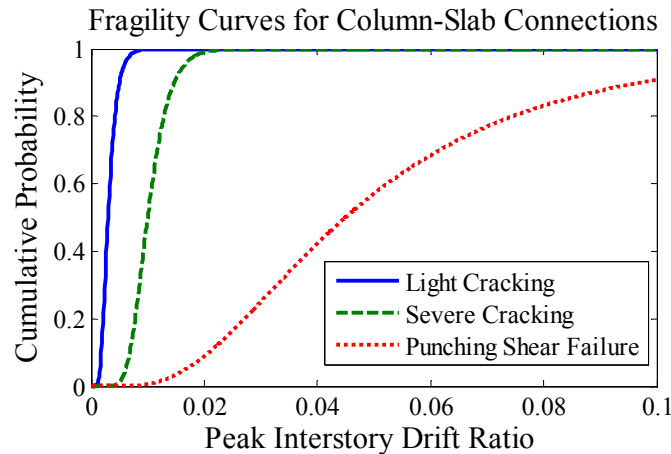


Figure 3.2 Fragility functions for column-slab connections.

3.2.3 Drywall partitions and finish

Interior full-height non-fire-rated walls of the benchmark building use a single layer of 5/8" gypsum wallboard fixed with drywall screws to 3 5/8" metal studs with fixed (rather than sliding) top plates. Fire-rated walls (2 hr rating at elevator shafts and stairwells) use multiple layers of wallboard. These additional layers make the walls stiffer and more resistant to interstory displacements (Pardoen et al. 2000). Therefore, these walls are considered to be robust and are not included in the loss analysis. Modular office furniture is used for partial-height partitions, which are assumed to be anchored to the slab and thus rugged (not damageable) and therefore excluded from the damage and loss analysis.

The drywall partitions considered for the benchmark office building are 5/8" wallboard partitions on 3 5/8" metal stud with screw fasteners. The *EDP* used for the drywall partitions and finish is the peak transient drift ratio (*PTDR*). The fragility curves, shown in Figure 3.3, were developed by Porter (2000) and are based on Rihal's (1982) in-plane racking tests of 8' × 8' building partitions. These fragility functions are used to relate the

PTDR values from the structural analysis to probabilities of exceeding the two levels of damage: visible and significant.

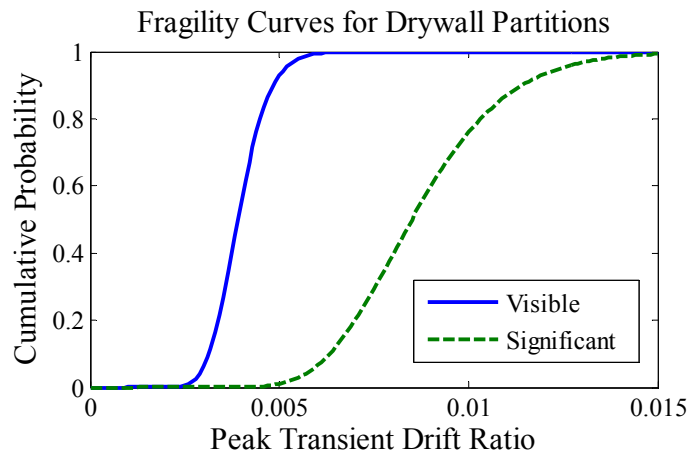


Figure 3.3 Fragility functions for the wallboard partitions.

Visible damage is repaired by patching cracks and possibly cutting out damaged pieces of wallboard and replacing them, then applying joint tape and joint compound (often called mud) to the cracks or seams, sanding, and repainting. Significant damage is repaired by demolishing and replacing the partition. Interior partitions with gypsum wallboard on both sides are treated as two separate assemblies: one that includes the framing and gypsum wallboard on one side, the other includes only the gypsum wallboard finish on the other side. Again, the cost associated with the repair effort to return the damaged wallboard partitions and finish to an undamaged state was calculated by professional cost estimators in Beck et al. (2002). The results used in this study are summarized in Table 2.5. Inflation is again taken into account through the inflation factor, C_i .

3.2.4 Interior paint

Researchers have shown that interior paint has a considerable contribution to the total repair costs of a damaged structure, especially for low levels of shaking (Beck et al. 2000). These researchers used a line-of-sight method to account for the needed interior painting of a damaged structure. This line-of-sight method assumes that damage on any wall of a room

or hallway that requires repainting leads to the repainting of that entire room or hallway. Thus, they consider the need for owners to repaint areas that are not damaged, to achieve a reasonable uniform appearance. This approach works in a Monte Carlo simulation but not when using FOSM (a first-order second-moment method used to estimate uncertainty) or the direct probability approach used in this work, so for present purposes an approximation is required. We propose a simplified formula for calculating the mean area requiring a fresh coat of paint:

$$ATP = DA + UA \cdot P(\text{paint } UA | DA) \quad (3.3)$$

where ATP = mean area to paint, DA = damaged area, UA = undamaged area, and $P(\text{paint } UA | DA)$ = probability of needing to paint an entire floor as a function of the damaged area of wallboard partitions on the same floor.

The fragility function in Figure 3.4 shows the cumulative lognormal distribution of painting an entire floor, based on the ratio of damaged area to total area of wallboard partitions on the same floor. The shape of this distribution, dictated by the median ($x_m = 0.25$) and the logarithmic standard deviation ($\beta = 0.5$), is based on our own judgment of the owner's tipping point to paint an entire floor based on the known damaged area. The cost associated with interior painting was calculated by professional cost estimators in Beck et al. (2002). The median and logarithmic standard deviation of cost to paint one square foot of interior wall space is \$1.52 and 0.2, respectively. Again, inflation is taken into account through the inflation factor, C_i .

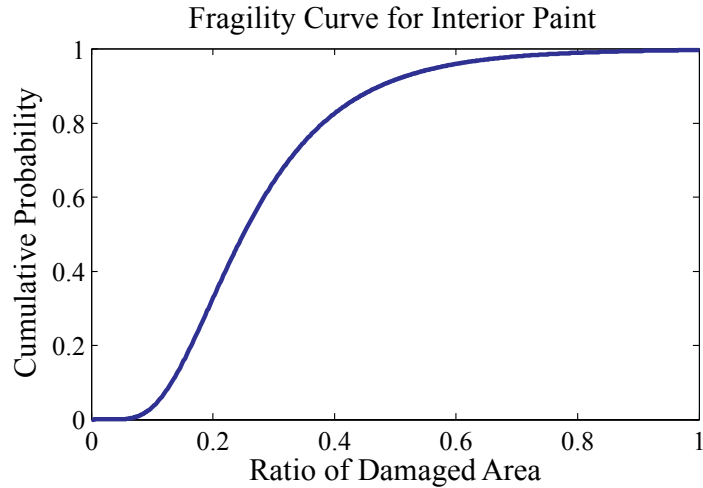


Figure 3.4 Fragility function for interior paint.

3.2.5 Exterior glazing

The exterior cladding system is composed of $5' \times 6'$ architectural glass assemblies with aluminum framing. A total of 1,060 glass assemblies make up the cladding for the benchmark building. We used a fragility function for a particular type of glazing system (Horizon Wall glazing) as documented by Porter (2000) and shown in Figure 3.5. The *EDP* for the exterior glazing is the peak interstory drift ratio. The fragility functions developed by Porter (2000) are based on Behr and Worrell's (1998) laboratory test data for in-plane racking capacity of glazing systems. The two damage states identified by Porter for the glazing (cracked and fallout damage) require replacing the damaged glass pane.

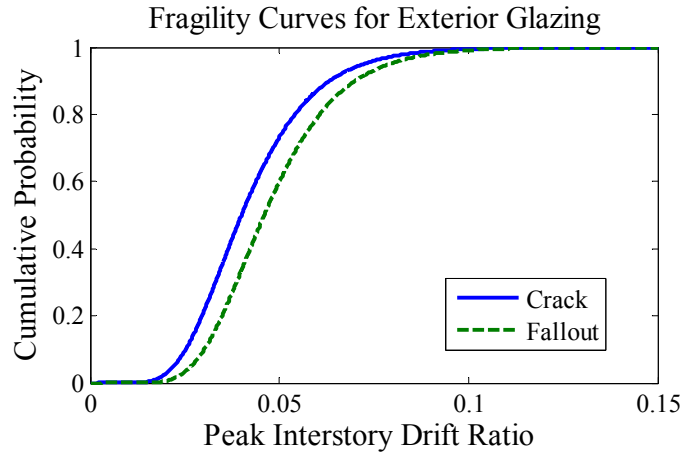


Figure 3.5 Fragility functions for exterior glazing.

3.2.6 Ceiling

The ceiling of the benchmark building consists of a grid-work of aluminum channels in the shape of an upside-down “T,” connected to the diaphragm above with splay wires that, in theory, provide lateral-force bracing along with vertical compression struts. These channels are in a regularly-spaced pattern made up of a 2’×4’ grid and support lightweight acoustical ceiling tiles. A total of 81,000 square feet of acoustical tiles make up the ceiling for the benchmark building.

The *EDP* used for the acoustical ceilings is the maximum of the peak floor diaphragm accelerations in either orthogonal direction. The collapse fragility of these ceilings depends on the ceiling plan dimensions. The collapse fragility curve shown in Figure 3.6 and associated repair effort to replace the ceiling component was developed by Porter (2000), based on a theoretical approach.

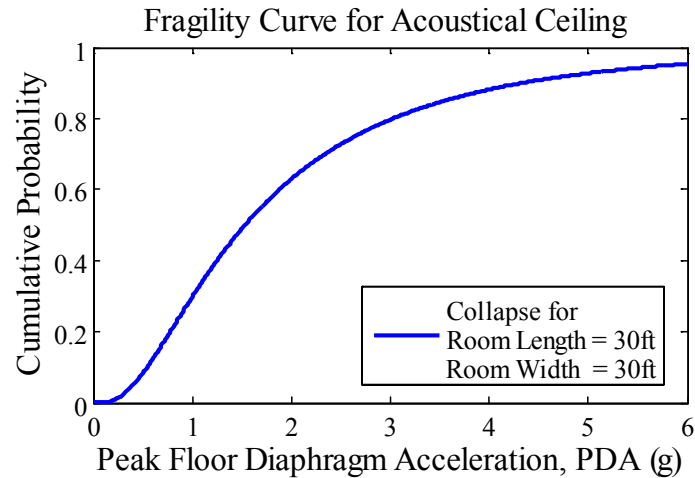


Figure 3.6 Fragility function for acoustical ceiling.

3.2.7 Sprinklers

The benchmark building uses an active fire protection system (or wet automatic sprinklers), shown in Figure 2.5 and Figure 2.6, to protect against damaging fires. Each floor of the benchmark building has an area of 21,600 ft², which is within the allowable range for sprinkler-protected area for office buildings and categorized as “light hazard” according to the *National Fire Protection Association’s Automatic Sprinkler Systems Handbook* (NFPA-13 2002). The area/density approach of the NFPA handbook (NFPA-13 2002) is used to design the sprinkler system. The minimum required area of sprinkler operation for an office building is 1,500 ft² and an area of operation of 2,000 ft² is assumed for the design of the sprinkler system. Assuming that each sprinkler provides 125 ft² of coverage, the hydraulic calculation assumes that a minimum of 16 sprinklers operate simultaneously during a fire emergency. The piping necessary for these requirements is 2,241 linear feet in the first story and 2,418 linear feet for all stories above. The sprinkler pipe weight is supported by hanger rods and the pipes are braced every 12 feet to restrain lateral and longitudinal displacements.

The *EDP* used for the sprinkler is the maximum of the peak floor diaphragm accelerations in either orthogonal direction. The fragility function presented in Figure 3.7 was developed by Porter (2000) and are based on damage data compiled by Sprinkler Fitters U.A. Local

483 (1989). The damage state corresponds to the replacement of 12-foot (3.7m) segment of pipe, and repair or replacement of wetted nonstructural components. A pressurized sprinkler that is fractured during a seismic event will lead to the wetting of exposed nonstructural components near the break of the sprinkler pipe. Since little data exists to determine the fraction of wetted items that should be considered worthless, it is assumed in Porter (2001) that all wetted ceiling tiles must be replaced as well as all wetted computer equipment (2001). In addition, Porter (2001) assumes that repair cost to carpets and wall finishes amounts to 25% of their replacement cost. Therefore, the “fracture” damage state of the braced automatic sprinklers considered for this benchmark building corresponds to pipe replacement as well as the repair or replacement of wetted nonstructural components.

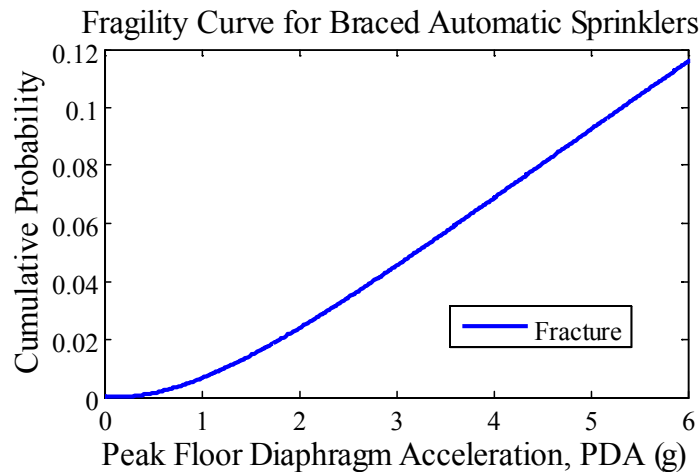


Figure 3.7 Fragility function for braced automatic sprinklers.

3.2.8 Elevators

The benchmark building has two passenger hydraulic elevators that serve all story levels and comply with the 2003 International Building Code (ICC 2003) and the *American Society of Mechanical Engineers Safety Code for Elevators and Escalators* (ASME 2000). Also, the benchmark building abides by the *Americans with Disabilities Act Design Requirements for Accessible Egress* (ADAAG 2002), which requires at least one passenger elevator for private facilities that have more than 3000 square feet per story and that are at least three stories tall. The ADA's requirements for wheelchair access in

elevator cars are as follows: the elevator door must provide 36” minimum width clearance; the width of the elevator car must be a minimum of 80” and the depth of the elevator car must be a minimum of 54” (ADAAG 2002). In fulfillment with these requirements, the dimensions of the elevator cars in the benchmark building are 81” wide and 114” deep.

There is little data available about performance of hydraulic elevators from past seismic events or from experimental studies. Porter (2007) developed the fragility function for hydraulic elevators (reproduced as Figure 3.8 below) based on data collected after the Loma Prieta and Northridge earthquakes. These functions lump several damage scenarios, including “damage to car guide shoes, cab stabilizers, and cab interior, snagged ropes and traveling cables, and failure of equipment anchorage and hydraulic cylinder or piping” (Porter 2007), into the *failure* damage state. The repair effort includes inspection of the elevator and the materials and labor needed to repair the damage (Schiff, 2006), which varies for the above-mentioned scenarios and is reflected by the coefficient of variation of the repair cost given in Table 2.5. The engineering demand parameter used for the fragility function is peak ground acceleration. This is the only case in this study where the *EDP* is independent of the building’s response; the loss associated with elevator damage is equal for all design variants.

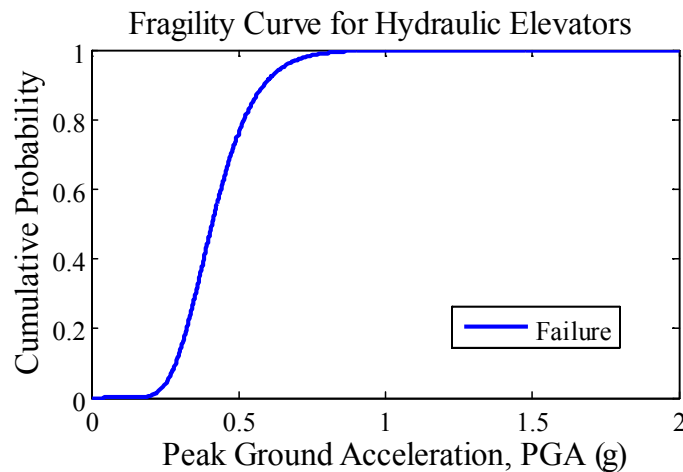


Figure 3.8 Fragility function for hydraulic elevators.

3.3 Damage results for benchmark study

The methodology for calculating the probability of the structural components being damaged is described above in Section 3.1. Some results of the damage analysis step are shown in Figure 3.9-Figure 3.21, showing plots against $IM=S_a$ of the average probability of reaching or exceeding each possible damage state for like components on each story level of the benchmark building. These plots show the average trend of damage of like components along the height of the structure and with increasing intensity level. The damage results can be used to quickly compare various designs and to estimate what will likely control the repair cost in future earthquakes. The designs and models considered are summarized in Table 3.3.

Table 3.3 Summary of benchmark building designs and structural models.

Design	Variant ID	Design and Model Description
A	1	Perimeter frame, designed with expected overstrength; fiber model, concrete tensile strength modeled, gravity frame included.
B	3	Same as Design A, but designed with bare code-minimum strengths; modeled same as VID #1.
C	2	Same as Design A, but designed with uniform beams and columns over height; modeled same as VID #1.
D	9	Same as Design C, but no SCWB provision enforced (not code-conforming); modeled same as VID #1.
E	6	Baseline space frame; fiber model, concrete tensile strength modeled.
A	11	Same as Design A; modeled same as VID #1, but concrete tensile strength and stiffness not modeled.
A	12	Same as Design A; modeled same as VID #1, but gravity frame not modeled.
A	13	Same as Design A; lumped plasticity model with secant stiffness through yield (K_{yld}).
A	14	Same as Design A; lumped plasticity model, with secant stiffness through 60% of yield.
A	15	Same as Design A; lumped plasticity model with secant stiffness through 40% of yield (K_{stf}).

As expected, these figures show that the probability of exceeding each damage state increases with increasing shaking intensity and can be utilized to help predict the location in the building of greatest damage. The greatest damage to the columns (see Figure 3.19) occurs in the first story for all the variants, which is an anticipated behavior of reinforced concrete structures under seismic loading (Moehle 1991). This output from the toolbox can

be a great asset to engineers who would like to optimize their design choices, and to their clients who can benefit from this information.

The variant that does not include code's strong-column weak-beam provision (Variant #9, Figure 3.13) has the most damage (or smallest probability of "no damage") to its columns throughout the height of the structure and even at small hazard levels, as compared to the other perimeter-frame designs (see Figure 3.19). The lowest probability of damage (or largest probability of "no damage") to the columns, beams, and partitions of the perimeter-frame designs occurs in the variant conservatively designed using the same beams and columns throughout (Variant #2, Figure 3.10 and Figure 3.20). The space-frame baseline design (Variant #6, Figure 3.12) acquires a significant amount of damage to the columns in the first story, but it better withstands damage to the beams and partitions as compared to the perimeter-frame designs (see Figure 3.19 and Figure 3.21).

This suggests that either Variant #2 or Variant #6 is likely to have the least expensive repairs. Also, all these damage plots show that significant damage to wallboard partitions has an early onset (at all story levels) for most of the variants considered in this study. As will be shown later, this early onset of damage in the nonstructural elements is a major contributor to the mean total repair costs for low levels of shaking and to expected annual loss, since these lower-level ground motions are more likely to occur.

A more detailed comparison of Variants #1 (Figure 3.9) and #2 (Figure 3.10) demonstrates what is gained and lost with the more conservative design that uses the same beams and columns throughout the height of the building. The design of Variant #2 with the same structural members over the height of the building makes the building significantly stiffer and stronger than required by the minimum code requirements. This design change specifically causes the members to be larger and stronger in the upper stories. This results in lower interstory drifts in the upper two stories of Variant #2, causing the building to suffer less damage in these stories. However, the stiffening and strengthening of the upper stories causes the damage to concentrate more in the first story columns, thus causing more structural and nonstructural damage in the first story (see Figure 3.19). An alternative to the

conservative design of Variant #2 is the design of Variant #9, which does not comply with the code's strong-column weak-beam (SCWB) provisions. The columns of stories 1-4 have lower probability of "no damage" (and have a higher probability of reaching the severe and collapse damage states in stories 1-2) for Variant #9 than for Variant #2; the beams in stories 2-4 for Variant #9 are also more damaged. Also, the partitions at the top three stories of this non-code-conforming design are more significantly damaged at lower levels of ground shaking (see Figure 3.21).

These damage plots are also an effective way to compare modeling choices of the benchmark building. Some modeling assumptions can lead to over- (conservative) or under- (non-conservative) estimation of the structure's response. Variant #11 assumes that all the concrete is precracked and is not expected to perform as well as the perimeter-frame baseline model (Variant #1). A comparison of Figure 3.9 and Figure 3.14 shows that the structural members of Variant #11 have a higher average probability of reaching more severe damage states throughout the height of the building; the partitions for Variant #11 have an earlier onset and a higher probability of reaching the significant damage state. This model is therefore a conservative representation of the baseline perimeter-frame design.

Another alternative to the baseline model is ignoring the effect of the gravity-load resisting frames, which results in an overall loss of strength and stiffness and an overall increase in structural response. Variant #12, which does not model the gravity-load resisting frames, has a higher average probability of its components being damaged for nearly all the hazard levels, when compared the baseline design (Variant #1). The most notable difference between Figure 3.9 and Figure 3.15 can be seen in the wallboard partitions, where the average probability of being damaged exceeds 0.50 and 0.85 (both occur at story level 3) at only the second and third smallest hazard levels, respectively. Again, this model overestimates the structural response.

All the above-mentioned variants have used fiber models for the structural analysis. Another type of model, the lumped plasticity model is described in Section 2.4 and has been shown to better capture collapse behavior (Haselton 2006). The structural analysis

results using the lumped-plasticity models are not realistic at low hazard levels and so the initial stiffness used in these models was adjusted to match the results of the fiber model at these hazard levels. The damage results in Figure 3.16-Figure 3.18 correspond to Variants #13-#15 that use an initial stiffness defined as the secant stiffness through the yield point (K_{yld}), through 60% and through 40% of the yield moment (K_{stf}), respectively. Variant #13 underestimates the response of the structural components at low hazard levels, where there is little light or no damage until the 2%-in-50-yr event ($S_a = 0.82g$); the behavior of the structural components is captured a little better with Variant #14 and is best portrayed with Variant #15. The lumped plasticity models overestimate the response of the nonstructural components at low hazard levels (most notably in Variant #13, Figure 3.16), but the damage results of Variant #15 are most similar to the baseline fiber model.

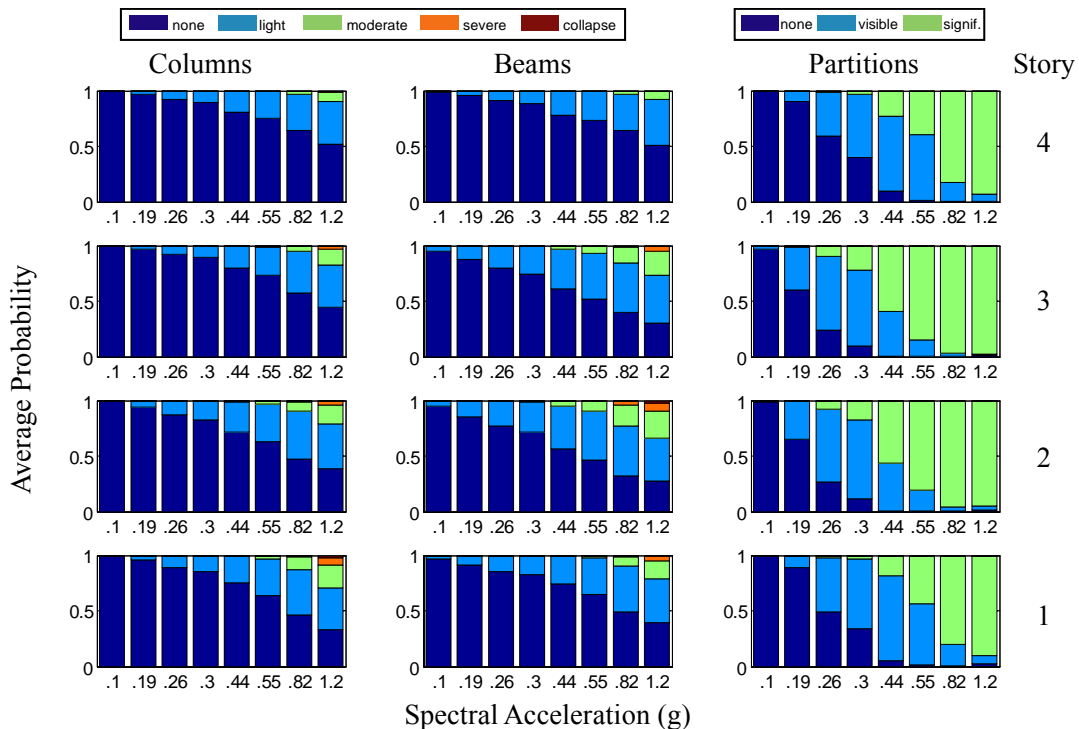


Figure 3.9 Average probabilities of damage per story level for variant #1.

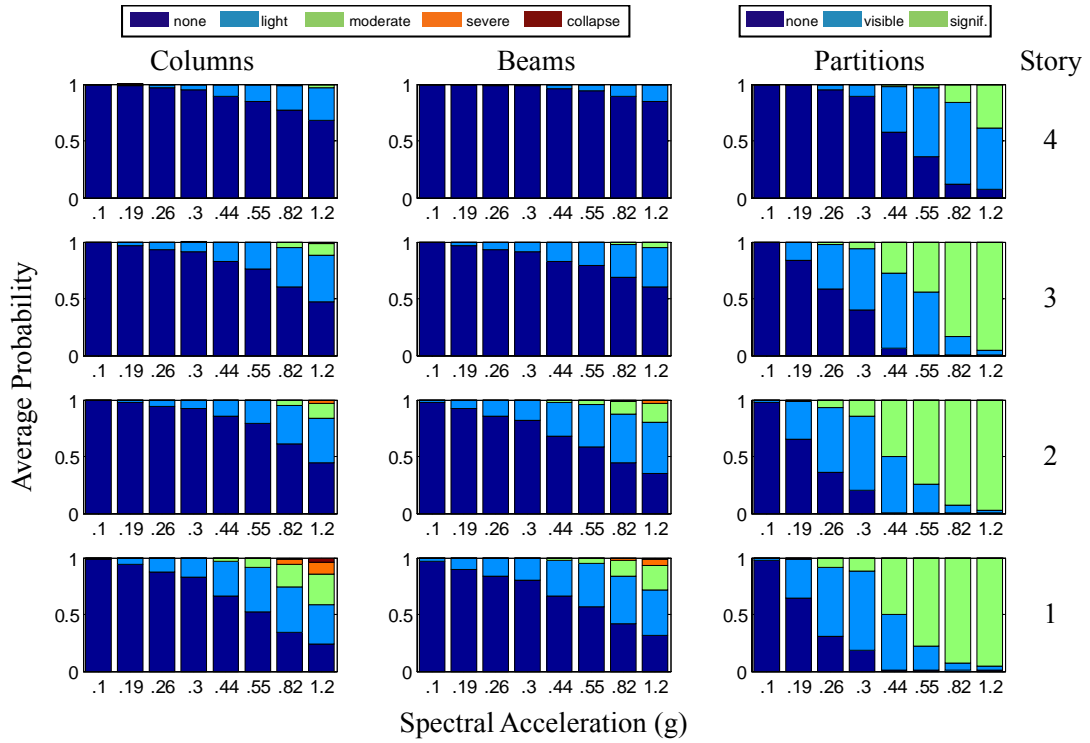


Figure 3.10 Average probabilities of damage per story level for variant #2.

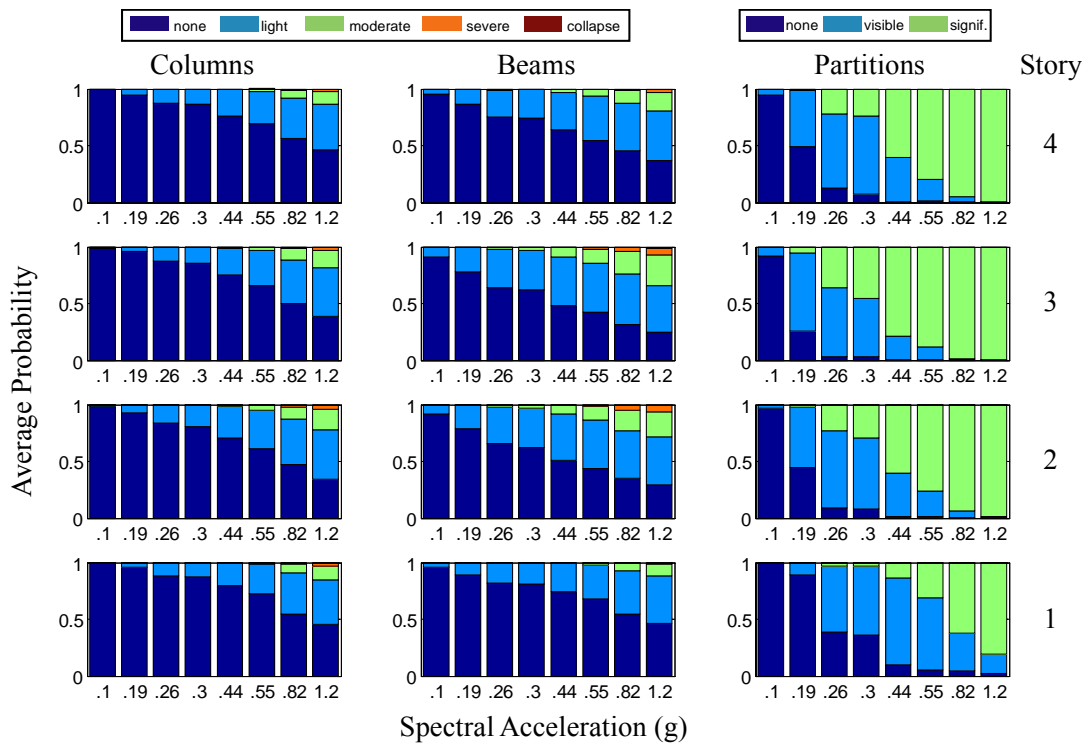


Figure 3.11 Average probabilities of damage per story level for variant #3.

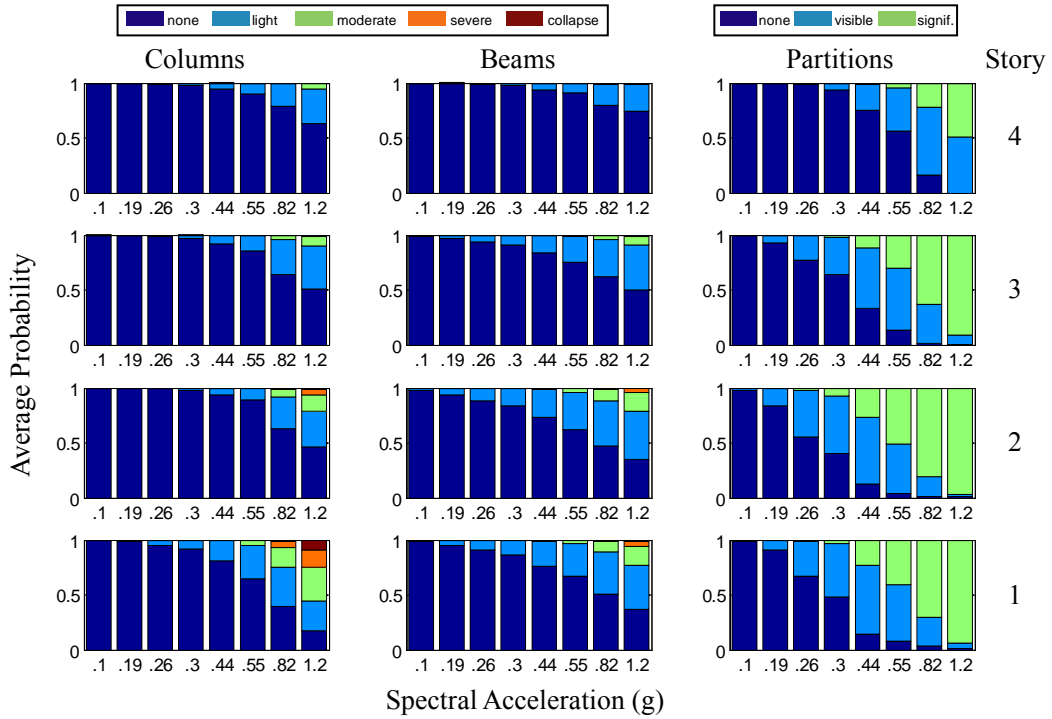


Figure 3.12 Average probabilities of damage per story level for variant #6.

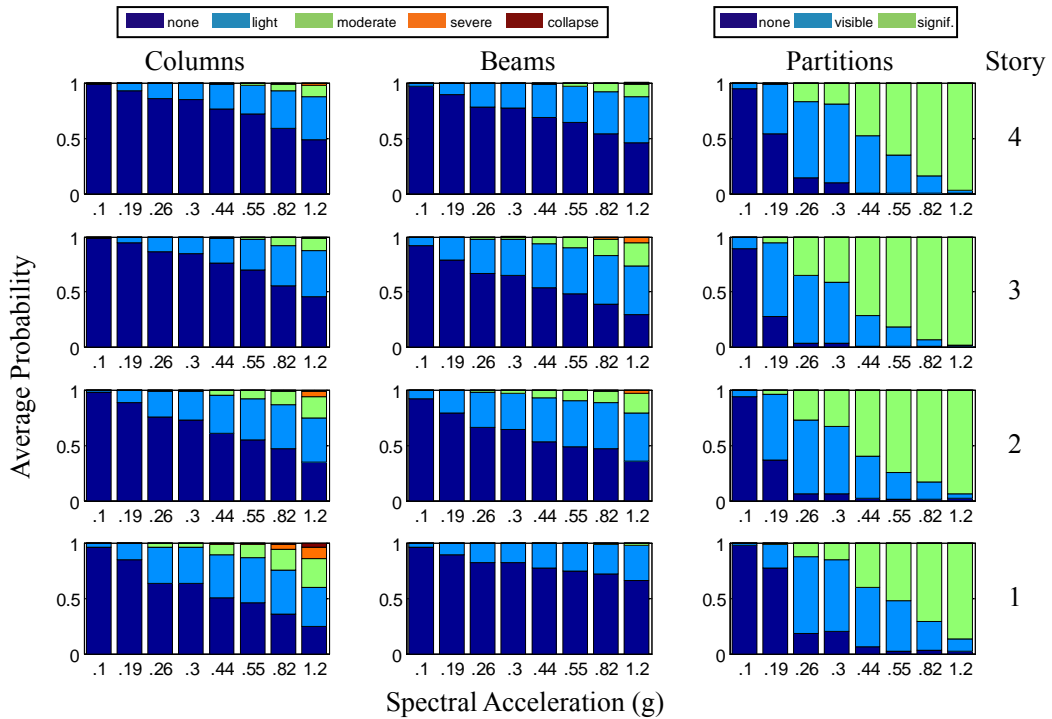


Figure 3.13 Average probabilities of damage per story level for variant #9.

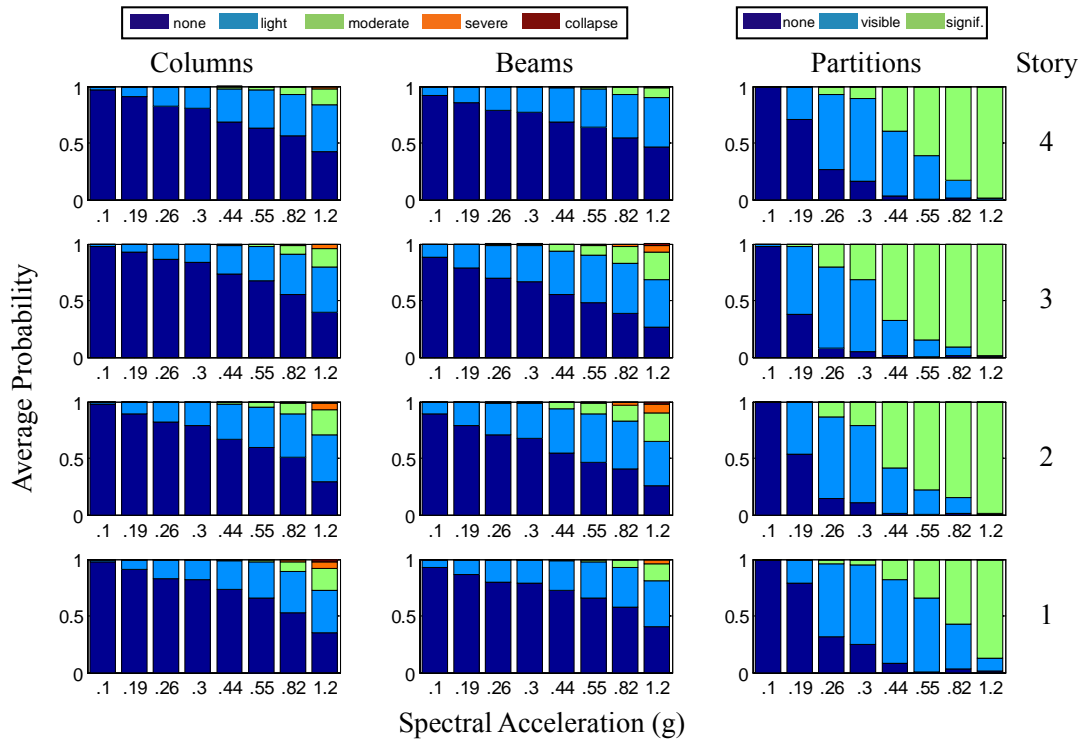


Figure 3.14 Average probabilities of damage per story level for variant #11.

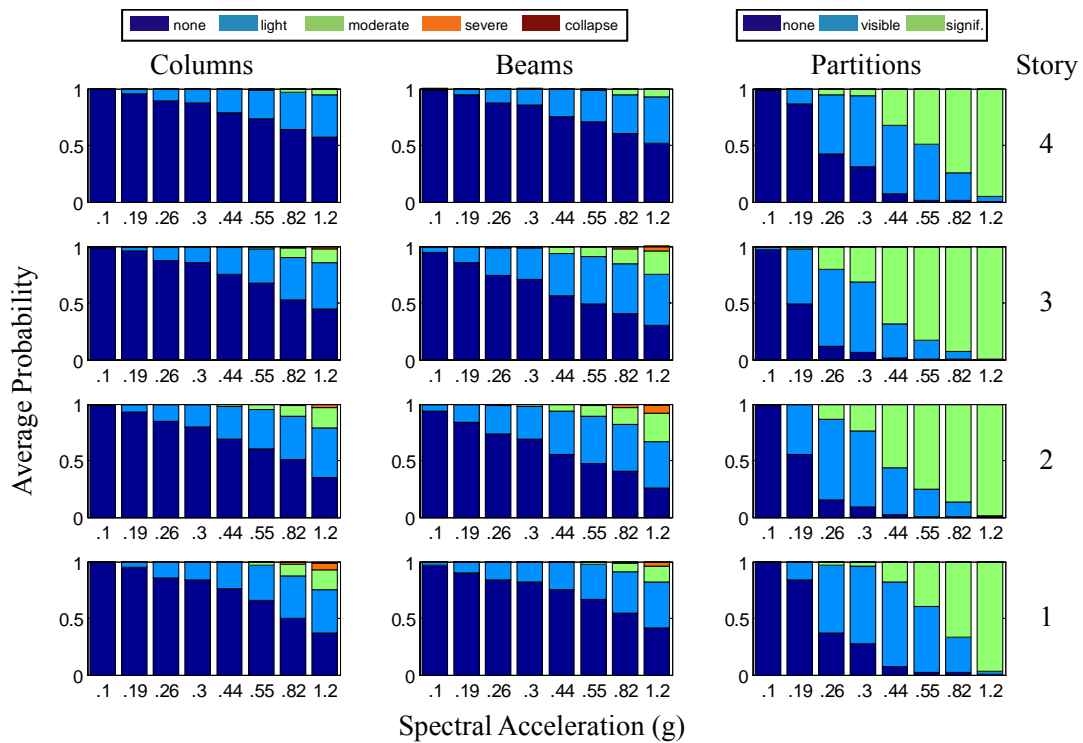


Figure 3.15 Average probabilities of damage per story level for variant #12.

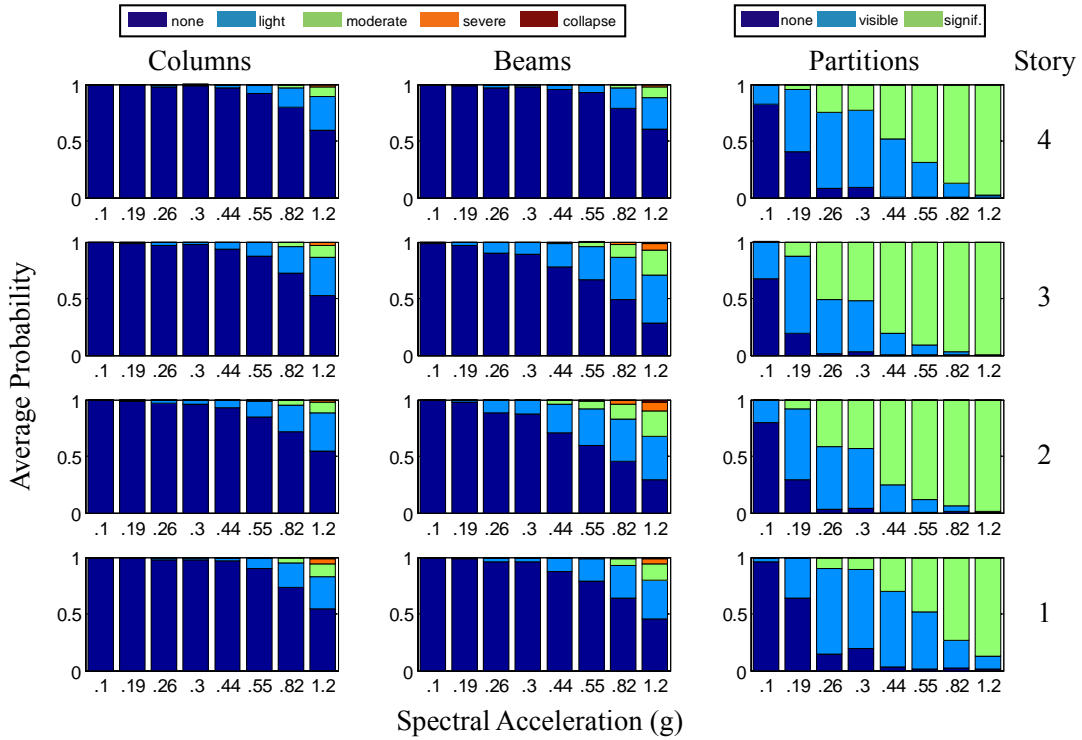


Figure 3.16 Average probabilities of damage per story level for variant #13.

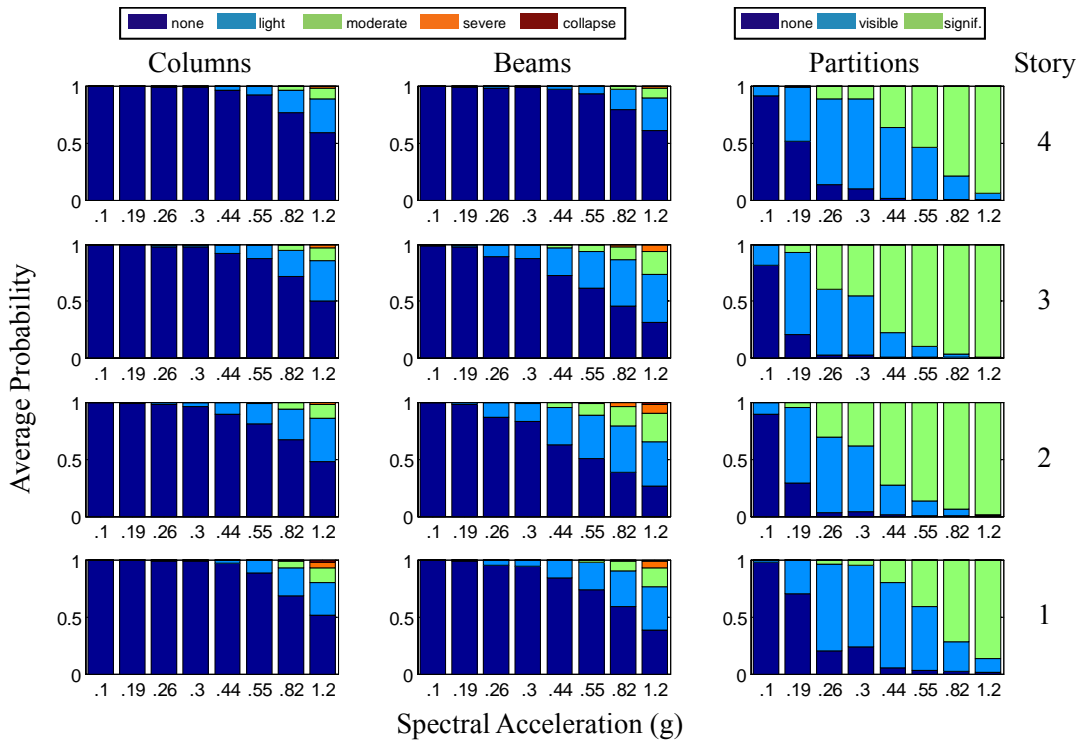


Figure 3.17 Average probabilities of damage per story level for variant #14.

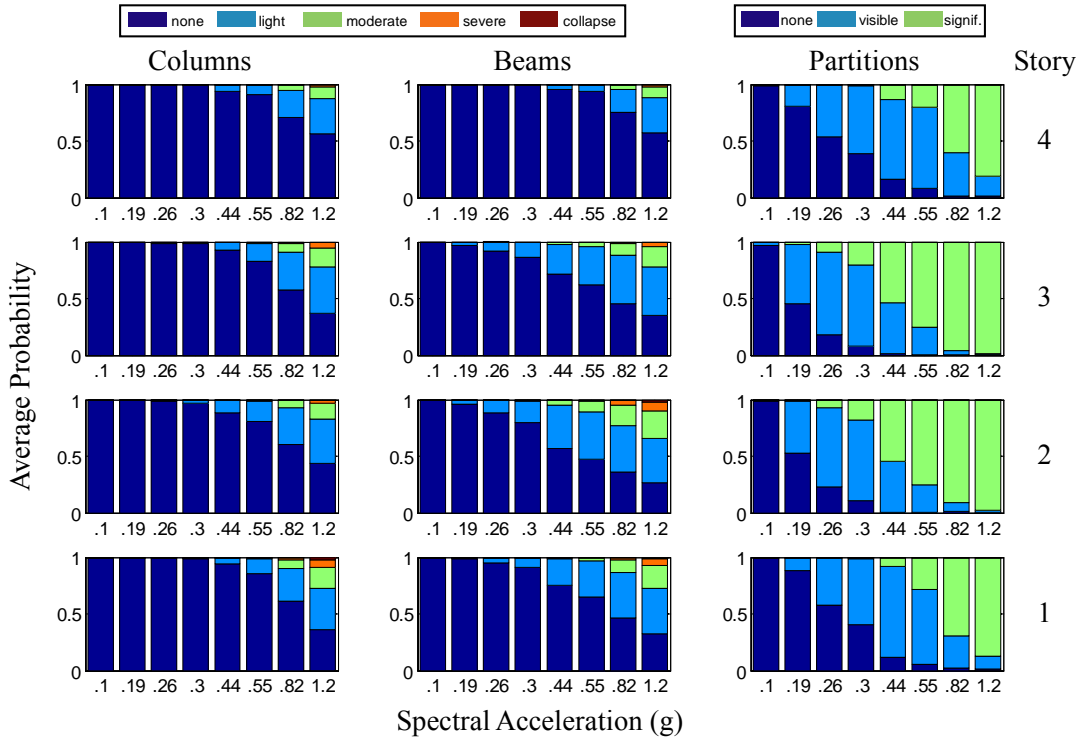


Figure 3.18 Average probabilities of damage per story level for variant #15.

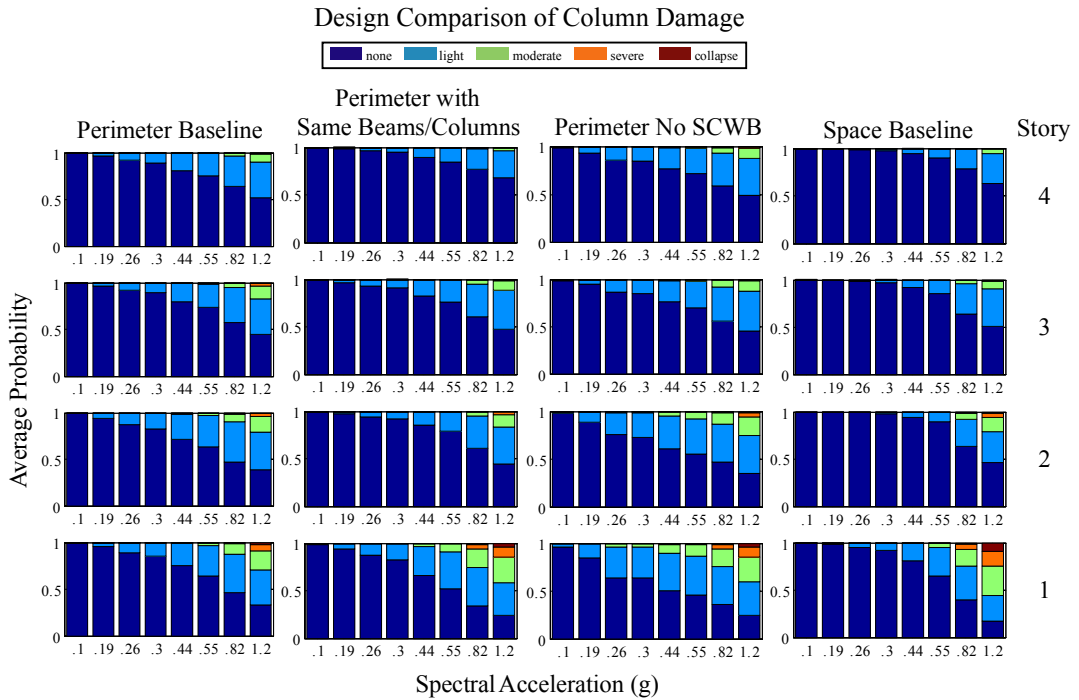


Figure 3.19 Comparison of the average probabilities of column damage per story level of design variants #1, #2, #9, and #6 (from left to right).

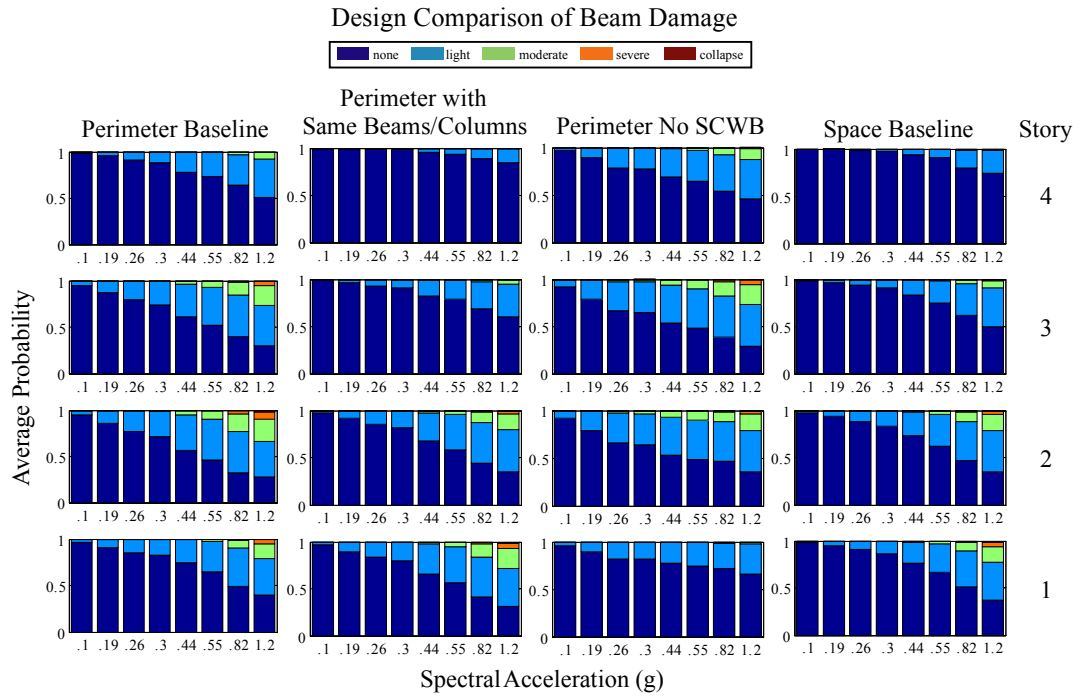


Figure 3.20 Comparison of the average probabilities of beam damage per story level of design variants #1, #2, #9, and #6 (from left to right).

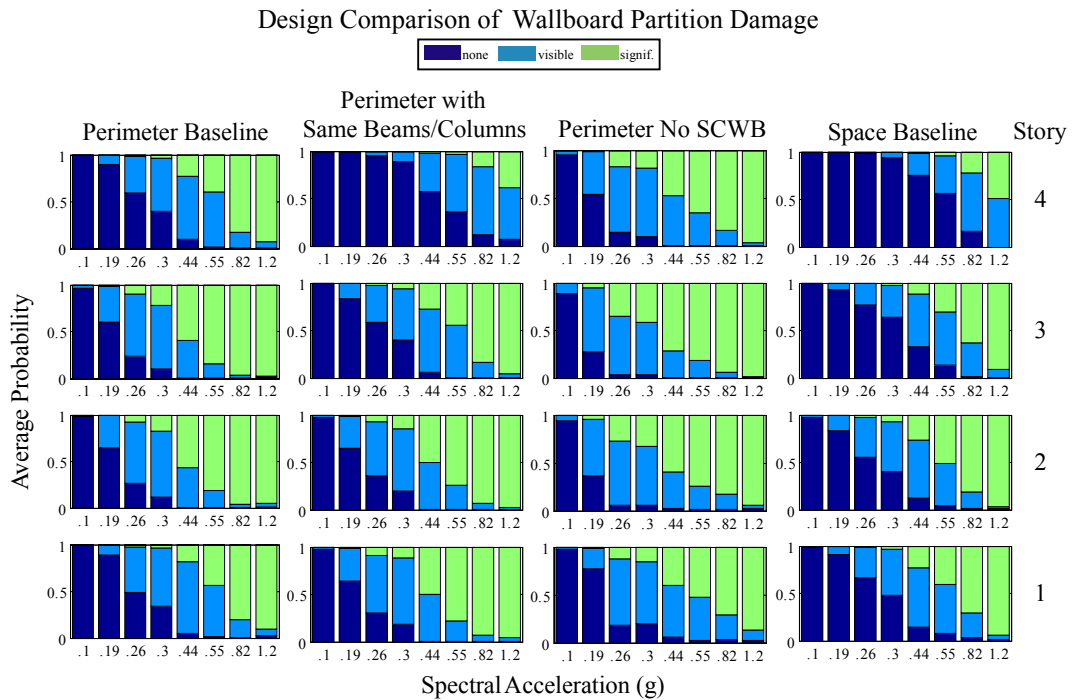


Figure 3.21 Comparison of the average probabilities of partition damage per story level of design variants #1, #2, #9, and #6 (from left to right).

CHAPTER 4

Building and Life Safety

The inspection of buildings and other structures after a seismic event helps to identify damage that may be life threatening to people, and to locate buildings that have collapsed or are in imminent danger of collapse. The estimated probabilities of damage and collapse resulting from the structural and damage analyses, respectively described in Chapter 2 and Chapter 3, are implemented in this chapter to develop a *virtual inspector* that can assess building damage. The virtual inspector has been designed to appropriately tag the building with the well-known red, yellow, and green safety placards abiding with current U.S. guidelines, and to locate the areas of concerning damage in the structure. The results of the damage analysis and the virtual inspection are used to estimate the number of fatalities in a building caused by partial or global collapse. The outcome of the virtual inspection and the fatality model are presented for several designs of the benchmark building across hazard levels.

4.1 Building safety

The biggest threat to human life and limb during an earthquake is the built environment; this threat can be greatly reduced or even eliminated by making structures safer. The development of analysis methods for predicting building safety and life loss is a relatively neglected area of research. The study of building safety and injury/casualty modeling is imperative to search and rescue planning, emergency preparedness, and design of safer

structures. This chapter investigates the role that building safety and casualty models can and should play in the design process. The goal of this chapter is to present the current state of building safety assessment procedures and of injury/casualty modeling for seismic events, to introduce improved safety and casualty models, and to show results of the proposed models applied to the PEER benchmark study described in Section 2.2.

4.1.1 ATC 20

The Applied Technology Council's *Procedures for Postearthquake Safety Evaluation of Buildings* document (ATC 20 1989; ATC 20-2 1995; ATC 20-3 1996a) offers guidelines for postearthquake safety inspections of buildings. The earliest document, ATC 20 (1989) was written to provide clear guidelines for postearthquake building evaluation using a three-level evaluation methodology: rapid evaluation (may be completed in less than 30 minutes; emphasis is on exterior of building; interior inspections are recommended for a few special circumstances), detailed evaluation (typically recommended after rapid evaluation; may be completed in a few hours; thorough examination of interior and exterior), and engineering evaluation (recommended when visual inspections are not sufficient to determine damage to building; can take up to a week or more to complete by structural engineers; responsibility of owner). The outcome of these evaluations is to tag the buildings with red, yellow, or green placards that designate a building as unsafe, restricted for use, or apparently safe, respectively.

These documents offer specific guidelines for building safety inspections for the rapid and detailed evaluations; they also provide some guidance for the engineering evaluation on evaluating when a structure is safe for use. The first of these guidelines, ATC 20 (1989) was initiated because existing procedures for damage assessment were vague and resulted in subjective evaluations. This document outlines specific postearthquake damage conditions for a variety of building types: wood frame, masonry, tilt-up, concrete, and steel-frame structures. Geotechnical and nonstructural damage conditions are also presented. The guidelines have been improved since their original 1989 publication and

after being field tested in a few damaging earthquakes. The most notable modifications are: a loss-value estimation procedure to “help determine the total damage the community actually suffered” (ATC 20-2 1995), updated placards with clear instructions of building-use restrictions (ATC 20-2 1995), and more than fifty case studies of postearthquake building safety evaluations using the rapid evaluation method described above (ATC 20-3 1996a).

4.1.2 Virtual inspector

The ATC-20 guidelines described above are used to create a “virtual inspector,” or a computer model that probabilistically estimates building safety using the damage analysis procedures described in Chapter 3. The damage descriptions from the fragility functions of the structural and nonstructural components are matched up with the damage descriptions from the ATC-20 guidelines to recreate the first two levels of the building evaluation procedure: rapid and detailed. The basic structure for this virtual inspector is given in the form of an event tree and shown below in Figure 4.1. The first block of the methodology, (a), corresponds to ATC-20’s rapid evaluation, which evaluates the structural integrity of a building and the probability of a red, yellow or a green tag being posted, based on what would be a speedy inspection of the exterior structural components. The second block, (b), relates to ATC-20’s detailed evaluation and includes a more thorough inspection of the structural components in the exterior as well as the interior of the building. Nonstructural damage does not play a role in this safety evaluation, but it used to determine any limitations of the building’s use and occupancy, which will be described in more detail in Section 6.1.

The level of detail that may be achieved for this “virtual inspector” really depends on the scale of the damage analysis. For example, do the fragility functions lump like elements at each story level? Also, what damage states are considered in the fragility functions for each damageable component in the building? The first branch of the event tree in Figure 4.1 determines the probability of a building’s red tagging due to severe leaning and/or collapse

(global or local) of the structure. The complement of this branch is for the event where the building does not collapse in any way nor is seriously out of plumb; this branch breaks off into three others that classify the overall damage to the exterior structural members as “severe,” “moderate,” and “none or light.” The structural analysis is used to determine the probability of building collapse and to determine the probability of damage of the structural elements, which are then used to determine the probabilities of a building being red, yellow and green tagged, given an intensity measure and completion of a rapid evaluation:

$$\begin{aligned}
 P[TAG_R | im, RE] &= P[C | im] + P[\text{severe ext. struct. damage} | im, NC]P[NC | im], \\
 P[TAG_Y | im, RE] &= P[\text{moderate ext. struct. damage} | im, NC]P[NC | im], \\
 P[TAG_G | im, RE] &= P[\text{light or no ext. struct. damage} | im, NC]P[NC | im],
 \end{aligned} \tag{4.1}$$

where TAG_R , TAG_Y , TAG_G correspond to red, yellow and green tags, respectively; RE denotes rapid evaluation; $P[C|im]$ is the probability of collapse given an intensity measure; $P[NC|im]$, the probability of no building collapse, is equal to $1 - P[C|im]$; and $P[\text{severe ext. struct. damage}|im]$, $P[\text{moderate ext. struct. damage}|im]$, $P[\text{light or no ext. struct. damage}|im]$ are the probabilities of severe, moderate, and light or no damage, respectively, to the exterior structural members given that the building has not collapsed and for a given intensity measure, as calculated in Equation (3.1).

If the tagging of a building is not determined to be red or green after the rapid evaluation, a detailed evaluation is typically recommended by building inspectors. The detailed evaluation procedure, (b) in Figure 4.1 below, follows the rapid evaluation’s yellow tagging. Again, the quality of the “virtual inspector” to determine the probability of tagging in this step depends on the amount of information available from the structural and damage analyses. The “virtual inspector” diverges from the ATC-20 guidelines in one respect for the detailed evaluation. In reality, the detailed evaluation of a building that has been yellow tagged can result again in a yellow tag if the inspector feels that visual inspection of the structure is not sufficient to estimate the degree of damage to the building. The inspector would then recommend that the owner contract a structural engineer to conduct the

engineering evaluation. However, the nonlinear dynamic structural analysis described in Chapter 2 and the damage analysis described in Chapter 3 offer information similar to that of the engineering evaluation. For this reason, the detailed evaluation of the “virtual inspector” is assumed to terminate with a red or a green tag. The probabilities of a building being red and green tagged, given an intensity measure and the completion of a detailed evaluation are:

$$\begin{aligned}
 P[TAG_R | im, DE] &= P[\text{severe int. struct. damage} | im, NC]P[NC | im], \\
 P[TAG_G | im, DE] &= P[\text{nonsevere int. struct. damage} | im, NC]P[NC | im], \\
 P[DE | im, RE] &= P[TAG_Y | im, RE],
 \end{aligned} \tag{4.2}$$

where DE denotes detailed evaluation; and $P[\text{severe int. struct. damage} | im, NC]$, $P[\text{nonsevere int. struct. damage} | im, NC]$ are the probabilities of severe and nonsevere (i.e., none, light, or moderate) interior structural damage, respectively, given that the building has not collapsed and for a given intensity measure. Note that *any* structural member (exterior or interior) in the severe damage state is considered to produce a red tag, and *any* exterior structural member in the moderate damage state produces a yellow tag. The probability of the benchmark building being red tagged and green tagged is computed from:

$$\begin{aligned}
 P[TAG_R | im] &= P[TAG_R | im, RE] + P[TAG_R | im, DE]P[DE | im, RE], \\
 P[TAG_G | im] &= P[TAG_G | im, RE] + P[TAG_G | im, DE]P[DE | im, RE].
 \end{aligned} \tag{4.3}$$

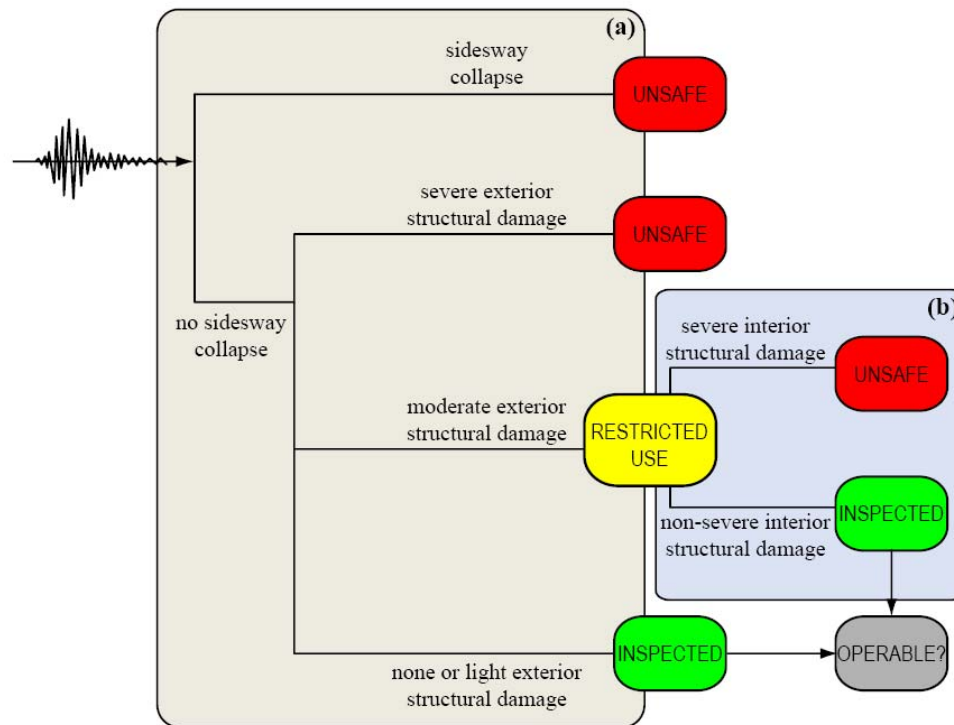


Figure 4.1 Event tree model for building safety evaluation based on ATC-20's (1985, 1995, 1996a) (a) rapid evaluation, and (b) detailed evaluation procedures.

4.1.3 Building safety results for benchmark study

As already mentioned, the power of the virtual inspector depends on the level of detail in the structural and damage analyses. A two-dimensional model (OpenSees, 2006) of a four-bay frame was used to analyze the benchmark building. The structural analysis employs plastic-hinge and fiber models to assess the building response at low and high intensity levels, respectively. The plastic-hinge model described in Chapter 2 captures sideways collapse of the structure, defined as the point of dynamic instability when interstory drift increases without bound; this is used to estimate the probability of collapse for all design variants in the PEER benchmark study. This sideways collapse will lead to a partial or total collapse of the structure, which warrants a red tag according to ATC-20's checklist for red tagging of a structure during a rapid evaluation (ATC 20-3, 1996a). The probability of the building needing a red tag due to sideways collapse is equal to $P[C | im]$, or the probability

of collapse as determined by the plastic-hinge model. The damage analysis of the fiber model results are used to estimate the probability of tagging in the event that there is no sidesway collapse of the building (all other branches of the event tree in Figure 4.1).

The probability of the benchmark building being posted with a red and green tag is calculated using Equation (4.3). The methodology for virtual building-safety tagging presented here attempts to closely mimic the post-seismic conditions encountered by building inspectors. It is likely that a building would have distributed damage after a sizeable earthquake, but the components with the most significant damage will be the ones to raise flags of concern with the inspectors who are assessing the structure. These are taken to be the exterior and interior components with the largest probability of severe damage in order to give a simplified procedure for estimating the probability of severe exterior (or severe interior) structural damage; however, the probability of damage for all components is considered in the virtual inspector's damage notes in Table 4.1. In the analysis of the perimeter-frame designs, the $P[\text{severe ext. structural damage} \mid \text{NC, im}]$ is therefore taken to be the maximum probability that the perimeter moment frames have serious cracking, spalling or crushing (i.e., beams or columns of moment frame have $\text{DM} = \text{severe or collapse}$) and the $P[\text{severe int. structural damage} \mid \text{NC, im}]$ is taken to be the maximum probability that the two-way slab has punching shear cracking or failure at columns (i.e., slab-column joints have $\text{DM} = \text{punching shear failure}$). In the analysis of the space-frame design, $P[\text{severe ext. structural damage} \mid \text{NC, im}]$ and $P[\text{severe int. structural damage} \mid \text{NC, im}]$ are similarly taken to depend on the maximum probability of severe damage to the columns and beams in the exterior and interior frames, respectively. Although the maximum probability of any of the structural members to be in a severe state is used as an approximation when computing the overall probability of tagging, the probability of structural damage in all components is considered when making the notes accompanying the tag in Table 4.1 (e.g., UNSAFE due to severe spalling of concrete of interior moment-frame column in ground story, but also severe damage to beams on second story above this column).

The probabilities of safety tagging are calculated at each hazard level, using the procedures of the rapid and detailed evaluations. Figure 4.2 shows a comparison of the tagging results from the rapid and detailed evaluations of a design that includes the SCWB provision (design C, VID #2) and one that does not (design D, VID #9). This plot demonstrates that the design without the SCWB provision performs considerably worse than the one including this important provision. Design C (VID #2) has a near-zero probability of receiving a red tag resulting from a detailed evaluation for earthquakes with hazard levels less than or equal to $S_a=0.55g$, and then the probability of red tag increases beyond this hazard level to about 40% at $S_a=1.2g$. On the other hand, after a detailed evaluation, Design D (VID #9) reaches the 50% probability of a red tag at a lower hazard level, near $S_a=0.90g$. The SCWB was introduced to building codes to lessen damage from the columns, which can lead to collapse; ignoring this provision is thought to be dangerous, which is supported by our virtual inspection of the building. Additionally, an interesting cross over occurs with the data for the probabilities of a green tag after rapid and detailed evaluations for design D (Variant #9). When the dashed green curve has values less than those of the solid green curve, it indicates that the information from the detailed evaluation informs the inspector that the damage assessment of interior structural members implies that there is more damage than expected from just the exterior evaluation. Furthermore, the damage notes of Table 4.1 show that the design without the SCWB provision suffers more damage of the interior structural components, based on the damage assessment of the column-slab connections. This interior damage controls the tagging results for this design.

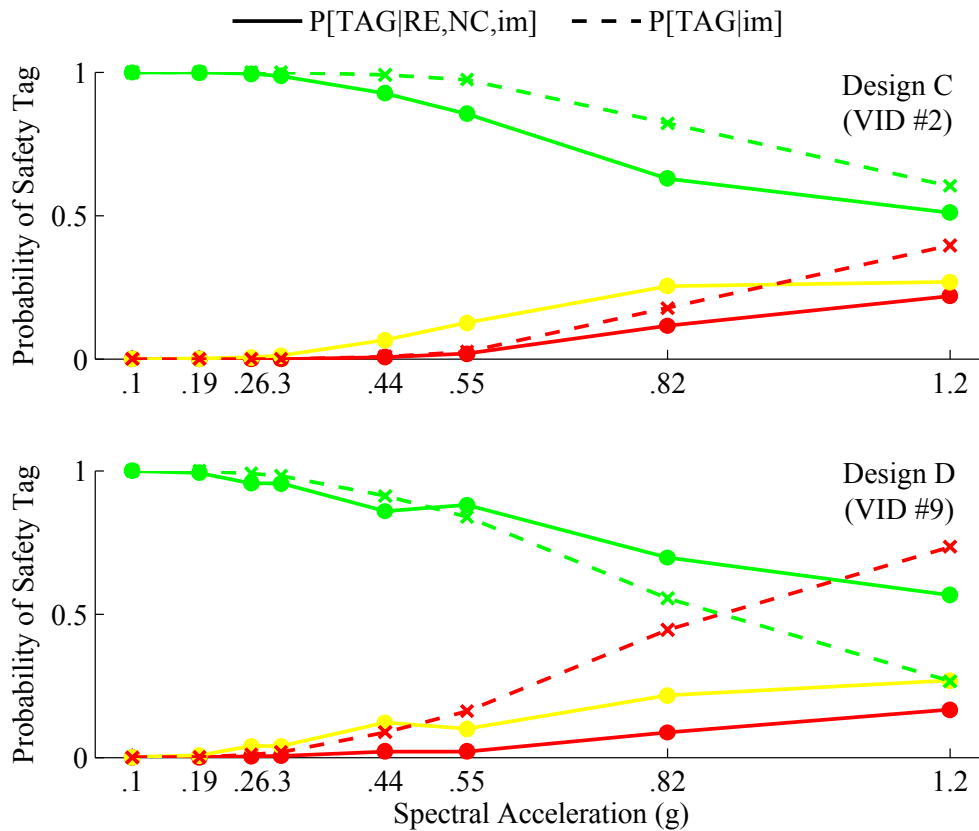


Figure 4.2 A comparison of the probabilities of building safety tagging between a design that includes the SCWB provision (VID #2) and one that does not (VID #9). The solid lines represent tagging after a rapid evaluation and the dashed lines represent tagging after a detailed evaluation; the color of the lines correspond to ATC-20's (1996a) red ("UNSAFE"), yellow ("LIMITED ENTRY"), and green ("INSPECTED") tags.

The virtual-inspector results for five designs of the benchmark building are presented in Table 4.1. This table gives the probability of the building receiving a red tag, $P[\text{TAG}_R|\text{im}]$, for the three highest hazard levels ($S_a = 0.55\text{g}$, 0.82g , 1.2g), and the associated damage notes that lead to an UNSAFE posting. Note that $P[\text{TAG}_G|\text{im}] = 1 - P[\text{TAG}_R|\text{im}]$. The probability of red tagging is comparable for the baseline perimeter-frame design (Design A) and the code-minimum design (Design B); failure of the floor slab system in the upper two stories leads to an UNSAFE tagging for both of these designs.⁶ The code-minimum design surprisingly has a lower probability than the baseline design of being red-tagged at

⁶The design of the interior columns was controlled by the slab shear check (Haselton et al., 2006).

the highest hazard level; this trend is also seen when comparing the probabilities of collapse and the losses of structural/nonstructural components of these designs (see Section 5.2). The other three designs (Design C, D, and E) are susceptible to severe damage in the first story columns, all predominantly in the NS-direction. As expected, Design D that ignores the strong-column weak-beam provision mandated by current building codes has high probability of badly damaged first-story columns, a high probability of collapse, and is highly likely to suffer damage to its floor-slab system in the upper two stories; three stories of this design are potentially hazardous to its occupants. The space-frame design (E) outperforms all the other designs in regard to safety tagging, at all hazard levels; this result is not surprising because the space frame has a lateral-resisting moment frame at every column line, and is better equipped to resist ground motions and thus it is safer. Design C has the same structural members in its first story as the baseline perimeter frame design (Design A). Design C, however, uses the same columns and beams throughout the height of the building. The additional weight of the larger structural members in the upper stories generates larger axial forces for first-story columns, which decreases their moment capacity. As shown in Section 3.3, this increases the probability of severe damage to the first-story columns of Design C, producing an increased probability of receiving an UNSAFE red tag.

The results of the virtual inspector stand on their own as essential information for building stakeholders. The results of this inspection, however, will later be incorporated into downtime modeling and used to estimate indirect losses associated with business interruption and delayed mobilization time prior to commencement of building repairs.

Table 4.1 Summary of virtual inspector results of various benchmark building designs for three largest hazard levels.

Design	$im=S_a(g)$	$P[C im]$	$P[TAG_R im]$	Higher Probability Damage States
A (VID#1): Perimeter frame, designed with expected overstrength.	0.55	0.006	0.02	Signs of distress in third floor beams of the perimeter frames, and punching shear failure in the slab of the third floor.
	0.82	0.034	0.10	Signs of distress in first story columns and third floor beams of the perimeter frames, and punching shear failure in the slab of the third floor.
	1.2	0.121	0.33	Signs of distress in first story columns and third floor beams of the perimeter frames, and punching shear failure in the slab of the second and third floors.
B (VID#3): Same as Design A, but designed with code-minimum strengths.	0.55	0.002	0.04	Signs of distress in fourth floor beams of the NS-directional perimeter frames, and punching shear failure in the slab of the third and fourth and floors.
	0.82	0.019	0.15	Signs of distress in fourth floor beams of the NS-directional perimeter frames, and punching shear failure in the slab of the third and fourth and floors.
	1.2	0.102	0.24	Signs of distress in fourth floor beams of the NS-directional perimeter frames, and punching shear failure in the slab of the third and fourth and floors.
C (VID #2): Same as Design A, but designed with uniform beams and columns over height.	0.55	0.005	0.03	Severe damage to first story columns of the NS-directional perimeter frames and punching shear failure in the slab of the second floor.
	0.82	0.038	0.18	Severe damage to first story columns of the NS-directional perimeter frames and punching shear failure in the slab of the second floor.
	1.2	0.147	0.40	Severe damage to first story columns of the NS-directional perimeter frames and punching shear failure in the slab of the second floor.
D (VID #9): Same as Design C, but no SCWB provision enforced (not code-conforming).	0.55	0.141	0.16	Signs of distress in first story columns of the perimeter frames and punching shear failure in the slab of the third and fourth floors.
	0.82	0.379	0.45	Severe damage to first story columns of the NS-directional perimeter frames and punching shear failure in the slab of the third and fourth floors.
	1.2	0.664	0.73	Severe damage to first story columns of the NS-directional perimeter frames and punching shear failure in the slab of the third and fourth floors.
E (VID #6): Baseline space frame.	0.55	0.003	0.01	Severe damage to first story columns and third floor beams in the space frames.
	0.82	0.027	0.12	Severe damage to first story columns in the space frames.
	1.2	0.131	0.43	Severe damage to first story columns in the space frames.

4.2 Life safety

The safeguarding of human lives is a top priority for engineers when designing buildings. That said, the estimation of human fatalities and/or injuries during a seismic event has had a limited role in current and past design practice. This section proposes a methodology for estimating fatalities for a specific building that can be used as a decision variable (*DV*) in performance-based earthquake engineering. The methodology presented incorporates many efforts towards this end from the past thirty years.

4.2.1 History of fatality modeling

The earliest publication (known to the author) to propose estimates of earthquake casualties is a report by NOAA for the Office of Emergency Preparedness (1972). This report lays the groundwork for fatality modeling and outlines several important factors that should be included in casualty and serious-injury models: (1) empirical data from relevant events, such as data from damaging U.S. earthquakes or from comparable events in other countries; (2) building inventory (e.g., number of concrete vs. number of steel frame buildings) and/or the physical properties of an individual building (e.g., material, height, gross area); and (3) population estimates including the population of a study area (e.g. a city or county), and the number of building occupants of a specific building. These factors as well as a few others highlighted in the earthquake morbidity/mortality literature are addressed in more detail in the following sections.

EMPIRICAL DATA

The work by NOAA (1972) summarizes the casualties due to major U.S. earthquakes between 1886 and 1971; their empirical data are reproduced in Table 4.2. This table does not describe the injury mechanisms (e.g., crushed by fallen ceiling, head injured by fallen bricks from damaged masonry wall), which this author and others (Wagner et al., 1994; Jones et al., 1990; Mahue-Giangreco et al., 2001) consider to be extremely important for

accurate building-specific fatality modeling. However, the NOAA data does provide a means to forecast the numbers of fatalities and serious injuries in future events having similar attributes and comparable building stocks as those listed in Table 4.2. The last entry of this table contains the number of deaths per 100,000 people due to the Loma Prieta earthquake; this was calculated based on data from coroner and medical examiner reports (Eberhart-Phillips et al., 1994). Other prominent studies propose estimates for future earthquake casualties: (1) FEMA's collaborative work with the National Security Council (FEMA 1980) provides numbers for deaths and hospitalized victims (categorized by occurrence times) for earthquakes occurring along four different Californian faults; (2) the Applied Technology Council (ATC 1985) provides estimates for fatalities, minor injuries, and serious injuries based on building type and mean damage factor (including structural and nonstructural components); and (3) the technical manual for FEMA's HAZUS99-SR2 earthquake loss analysis software (HAZUS 2002) provides casualty estimates (ranging from injuries requiring basic medical aid to fatal injuries) for various levels of structural damage (from slight structural damage to complete structural damage with collapse) and based on building type (the extensive list includes 36 building types). The casualty ratios from (2) and (3) are given below in Table 4.3.

There is also vast knowledge of earthquake casualties due to disastrous seismic events from around the world, including studies of the 1976 Guatemala earthquake (Glass et al., 1977), several Japanese earthquakes (Ohta et al., 1986), the 1986 San Salvador, El Salvador earthquake (Durkin 1987), the 1988 Spitak, Armenia earthquake (Murakami 1992), the 1999 Izmit, Turkey earthquake (Shoaf and Seligson, 2005), and a study of many international seismic events (Coburn et al., 1992). It is problematic to use casualty earthquake data from countries other than the U.S. because of the great differences in the seismic/geophysical characteristics (e.g., Peek-Asa et al., 2003), inconsistencies with construction practices (e.g., Glass et al., 1977),⁷ differences in population density (e.g., Samardjieva and Badal, 2002), or the disparate levels of earthquake preparedness (e.g.,

⁷ As an extreme example of the significance of these differences, all the deaths and serious injuries in the village of Santa Maria Cauque after the 1976 Guatemalan earthquake occurred in one-room adobe shelters (Glass et al., 1977).

Tierney 1990).⁸ However, if a careful examination of the international data proves that in some cases similar characteristics may be established between the events in these countries and those in the U.S., it is reasonable to use the empirical data (in those cases) to better inform casualty models of future U.S. events. In cases where data have been categorized by injury mechanisms, damage extent, or by building construction type, it is possible to use these results from international events together with the probabilities of these conditions occurring to estimate casualties for buildings in U.S. seismic regions.

Table 4.2 Death and injury ratios from some major U.S. earthquakes. All entries, but the last, are from NOAA (1972).

Earthquake	Date	Time of Occurrence	Deaths per 100,000 Population	Injuries per 100,000 Population
Charleston, SC	08/31/1886	21:51	45 outright, 113 total	---
San Francisco, CA	04/18/1906	05:12	320	211
Santa Barbara, CA	06/29/1925	06:42	45	119
Long Beach, CA	03/10/1933	17:54	26	1300
Imperial Valley, CA	03/18/1940	20:37	18	40
Puget Sound, WA	04/13/1949	23:56	1	---
Kern County, CA	07/21/1952	04:52	500	---
Bakersfield, CA	08/22/1952	15:41	3	47
Anchorage, Alaska	03/27/1964	17:36	9	315
San Fernando, CA	02/09/1971	06:01	12 excl. VA Hosp., 64 incl. VA Hosp.	180
Loma Prieta, CA	10/17/1989	17:04	1.4*	---

* This is the number of deaths per 100,000 population calculated from Loma Prieta mortality data (Eberhart-Phillips et al., 1994) and from the 1980 population of seven Bay Area counties (U.S. Census, 1980).

BUILDING CHARACTERISTICS AND OCCUPANCY

An extensive study of worldwide earthquakes between 1900 and 1992 (Coburn et al., 1992), shows that nearly 75% of earthquake-related deaths have been caused by building collapse, and specifically, 7% of total deaths have been caused by the collapse of RC buildings. Additionally, researchers found that 98% of direct earthquake fatalities were

⁸ After the 1998 Armenian earthquake, emergency care providers were unable to provide basic forms of treatment to many individuals, leading to deaths and severe injuries that would not have otherwise occurred (Tierney 1990).

caused by structural failures in the 1989 Loma Prieta earthquake. It is therefore important to investigate the relationship between structural behavior and human casualties during earthquakes. Building properties such as type, material, height, and area have an impact on the collapse mechanism of the building due to future seismic events, and play a very important role in casualty modeling (NOAA 1972; Ohta et al., 1986; Jones et al., 1990; Coburn et al., 1992; Murakami 1992; Shoaf and Seligson 2005). However, most of the available empirical earthquake casualty data have not been collected with these characteristics in mind and are therefore not disaggregated by building characteristics. Further, it is difficult to reconstruct these data after the fact due to confidentiality of hospital records and the redistribution of the original population from a study area. Fatality ratios that have been determined with consideration to some characteristics applicable to the benchmark study are given in Table 4.3. This table does not reflect consistent terminology for building types or the associated damage states, which is typical of the available empirical earthquake data since there is no existing standard for data collection. The fatality modeling effort would be greatly assisted if standardized post-event data collection forms, such as those developed by Choudhury and Jones (1996), would be adopted for U.S. reconnaissance efforts to ensure that valuable, perishable data is not lost.

The occurrence time of an earthquake greatly affects the casualty outcomes. FEMA (1980) describes residential buildings as the safest environment during a seismic emergency and so the safest (fewest casualties) time for a Californian earthquake is the nighttime. Additionally, FEMA (1980) reports that when an earthquake strikes in the daytime people are more at risk in the early afternoon because they are more vulnerable to the collapse of office buildings and failures of transportation systems. Several models take building occupancy at various times of the day directly into account when calculating earthquake casualties (NOAA 1972; Ohta et al., 1986; Coburn et al., 1992). NOAA's (1972) model uses the empirical data from Table 4.2 to estimate the number of deaths and victims with hospitalized injuries for future events occurring at three discrete times of day in the San Francisco Bay Area. Ohta et al. (1986) provide a periodic function, based on empirical data, to more accurately estimate the number of fatalities in Japanese homes through a 24hr period. Coburn et al. (1992) propose the most comprehensive occupancy model for a 24hr

period, considering occupancy patterns of buildings in rural agricultural societies and in residential and commercial buildings of urban societies; a modified version of their commercial building occupancy curve is presented in Figure 4.3.

OTHER IMPORTANT FACTORS FOR CASUALTY MODELING

Several other important factors contribute to casualties in seismic events: damage to nonstructural building elements; location of occupant in the building and their gender, age, and behavior during and immediately after the event; search and rescue immediately following the event; and quality and efficiency of medical treatment.

Although it is intuitive to attribute earthquake injuries to falling nonstructural elements and building contents, researchers (e.g., Durkin and Thiel, 1992) found that there was a low probability of these elements causing fatal injuries and that they were responsible instead for numerous minor and moderate injuries. In addition to falling objects, it is believed that a person's spatial location in a building during an event can also have an affect on their risk of injury. Wagner et al. (1994) show that a person has a higher risk of being injured if they occupy upper stories of a building instead of the first floor. Also, a study by Ohta et al. (1986) shows that small living spaces amplify the risk of casualty in a home.

Table 4.3 Comparison of fatality models that is disaggregated by building type and damage quantity (modified from Table 19 in Shoaf and Seligson, 2005).

Building Characteristics	Fatality Model	Damage Description	Conditional Fatality Probability
For all construction types except light steel and wood frame.	ATC-13 ^a (1985)	“none”	0
		“light”	0.00001
		“moderate”	0.0001
		“heavy”	0.001
		“major”	0.01
		“destroyed”	0.20
Reinforced concrete (non-near-field ground motions)	Coburn et al. ^b (1992)	“partial collapse (10% of volume”	0.082
		“partial collapse (50% of volume”	0.31
		“top-down collapse”	0.41
		“bottom-up collapse”	0.57
Midrise concrete moment frame	HAZUS 99-SR2 ^c (2002)	“moderate”	0
		“extensive”	0.00001
		“complete without collapse”	0.0001
		“complete with collapse”	0.1
Midrise non-ductile reinforced-concrete frame	Shoaf and Seligson ^d (2005)	“partial collapse”	0.015
		“total collapse”	0.131
^a Fatality ratios are based on NOAA’s report (1972) and expert opinion. ^b Fatality ratios are based on worldwide data from Coburn et al. (1990). ^c Fatality ratios are based on and revised from ATC-13 (1985). ^d Fatality ratios are based on population survey data from Golcuk, Turkey after the 1999 Izmit earthquake (Shoaf and Seligson 2005).			

Human characteristics can also play a role in the risk of people incurring injuries during seismic events. For example, the risk of injury is consistently greater for women than it is for men (Glass et al., 1977; Ohta et al., 1986). Also, several researchers demonstrate that children and elderly people are at a higher risk of being injured (Glass et al., 1977; Ohta et al., 1986; Mahue-Giangreco et al., 2001). Also, the behavior of people during and

immediately following an event can affect the risk of injury. For example, people on a ground floor are more likely to run out of a building during an earthquake,⁹ and Wagner et al. (1994) show that those people who stay inside a building during shaking have a higher risk (5 times more likely) of being injured than those who run outside. In addition, Durkin and Thiel (1992) found that in the absence of structural failure, peoples' behavior during and after the event contribute only in a small way to the probability of their being seriously injured, although it does contribute in a large way to minor injuries.

Most severe injuries and deaths are caused by entrapment in the structural debris of a damaged building. Wagner et al. (1994) found that being trapped by collapsing structures was the most significant risk for dying in the 1988 Armenian and the 1980 southern Italian earthquakes; these researchers estimate from empirical data that trapped people are 68-107 times more likely to die, and 5-11 times more likely to have non-lethal injuries than those who are not trapped. The Coburn et al. (1992) fatality model accounts for this in their "M3" factor. The time it takes to find victims in rubble and treat their injuries to prevent further deterioration is critical. Coburn et al. (1992) also include an "M5" factor in their earthquake injury model that accounts for the additional deaths of trapped victims that occur after an event. For example, after the 1998 Armenian earthquake, emergency care providers were unable to provide basic forms of treatment to many individuals that certainly would have prevented further deaths if available (Tierney 1990).

4.2.2 Methodology and example of fatality estimation

The literature on earthquake casualty modeling and earthquake epidemiology provides a number of factors that are likely to affect the risk of human injury during seismic events. In this work, the purpose of the casualty modeling is to inform the building design process. Therefore, although all the factors mentioned above are important, only those that may be

⁹ Statistical data on evacuation patterns are lacking, but tests have shown that people cannot get out of a building above the first floor in less than thirty seconds (based on Georgescu 1988, as cited in Coburn et al., 1992). It is reasonable to assume, as others have in their fatality models (Coburn et al. 1992; HAZUS 2002; Yeo and Cornell 2003) that 50% of people on a ground floor will run outside during ground shaking.

directly affected by a change in building design are considered in this dissertation. These include collapse states of the building (partial or complete), building occupancy, and spatial location of building occupants. The probability of local collapse (LC) and sidesway collapse (C) are evaluated from the virtual inspector output described in Section 4.1.2. The probability of a local collapse may be taken as the probability of a red tag conditioned on no collapse (even without the condition of sidesway collapse, a red tag post implies that there are life-threatening dangers in the building, i.e., severe damage to columns or beams). The first step in estimating fatalities in a building due to an earthquake is to determine the population at risk by considering the building occupancy and the spatial location of the occupants.

The benchmark building is a hypothetical structure, and so in order to estimate a realistic value for building occupancy, the recommendations of ATC-13 (1985) were used. ATC-13 provides tables for estimating the mean building daytime and nighttime occupancies based on building type and square footage, but they do not provide information about the uncertainty (e.g., the variance) of these occupancy estimates (1985). The calculated mean number of occupants for the benchmark building using Table 4.12 of ATC-13 (1985) is 346 people. The floor plans of the building, given in Figure 2.3-Figure 2.4, are used to estimate the distribution of this population throughout the building. The top three stories have exactly the same floor plans and are thus assumed to have the same mean number of occupants (95 people). The ground floor has many areas that are not designated as desk/continued-usage areas (the cafeteria, mail room and open lobby space), and so the ground floor is assumed to have near $2/3$ of the mean number of occupants as in the stories above (61 people). Also, using the result the fact that people on the ground floor tend to run out of the building during seismic events, it is reasonable to assume that 50% of the ground floor occupants will evacuate during ground shaking and therefore, will not be injured by any resulting structural damage inside the building.¹⁰ The mean number of occupants for the benchmark building minus the 50% of the first floor occupants assumed to evacuate at the first sign of an earthquake, O_N , is equal to 316. The occupancy patterns of Figure 4.3

¹⁰ The assumption of 50% evacuees was first introduced by Coburn et al. (1992), and has been adopted by HAZUS (2002) and Yeo and Cornell (2003).

must also be incorporated to account for the equal likelihood of earthquakes occurring at any hour of the day.

The proposed fatality model uses the non-residential (commercial) occupancy model of Coburn et al. (1992). It is reasonable to use this model for occupancy during weekdays; however, most typical businesses have many fewer employees on-site during weekends and holidays. Therefore, the occupancy pattern during these times is modeled as a fraction of the weekday occupancy during peak hours (both occupancy patterns are shown in Figure 4.3). It is assumed that an earthquake can occur at any time of any day with equal probability, and so the mean population at risk is calculated by:

$$n_{\text{weekday}} = O_N \cdot \int_0^{24} E[OF | \text{weekday}, t] \cdot p(t) dt,$$

$$n_{\text{weekend/holiday}} = O_N \cdot \int_0^{24} E[OF | \text{weekend/holiday}, t] \cdot p(t) dt, \quad (4.4)$$

$$n = n_{\text{weekday}} \cdot \left(\frac{\text{No. weekdays}}{365} \right) + n_{\text{weekend/holiday}} \cdot \left(\frac{\text{No. weekends/holidays}}{365} \right),$$

where n is the mean population at risk; $O_N = 316$, as determined above by assuming first-floor evacuations during the earthquake and the estimated occupancy of ATC-13 (1985); n_{weekday} is the mean number of occupants in the building during the weekdays over a 24hr period; mean $E[OF | \text{weekday}, t]$ is the mean fraction of occupants in the building for weekdays at a given hour of the day, which is given in Figure 4.3; $n_{\text{weekend/holiday}}$ is the mean number of occupants in the building during weekends and holidays over a 24hr period; mean $E[OF | \text{weekend/holiday}, t]$ is the mean fraction of occupants in the building during weekends/holidays at a given hour; and $p(t)$ is a uniform distribution equal to $1/24$ for $t \in [0, 24]$. In calculating n , we use 251 weekdays and 114 weekend/holidays (accounting for the 10 observed U.S. national holidays), respectively. Equation (4.4) then gives $n=133.4$ for the mean population at risk in the benchmark building. In the discussion that follows, fatalities are estimated for $n=133$.

Human fatalities due to strong seismic events can be estimated as a function of the population at risk and the probability of building damage. The probability of fatalities occurring, given the damage state of the structure, can be modeled with the binomial distribution given by:

$$P_{Y_n|DM}(y | DM) = \frac{n!}{y!(n-y)!} p_{DM}^y (1-p_{DM})^{n-y}, \quad (4.5)$$

where $P_{Y_n|DM}(y | DM)$ is the probability of y deaths occurring given the damage state of the building, and p_{DM} is the fatality probability (also known as fatality rate in epidemiology literature) given the damage state of the building. The fatality probability, p_{DM} , is given in Table 4.3 for reinforced-concrete buildings for various levels of damage. Note that the number of building occupants is also uncertain; the mean value of n calculated in Equation (4.4) is used here as a simplification for design purposes.

The mean and the variance of fatalities given the damage state of the building are computed as follows:

$$\begin{aligned} E[Y_n | DM] &= (np_{DM}), \\ \text{Var}[Y_n | DM] &= n \cdot p_{DM}(1-p_{DM}), \end{aligned} \quad (4.6)$$

where Y_n is the number of fatalities when there are n total occupants in the building at the time of the earthquake; $E[Y_n|DM]$ is the mean number of fatalities for the given damage state of the building; and $\text{Var}[Y_n|DM]$ is the variance of fatalities for the given damage state of the building. The mean and variance of the number of fatalities are calculated using the value $n=133.4$ for the benchmark building and the fatality probabilities given local collapse and global collapse. These are listed in Table 4.4, where the damage states “local collapse” and “collapse” are assigned to the appropriate damage descriptions given in Table 4.3: the “major” and “destroyed” damage states of ATC-13 (1985) are used for local collapse (LC) and collapse (C) in Table 4.4; the “partial collapse (50% volume)” damage state of Coburn

et al. (1992) is used for LC, and the average of the collapse damage states, “top-down collapse” and “bottom-up collapse,” is used for C in Table 4.4; the “complete without collapse” and “complete with collapse” damage states of HAZUS (2002) are used for LC and L, respectively, in Table 4.4; and the “partial collapse” and “total collapse” damage states Shoaf and Seligson (2003) are used for LC and L, respectively, in Table 4.4.

Event trees like the one used for the building safety-tagging model in Section 4.1.2 are also used by researchers for casualty modeling (Murakami 1992; HAZUS 2002; Yeo and Cornell 2003). The proposed event tree model to estimate earthquake fatalities for the example benchmark building in this work is given in Figure 4.4, which builds on Figure 4.1. The first block in the event tree of Figure 4.4 corresponds to the population of a building that is at risk, which was calculated using Equation (4.4). The event-tree branches leaving this block correspond to the probability of damage states for the building conditioned on the hazard level and then the fatality probabilities associated with these damage states.

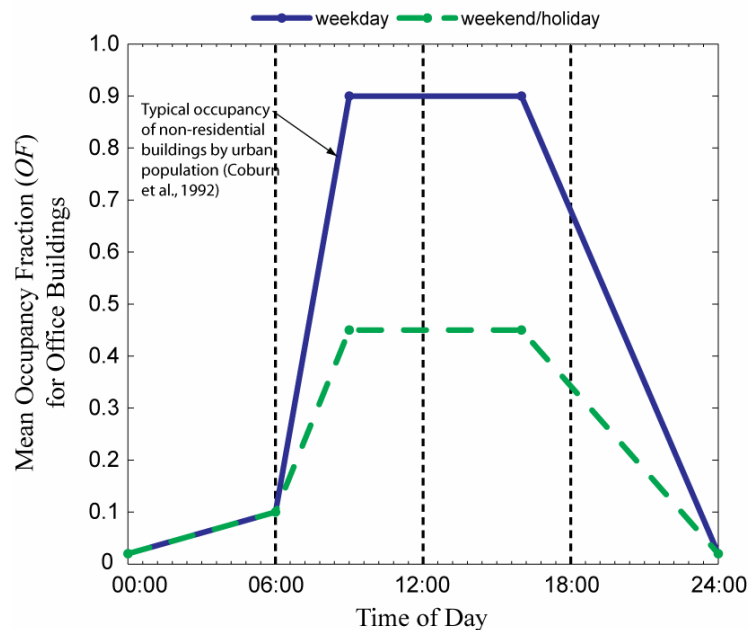


Figure 4.3 Fractional office building occupancy throughout the day, modeled after Coburn et al. (1992). The dashed version is the modified pattern used here to account for weekend and holiday occupancy.

Table 4.4 Mean and variance of fatality models for local collapse and global collapse of the building, calculated with equation (4.6).

Building Characteristics	Fatality Model	Damage State (DM)	P_{DM}	$E[Y_n DM]$	$Var[Y_n DM]$
For all construction types except light steel and wood frame.	ATC-13 (1985)	LC	0.01	1.33	1.32
		C	0.20	26.68	21.34
Reinforced concrete (non-near-field ground motions)	Coburn et al. (1992)	LC	0.31	41.35	28.53
		C	(0.57+0.41)/2	65.37	33.2
Mid-rise concrete moment frame	HAZUS 99-SR2 (2002)	LC	0.0001	0.01	0.01
		C	0.1	13.34	12.01
Mid-rise non-ductile reinforced-concrete frame	Shoaf and Seligson (2005)	LC	0.015	2.00	1.97
		C	0.131	17.47	15.19

The results from the damage analysis of Chapter 3 may be used to determine the expected number of deaths and the variance of deaths for each hazard level, given the building's damage state. Using the terminology of the event tree, the mean and variance of fatalities for a given hazard level are given by:

$$\begin{aligned}
 E[Y_n | im] &= E[Y_n | C]P[C | im] + E[Y_n | NC]P[NC | im] \\
 &= E[Y_n | C]P[C | im] + E[Y_n | LC, NC]P[LC | im, NC]P[NC | im] \\
 &= (np_C) \cdot P[C | im] + ((np_{LC}) \cdot P[LC | im, NC]) \cdot (1 - P[C | im]),
 \end{aligned} \tag{4.7}$$

$$\begin{aligned}
 E[Y_n^2 | im] &= E[Y_n^2 | C]P[C | im] + E[Y_n^2 | NC]P[NC | im] \\
 &= E[Y_n^2 | C]P[C | im] + E[Y_n^2 | LC, NC]P[LC | im, NC]P[NC | im] \\
 &= [np_C(1 - p_C) + (np_C)^2] \cdot P[C | im] + [np_{LC}(1 - p_{LC}) + (np_{LC})^2] \cdot P[LC | im, NC] \cdot (1 - P[C | im]),
 \end{aligned}$$

$$Var[Y_n | im] = E[Y_n^2 | im] - (E[Y_n | im])^2,$$

where $P[C|im]$ is the probability of collapse conditioned on the hazard level, which is estimated from the structural response simulated using the lumped plasticity model described in Section 2.4; $E[Y_n | NC, im] = E[Y_n^2 | NC, im] = 0$ assuming that there are no

fatalities if the building has no global or local collapse, and from the expression of conditional variance using first and second moments; $E[Y_n^2 | C, im] = Var[Y_n | C, im] + (E[Y_n | C, im])^2$ for the collapsed case and $E[Y_n^2 | NC, im] = Var[Y_n | NC, im] + (E[Y_n | NC, im])^2$ for the non-collapsed case; and $P[LC|im, NC]$ is the probability of a local collapse given the hazard level and that there is no global collapse. Note that $P[LC|im, NC]$ is equal to $P[TAG_R|im] - P[C|im]$, where values for $P[TAG_R|im]$ and $P[C|im]$ for each benchmark design are given in Table 4.1.

The mean number of fatalities conditioned on the hazard level is calculated from Equation (4.7) and then combined with the hazard function (described in Section 2.3) to compute the expected annual number of fatalities:

$$EANF = \lambda_0 \int_{im} E[Y_n | im] p(IM | im \geq im_{cr}) dim, \quad (4.8)$$

where im_0 refers to a value of IM below which repair cost is probably negligible (here taken as 0.1g), λ_0 is the mean annual rate of events with $IM \geq im_0$; $E[Y_n | im]$ is calculated as in Equation 4.7; and $p(im | IM \geq im_0)$ is the probability density function of damaging IM values, i.e., $p(im | IM \geq im_0) dim$ is the probability that the building will experience $IM = im$, given that it experiences an event with $IM \geq im_0$.

The expected annual number of fatalities has been calculated for the five benchmark building designs, using the fatality probabilities of Shoaf and Seligson (2005) listed in Table 4.4 and the results are given in Table 4.5. The expected annual number of fatalities for designs A, B, C, and E range between 0.0005 and 0.0021. The expected annual number of fatalities increases drastically to 0.023 for design D, which does not include the SCWB provision; this is consistent with 0.024 reported as the annual number of fatalities for a post-Northridge steel moment resisting frame building, assuming various occupancy values in a 24hr period (Yeo and Cornell 2003). The expected loss of life during a seismic event is perhaps the decision variable that owners and policy makers will be most interested in

mitigating. The fatality estimation carried out for the benchmark building provides a methodology for comparing this important value for various building designs, and enables informed decision making during the design process.

Table 4.5 Design variant descriptions and corresponding EANF results.

Design (VID): description	EANF (*10⁻³)
A (VID #1): Baseline perimeter frame design.	1.4
B (VID #3): Same as A, but with code-min strengths.	1.3
C (VID #2): Same as A, but with uniform beam/column throughout.	1.6
D (VID #9): Same as C, but no SCWB provision.	22.8
E (VID #6): Baseline space frame design.	1.0

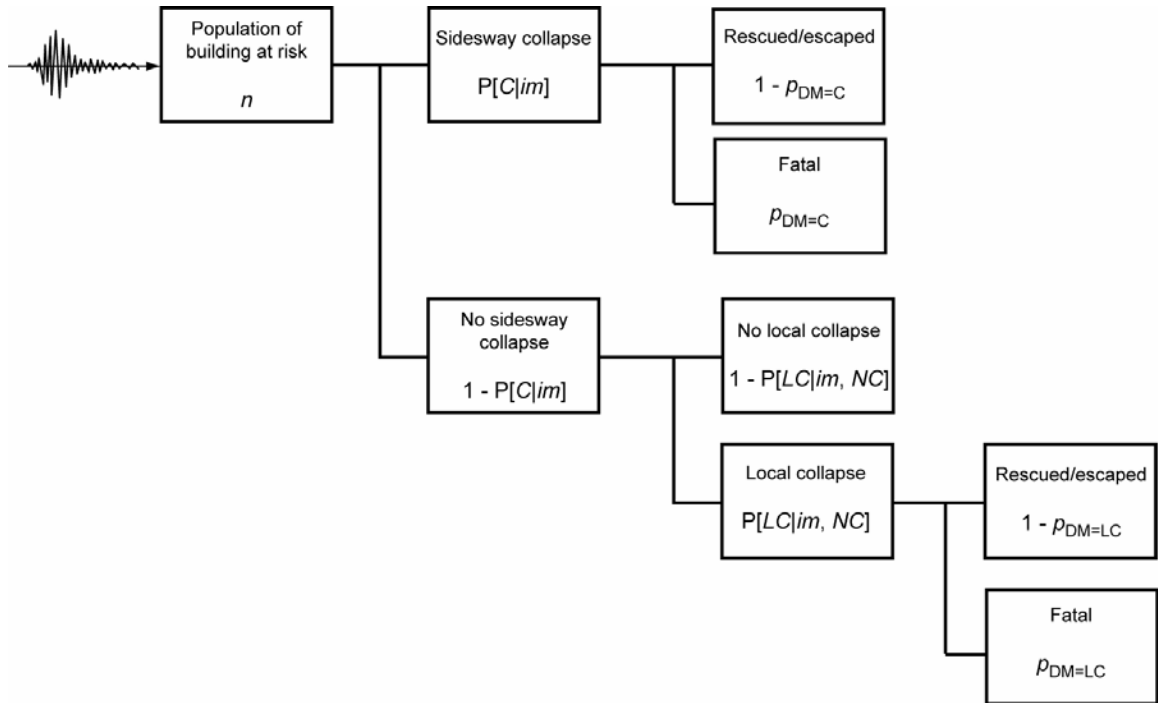


Figure 4.4 Event tree model for fatality estimation of a specific building, considering the probabilities of local and global collapse at every hazard level.

CHAPTER 5

Estimation of Direct Losses

The term *direct loss* is used in this dissertation to represent the building repair cost of earthquake-induced damage, a decision variable of the PBEE framework. The mean total repair cost is calculated by summing the mean repair cost over all damageable components in the building and across all hazard levels. The equations and results for mean total repair cost for each hazard level, that is the vulnerability functions, are given in this chapter. The vulnerability functions are presented for various design and model variants of the benchmark building, and comparisons of these variants are described using the repair cost *DV*. Additionally, the calculation of the dispersion of these results, represented by the coefficient of variation, is also presented in this chapter. The contribution of the damageable building components to total repair cost is represented by a vulnerability function for each of these components. The repair costs and hazard function are used to estimate the expected annual loss, by which is meant the amount one could expect to pay on average every year to repair earthquake damage, considering the uncertain occurrence and severity of earthquakes.

5.1 Procedure for establishing vulnerability functions

The vulnerability functions, a product of the last step of PEER's PBEE methodology, are the relationship between repair costs and shaking intensity level. The vulnerability functions are given by:

$$\begin{aligned}
E[TC | im] &= E[TC | NC, im] \cdot (1 - P[C | im]) + E[TC | C, im] \cdot P[C | im], \\
E[TC^2 | im] &= P(NC | im) \cdot E[TC^2 | NC, im] + P(C | im) \cdot E[TC^2 | im, C], \\
Var[TC | im] &= E[TC^2 | im] - (E[TC | im])^2,
\end{aligned} \tag{5.1}$$

where $E[TC | im]$ is the expected total repair costs conditioned on $IM=im$, $E[TC | C, im]$ is the replacement cost of the structure, and $P[C | im]$ is the probability of collapse, which is estimated from the structural response simulated using the lumped plasticity model described in Section 2.4. Similarly, $E[TC^2 | im]$ is the mean-square of the total repair costs conditioned on $IM=im$ and $Var[TC | im]$ is the variance conditioned on $IM=im$. The expected total repair cost conditioned on the structure not collapsing and on IM , $E[TC | NC, im]$, is calculated by:

$$\begin{aligned}
E[TC | NC, im] &= (1 + C_{OP}) \cdot C_I \cdot C_L \sum_{i=1}^{na} Nu_i \cdot E[RC_i | NC, im], \\
E[RC_i | NC, im] &= \sum_{j=1}^{nds_i} E[RC_i | DM_{ij}] \cdot P[DM_{ij} | NC, im],
\end{aligned} \tag{5.2},(5.3)$$

where C_{OP} , C_I , and C_L are factors to account for contractor overhead and profit, inflation, and location, respectively; na is the number of damageable assembly groups; Nu_i is the number of units in assembly group i ; RC_i is the repair cost for one unit in assembly group i ; and nds_i is the number of damage states for one unit in damageable assembly group i . Note that an assembly group is defined as the set of damageable components of the same type that are sensitive to the same EDP value. Their damage states and repair costs are modeled as perfectly correlated and conditionally independent given EDP from all other assembly groups.

5.2 Component cost distribution for benchmark study

The mean total repair cost given no collapse is the sum of the mean repair costs of the considered structural and nonstructural assembly groups, which is then scaled by inflation,

location, and overhead and profit factors. A breakdown for the mean total repair cost given no collapse against $IM=S_a$ is given in Figure 5.1-Figure 5.6

The cost contribution curves in these figures increase monotonically with increasing S_a for all the building assembly groups except for one; the contribution of paint repair costs plateaus for all of the variants (occurring at about $S_a=0.26g$ for most variants), which is the result of needing to repaint all areas (undamaged or not) to achieve a uniform appearance (Section 3.2.4). The cost to repair beams is greater than the cost to repair columns at most hazard levels for all the variants designed using the SCWB provision, except for Variant #2 (Figure 5.1b). The additional axial load from the heavier structural members in the upper two stories for Variant #2 reduces the flexural capacity of the columns in the first story, which results in costlier repairs for the columns than for the beams. Variant #9, which ignores the SCWB provision, is expected to have more yielding and costlier repair efforts in its columns (rather than for its beams), which is shown to be true in Figure 5.3a.

These cost contribution figures demonstrate that the contribution of wallboard partitions is significant for all hazards levels and that the contributions of glazing, column-slab connections, sprinkler piping, ceilings and elevators do not play a major role in the total repair costs. The largest repair loss for nonstructural components over most hazard levels corresponds to the non-code-conforming design for $S_a < 0.44g$ (Variant #9, Figure 5.3a) and to the minimum-code design (Variants #3) for $0.44g \leq S_a \leq 0.82$ (Figure 5.6b); the smallest repair loss for nonstructural components for $S_a \leq 0.82$ corresponds to the space-frame design (Variant #6, Figure 5.6b) and to the design that uses the same beams and columns throughout the height of the building (Variant #2, Figure 5.1b and Figure 5.6b). The lumped plasticity models with a secant stiffness through the yield moment (Variant #13, Figure 5.4b) and through 60% of the yield moment (Variant #14, Figure 5.5a) do not accurately predict the structural response at low levels of ground shaking and leads to large economic losses for the nonstructural components, which are the most likely damaged components at these levels. Note that the losses due to damaged wallboard partitions are comparable to the losses associated with structural damage for the space-frame design

(Variant #6, Figure 5.2b); this is because the number of lateral resisting frames is greater in the space-frame design, which gives a large increase in repair costs of beams and columns for this variant at higher hazard levels (Figure 5.6a), while the wallboard partition losses are reduced compared with the baseline perimeter-frame design (Variant #1, Figure 5.1a).

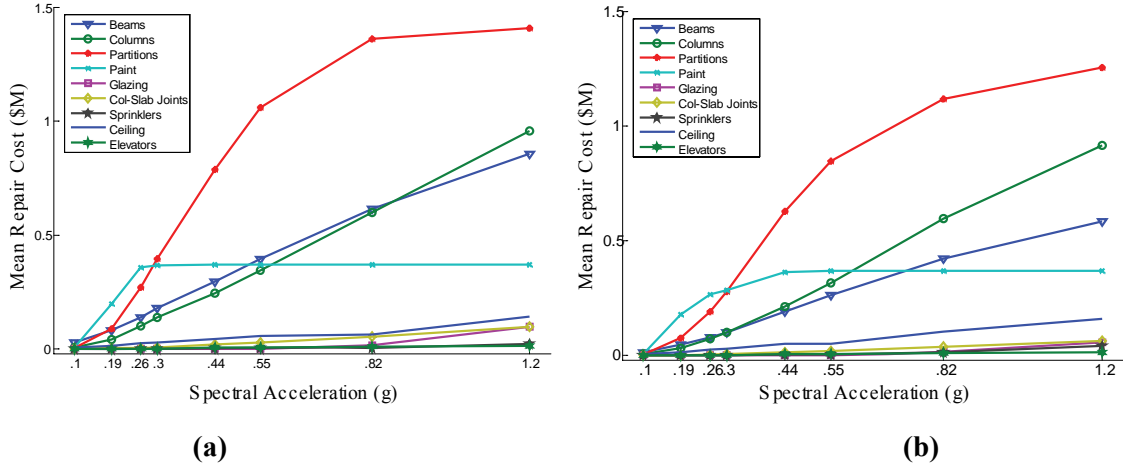


Figure 5.1 Contributions to mean total repair cost for (a) variant #1, and (b) variant #2.

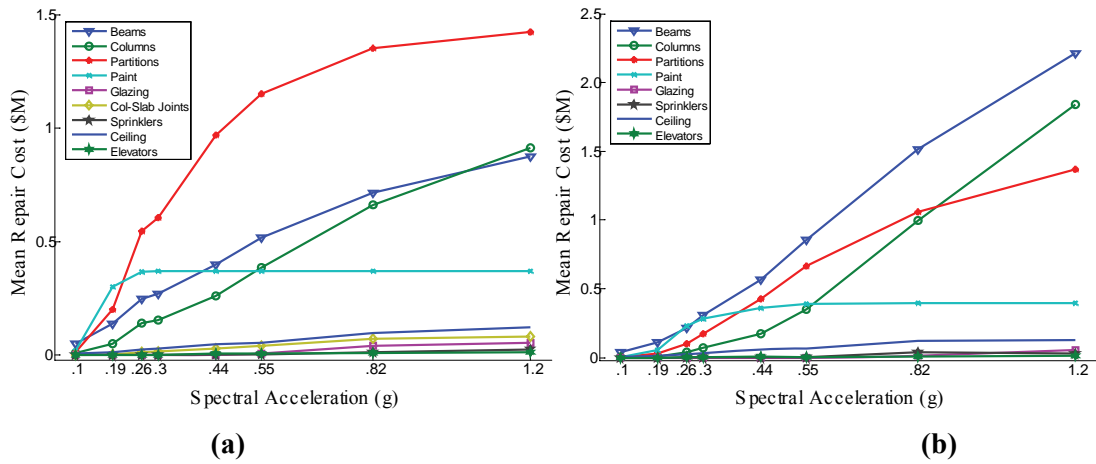


Figure 5.2 Contributions to mean total repair cost for (a) variant #3, and (b) variant #6.

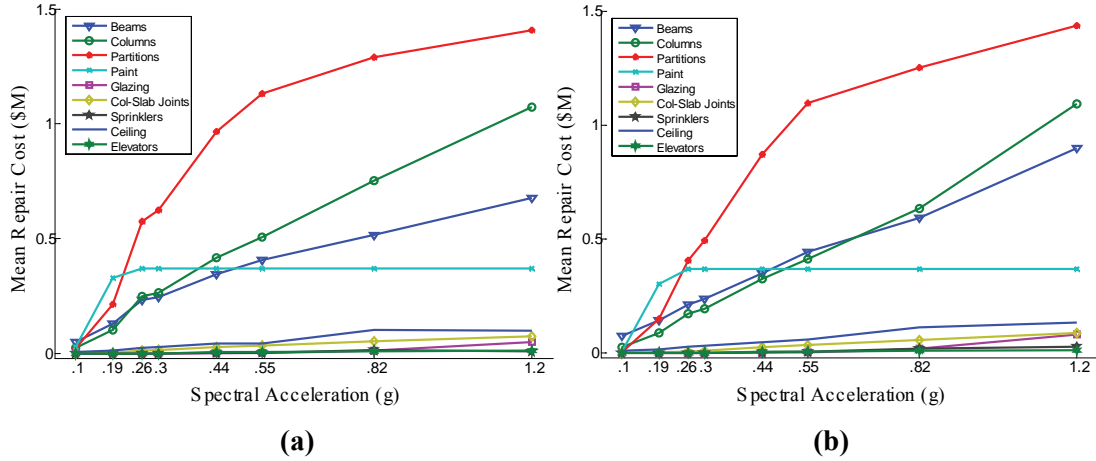


Figure 5.3 Contributions to mean total repair cost for (a) variant #9, and (b) variant #11.

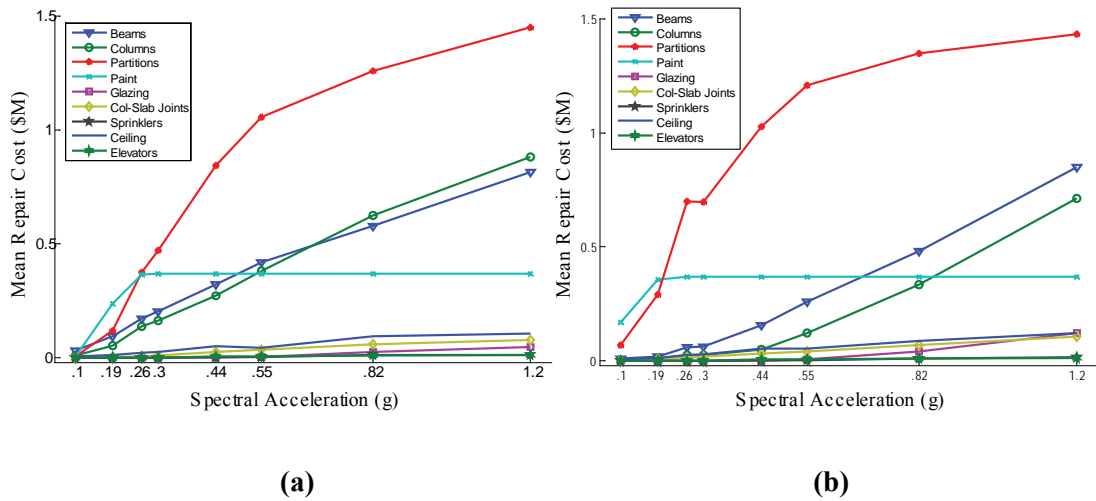


Figure 5.4 Contributions to mean total repair cost for (a) variant #12, and (b) variant #13.

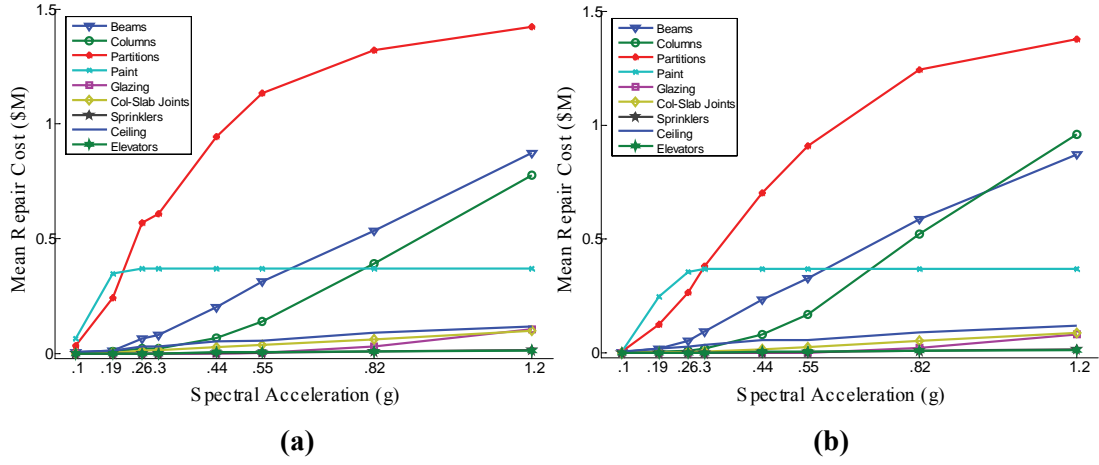
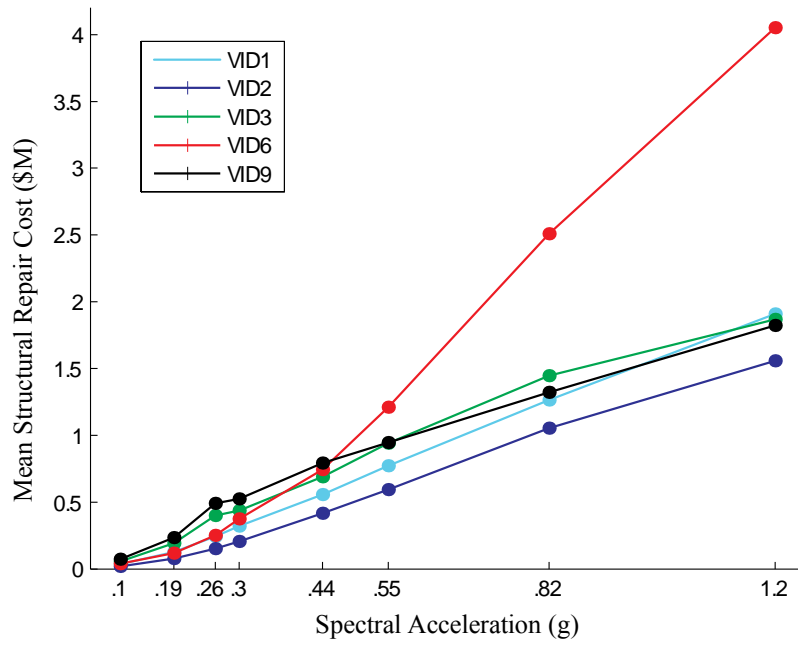
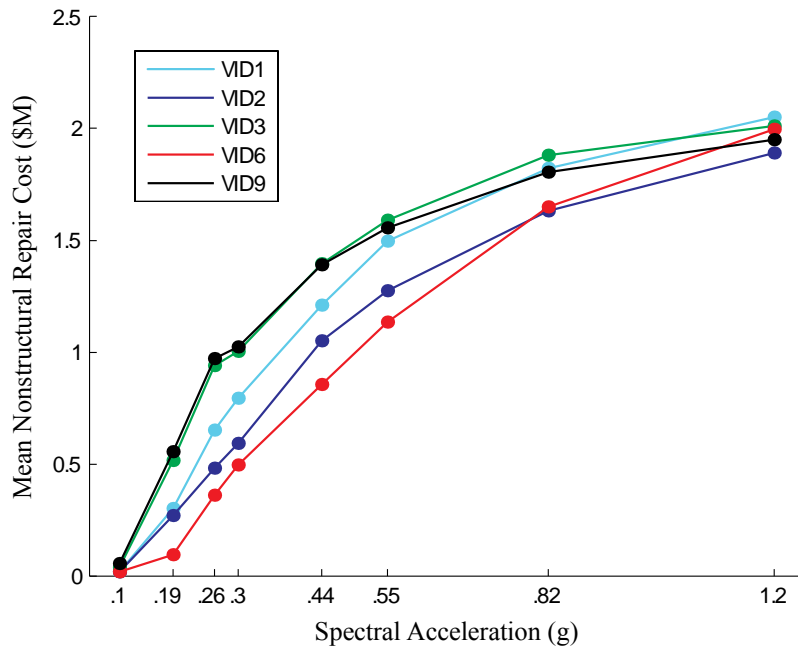


Figure 5.5 Contributions to mean total repair cost for (a) variant #14, and (b) variant #15.



(a)



(b)

Figure 5.6 Design comparisons of mean repair costs for (a) all structural components, and (b) all nonstructural components.

5.3 Results of vulnerability functions for benchmark study

The vulnerability functions for the design variants are shown and discussed in Sections 5.3.1 and 5.3.2 below.

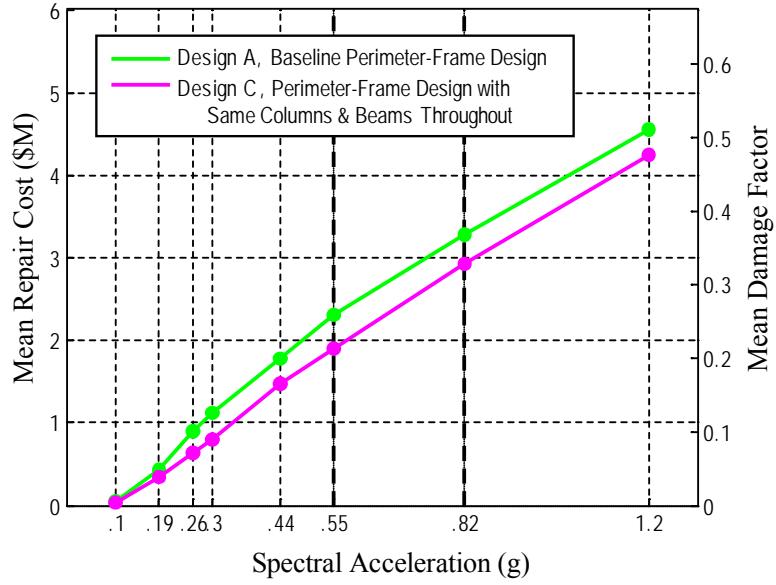
5.3.1 Results for design comparisons

The vulnerability functions (using $C_{op}=0.175$; $C_i=1.13$; and $C_L=1.085$) for variants having different structural designs are shown in Figure 5.7 and Figure 5.8, where the black dashed vertical lines at $S_a = 0.55g$ and $S_a = 0.82g$ correspond to the 10%-in-50yr event (475 year return period) and the 2%-in-50yr event (2475 year return period), respectively, for the site. The mean total repair cost is represented in these figures as \$USD and as a ratio over the mean building replacement cost, known as *mean damage factor*. The replacement cost is kept the same for all perimeter-frame variants. Some interesting comparisons of design choices are made from these results.

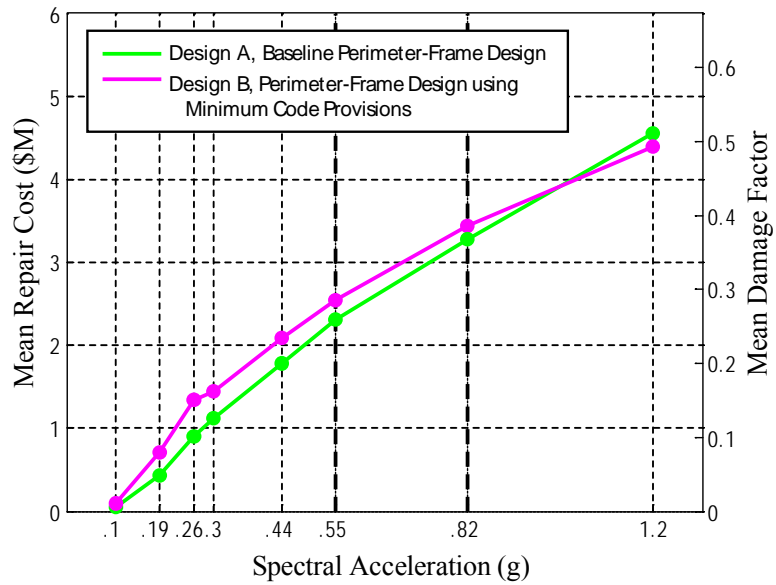
In Figure 5.7(a), the curve for Variant #1 (Design A) corresponds to a perimeter-moment-frame design, considering the gravity frame and a flexible base; the curve for Variant #2 (Design C) corresponds to a similar structural model except the structural design uses the same beams and columns throughout, which makes the structure stiffer and more conservative. This more conservative design variant has smaller structural responses and thus smaller mean losses, at every level of S_a . Another interesting comparison in Figure 5.7(b) shows the vulnerability functions for Variants #1 (Design A) and #3 (Design B). These variants are both perimeter-frame designs, except Variant #3 is a code-minimum design. The code-minimum design has higher losses for every level of S_a , except at $S_a=1.0g$ because losses associated with building collapse significantly contribute to mean total repair cost at this hazard level, and because the probability of collapse for the code-minimum design is smaller than for the baseline design at this level.

In Figure 5.8(a), the curve corresponding to Variant #1 (Design A), the perimeter-moment-frame baseline design, is shown along with the curve for Variant #6 (Design E) corresponding to the space-frame baseline design. Since up-front costs are significantly different for these designs, the vulnerability function is only plotted using the mean damage factor when comparing these two variants. The space-frame design should better withstand lateral motions since it has lateral force-resisting moment frames on every grid line, which is consistent with Figure 5.8(a) up until $S_a = 0.55g$. The beams and columns are heavily damaged at the two highest hazard levels for simulation ($S_a = 0.82g$ and $S_a = 1.2g$) and because there are more of them to repair in the space-frame design than there are in the perimeter-frame design, their contributions to the total repair cost dominate the contributions of the other damageable components. In fact, the contribution to mean total repair cost from the beams surpasses that of the partitions in the space-frame design at all levels of S_a , which does not occur in any of the perimeter-frame variants.

One building design, Variant #9, was chosen to investigate the importance of the strong-column weak-beam design provision (ACI 2002). Figure 5.8(b) shows this design (Design D) in addition to its code-conforming counterpart, Variant #2 (Design C). The losses increase at every hazard level when the SCWB provision is ignored. In fact, the largest value of mean repair cost is 1.5 times larger than the mean repair cost for any of the other designs considered in this section. This comparison is also significant for the expected annual loss, which is found in Section 5.4.

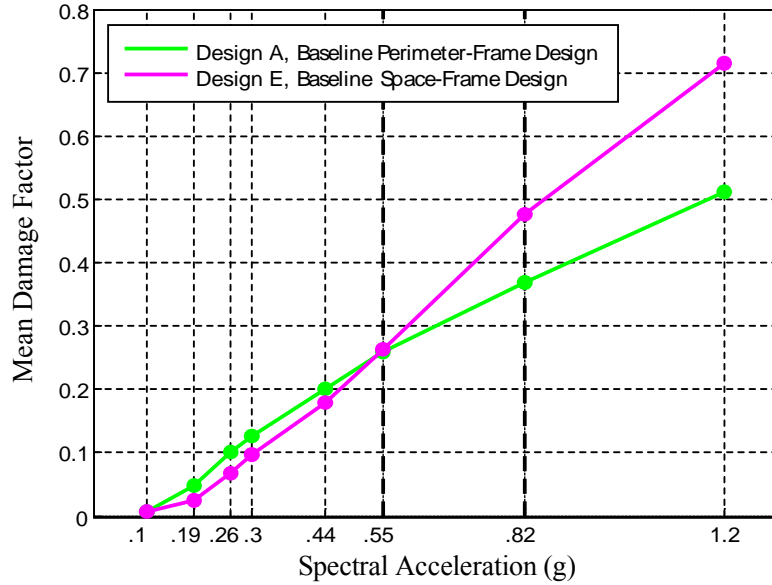


(a)

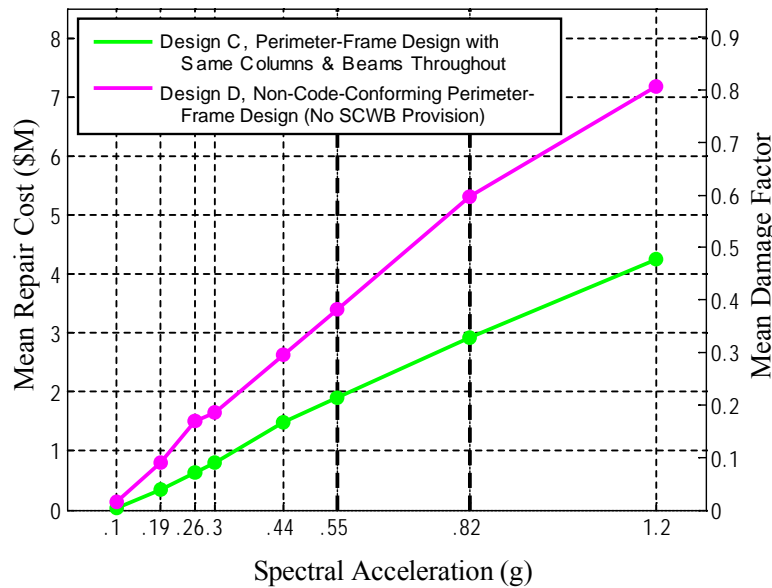


(b)

Figure 5.7 (a) Vulnerability functions for variants #1 and #2, and (b) for variants #1 and #3.



(a)



(b)

Figure 5.8 (a) Vulnerability functions for variants #1 and #6, and (b) for variants #2 and #9.

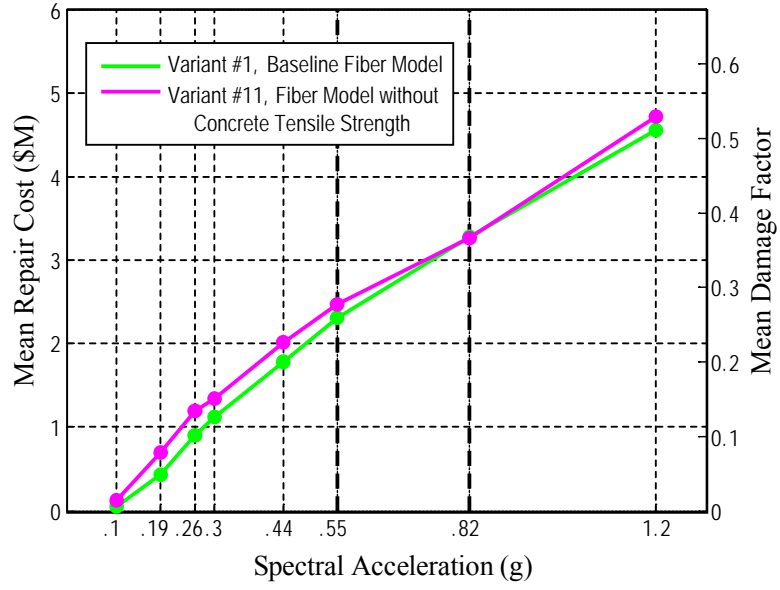
5.3.2 Results for modeling comparisons

The vulnerability functions for variants having the same design (Design A), but different structural models are shown in Figure 5.9 and Figure 5.10, where, again the black dashed

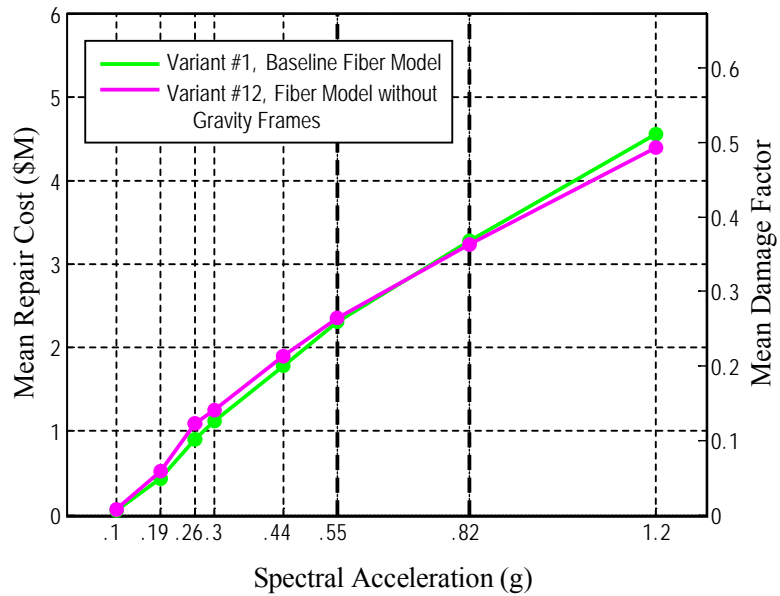
vertical lines correspond to the 10%-in-50yr and the 2%-in-50yr events. Some interesting comparisons are made from the results of variants with varied modeling choices.

In Figure 5.9(a), the curve for Variant #11 corresponds to a perimeter-moment-frame design excluding the tensile strength of the concrete. This structural model assumes that all the concrete is pre-cracked and therefore is expected not to perform as well as the perimeter-frame baseline model (Variant #1), which has smaller mean losses at every level of S_a except at $S_a = 0.82g$, where they are close numerically. A comparison of Variants #1 and #12 (Figure 5.9b) shows the significance of modeling the gravity frame. Variant #1 includes the gravity frame in the model, which adds stiffness and strength relative to Variant #12, which ignores the gravity frame. One would expect to see larger structural responses without the gravity frame (Variant #12), and thus larger mean losses; this expectation is borne out in Figure 5.9(b), except at the largest hazard levels.

In Figure 5.10, the curve for Variant #13 corresponds to the baseline perimeter-moment-frame design using a lumped-plasticity model with initial stiffness defined as the secant stiffness through the yield point (K_{yld}); the curves for Variants #14 and #15 correspond to a similar design except that the initial stiffness is defined as the secant stiffness that respectively correspond to 60% and 40% of the yield moment (K_{stf}); Variant #1 is given again in this plot to compare the baseline-fiber model with these lumped-plasticity models. Note that the fiber model results are consistent with the ones from the lumped plasticity model using K_{stf} until $S_a = 0.19g$, where the two curves diverge and the mean total repair costs become greater than for the fiber model for all values of $S_a > 0.19g$. This is consistent with the behavior shown in the static pushover curves in Figure 2.8. The lumped-plasticity models using K_{yld} and a secant stiffness corresponding to 60% of the yield moment result in greater losses at low levels of ground shaking and lower losses at higher levels of ground shaking; this switch occurs near $S_a = 0.30g$.



(a)



(b)

Figure 5.9 (a) Vulnerability curves for variants #1 and #11, and (b) for variants #1 and #12.

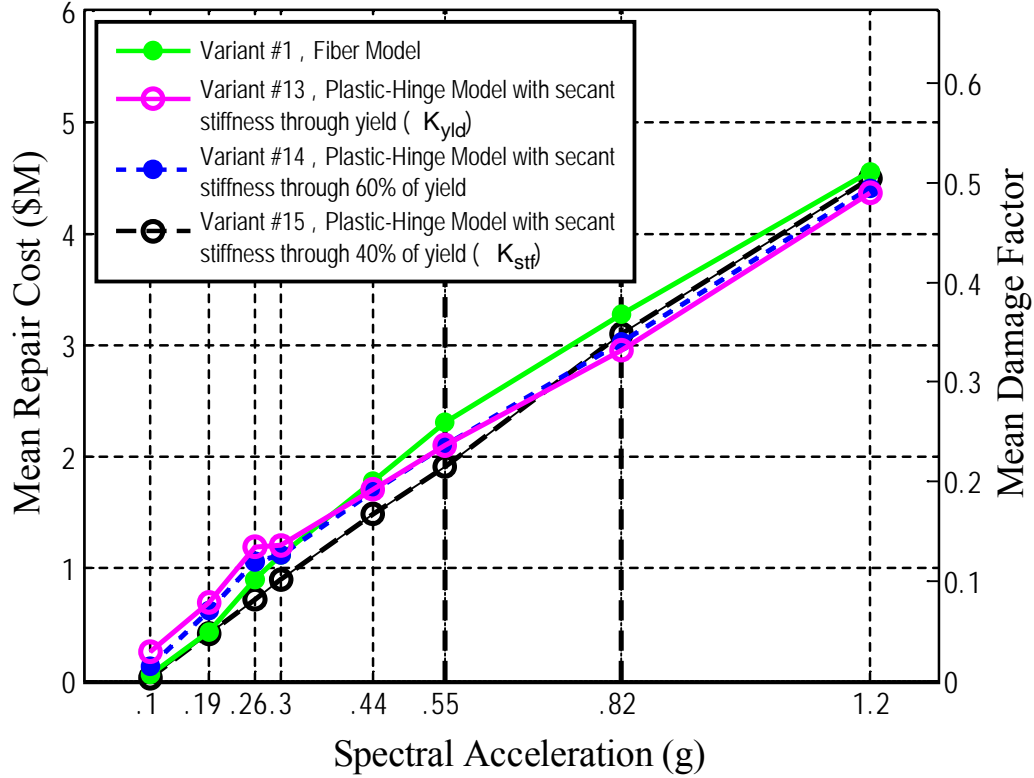


Figure 5.10 Vulnerability curves for variants #1, #13, #14 and #15.

5.4 Calculation of expected annual loss due to repairs

The expected annual loss (EAL) is calculated consistently with other researchers (e.g. Porter et al. 2004a, Baker and Cornell 2003) as the product of the mean total rate of occurrence of events of interest and the mean loss conditional on an event of interest occurring, which may be expressed as:

$$EAL = \lambda_0 \int E[TC | im] p(im | IM \geq im_0) dim, \quad (5.4)$$

where im_0 refers to a value of IM below which repair cost is probably negligible (here taken as 0.1g), λ_0 is the mean annual rate of events with $IM \geq im_0$; $E[TC | im]$ is calculated as in Equation 2.4; and $p(im | IM \geq im_0)$ is the probability density function of damaging IM values, i.e., $p(im | IM \geq im_0) dim$ is the probability that the building will experience

$IM \in [im, im + dim]$, given that it experiences an event with $IM \geq im_0$. The EAL results for the benchmark building are given in Table 5.1.

5.4.1 Disaggregation of EAL

The expected annual loss can be disaggregated to illustrate the major contributors to loss across the hazard levels. A disaggregation of the *EAL* for design A (VID #1), given in Figure 5.11, shows that the beams/columns (31%), wallboard partitions (30%), and interior paint (34%) are the major contributors to *EAL*; the remaining nonstructural elements combined contribute only a mere 4% to *EAL* and the contribution from building collapse is 1%.

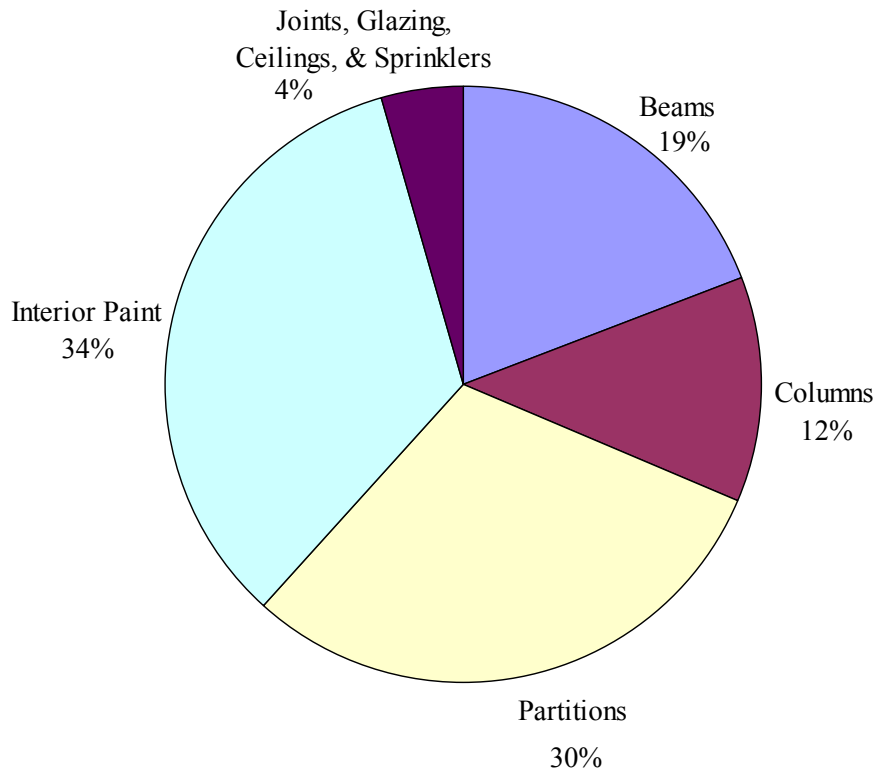


Figure 5.11 A disaggregation of the expected annual loss for Design A (VID #1).

Table 5.1 Design variant descriptions and corresponding EAL results.

Design and Model Descriptions	$Sa(T_I)$	Mean Total Repair Cost for Sa (g) in \$M								EAL (\$)
		Coefficient of Variation of Repair Cost								
		0.1	0.19	0.26	0.3	0.44	0.55	0.82	1.2	
Design A (VID #1): Perimeter frame, designed with expected overstrength; fiber model, concrete tensile strength modeled, gravity frame included.	Mean	0.06	0.43	0.9	1.12	1.78	2.31	3.28	4.56	66,585
	COV	0.52	0.17	0.15	0.16	0.2	0.24	0.33	0.36	
Design C (VID #2): Same as Design A, but designed with uniform beams and columns over height; modeled same as VID # 1.	Mean	0.04	0.35	0.64	0.8	1.48	1.9	2.92	4.25	51,933
	COV	0.62	0.18	0.16	0.17	0.21	0.27	0.41	0.46	
Design B (VID #3): Same as Design A, but designed with bare code-minimum strengths; modeled same as VID # 1.	Mean	0.1	0.71	1.34	1.44	2.09	2.54	3.43	4.39	95,656
	COV	0.37	0.13	0.12	0.12	0.11	0.13	0.23	0.35	
Design E (VID #6): Baseline space frame; fiber model, concrete tensile strength modeled.	Mean	0.06	0.22	0.61	0.87	1.6	2.36	4.29	6.43	49,422
	COV	0.51	0.25	0.15	0.14	0.16	0.17	0.19	0.16	
Design D (VID #9): Same as Design C, but no SCWB provision enforced (not code-conforming); modeled same as VID # 1.	Mean	0.13	0.8	1.51	1.64	2.63	3.41	5.31	7.18	112,930
	COV	0.36	0.33	0.4	0.51	0.64	0.66	0.53	0.34	
Design A (VID #11): Same as Design A; modeled same as VID # 1, but concrete tensile strength and stiffness not modeled.	Mean	0.12	0.7	1.19	1.34	2.01	2.47	3.26	4.72	92,721
	COV	0.35	0.13	0.13	0.14	0.18	0.22	0.33	0.33	
Design A (VID #12): Same as Design A; modeled same as VID # 1, but gravity frame not modeled.	Mean	0.06	0.52	1.09	1.25	1.9	2.35	3.23	4.39	76,069
	COV	0.49	0.15	0.14	0.15	0.19	0.23	0.34	0.38	
Design A (VID #13): Same as Design A; lumped-plasticity model with secant stiffness through yield (K_{yld}).	Mean	0.26	0.69	1.20	1.20	1.71	2.11	2.96	4.37	97,066
	COV	0.18	0.16	0.15	0.16	0.21	0.26	0.38	0.39	
Design A (VID #14): Same as Design A; lumped-plasticity model, with secant stiffness through 60% of yield.	Mean	0.12	0.63	1.07	1.13	1.69	2.11	3.03	4.41	82,433
	COV	0.29	0.15	0.15	0.17	0.21	0.26	0.37	0.38	
Design A (VID #15): Same as Design A; lumped-plasticity model with secant stiffness through 40% of yield (K_{stf}).	Mean	0.03	0.42	0.72	0.91	1.49	1.91	3.11	4.50	57,363
	COV	0.75	0.17	0.17	0.19	0.25	0.3	0.36	0.37	

5.4.2 Discussion of results

Based on the EAL in Table 5.1, the potential for financial loss is considerable. Loss modeling considering the moment-frame beams and columns, the column-slab connections, the wallboard partitions, the acoustical ceiling, the sprinkler piping, the exterior glazing, and the interior paint, indicates that mean annual losses from earthquakes are likely to be in the range of \$52,000 to \$97,000 for the various code-conforming benchmark building designs, or roughly 1% of the replacement cost of the building. Some important lessons learned from these simulations that may be transferable to other projects include the following:

- Expected annual loss (EAL) estimates are highly sensitive to the manner of estimating the initial stiffness of the structural elements. The EAL for the baseline perimeter-frame model using the fiber model is \$66,600 (0.75% of replacement cost); the EAL for the same design using the lumped plasticity model with secant stiffness through yield (K_{yld}) is \$97,100 (1.1% of replacement cost); the EAL using a secant stiffness through 60% and 40% of yield (K_{stf}) is \$82,400, and \$57,400, (0.9%, and 0.6% of replacement cost), respectively. If a lumped-plasticity approach is used to model structural behavior, the initial stiffness of the hinge element should be calibrated to test data and chosen carefully (similar to K_{stf}) to better model the building stiffness under frequent ground motions.
- Losses are sensitive to other modeling choices. If the tensile strength of the concrete is ignored by assuming all pre-cracked concrete (Variant #11) (this changes the initial stiffness of the element model), there is an increase of almost 40% in *EAL*. If the gravity frame is ignored in the structural model (Variant #12), thus neglecting the contribution of its strength and stiffness, there is an increase of almost 15% in *EAL*.

- Variant #2 (design C), a more conservative design than Variant #1 (design A) because it uses the same beams and columns throughout the building, produces an *EAL* that is 22% smaller. Variant #3 (design B), a code-minimum design, produces an *EAL* that is 44% larger.
- The strong-column weak-beam provisions are ignored for Variant #9 (design D), which drastically increases the *EAL* of the baseline model (Variant #1, design A) by 70%.

CHAPTER 6

Estimation of Indirect Losses and Benefit-Cost Analysis

After an earthquake, the repair cost will not be the only “loss” suffered by building stakeholders. The previous chapter focuses on *direct losses*, a term used in this work to represent the losses caused by an earthquake that arise from the repair effort needed to return a damaged building to its undamaged state. In a sizeable earthquake, there will likely also be some *indirect losses*, due to business interruption during the repair effort (described in this chapter), building closure taken as a safety precaution (detailed in Section 4.1), and human casualties caused by building failures during the seismic event (detailed in Section 4.2). This chapter outlines the methodology for estimating two types of indirect economic losses that are identified by PEER as decision variables of interest in their proposed PBEE methodology, those produced by building downtime and by human fatalities. The losses due to downtime and human fatalities are then added to the building repair cost calculated in Chapter 5 in order to estimate the total building loss, which is then used to perform a benefit-cost analysis of the benchmark building.

6.1 Building downtime

Building downtime is defined in this dissertation as the period of time between the occurrence of a seismic event and the completion of the building repair effort. There are various factors that can affect building downtime: building inspection, damage assessment, finance planning, architect/engineering consultations, a possible competitive bidding process, and the repair effort needed to return a building back to its undamaged state (Comerio 2006). One portion of downtime is attributed to the time needed to repair building damages and is considered as the *rational* component of building downtime (Comerio 2006). Although seemingly straightforward, this repair effort is contingent on the repair scheme and will vary from one owner to another. In this work, the rational component of downtime is estimated using a methodology modified from a repair-time model introduced by Beck et al. (1999), which considered several repair schemes for the purpose of calculating building life-cycle costs. The remaining portion of building downtime is difficult to model because it is highly dependent on *irrational* components, which include financing, relocation of functions, human resources, and economic and regulatory uncertainty (terminology as defined in Comerio (2006) and used here for consistency). Comerio proposes a downtime model for these irrational factors that is a function of the percentage of damaged building stock (2006). The downtime estimation model proposed in this thesis builds on this previous study on downtime and was developed to fit within the context of PEER's PBEE framework by exploiting the results from its hazard, structural, damage, and loss analysis modules.

6.1.1 Rational components of downtime

As described in Section 3.2, fragility functions describe the probability of realizing or exceeding a damage state given an appropriate EDP for each damageable building component. Each of these damage states is associated with a particular repair effort that is described by cost (dollar amount needed to cover the labor, material, equipment and overhead costs to repair the damaged component) and time (crew hours needed to complete

this repair effort). The former category of the repair effort (construction cost) is a direct loss, and is detailed in Chapter 5. The latter category of the repair effort, the time needed to repair building damage caused by an earthquake, is estimated in this chapter using the output of the damage analysis (Chapter 3) and repair times determined by a professional cost estimator (Hecksher 2006).

The repair duration for each damageable building assembly group is dependent on the repair crew and particulars of the damage; therefore, these durations should be treated as uncertain. Probability distributions for these uncertain durations were developed using the means and 90th percentiles of the repair times, provided by the professional cost estimator (Hecksher 2006) for the benchmark building assembly groups (these parameters are listed in Table 6.1). The expected repair time for the i^{th} assembly group, located in operational unit m (e.g., a rental unit), conditioned on IM and the structure not collapsing, $E[R_i(m) | NC, im]$, is calculated using an equation modified from Beck et al. (1999) by:

$$E[R_i(m) | NC, im] = Nu_i(m) \cdot E[R_i | NC, im] / w, \quad (6.1), (6.2)$$

$$E[R_i | NC, im] = \sum_{j=1}^{nds_i} E[R_i | DM_{ij}] \cdot P[DM_{ij} | NC, im],$$

where $R_i(m)$ is the repair time required to return all units of assembly group i , located in operational unit m , to their undamaged state, which is measured in days from the beginning of the repair effort; $Nu_i(m)$ is the number of units in assembly group i located in operational unit m ; R_i is the repair time for one unit of assembly type i , measured in hours; nds_i is the number of damage states for damageable component group i ; $w = \#$ workday hours (i.e., 8 hours for daytime crews and 7 hours for nighttime crews); DM_{ij} is damage state j for a given building for component of type i ; and $P[DM_{ij} | NC, im]$, is the probability of reaching (or exceeding) the damage state j for a given building component, conditioned on the structure not collapsing (NC) and on a given IM level. Again, note that an assembly group is defined as the set of damageable components of the same type that are sensitive to the same EDP . As with repair cost estimates, the damage states and repair times within an

assembly group are modeled as perfectly correlated and conditionally independent, given *EDP*, from all other assembly groups.

Table 6.1 Summary of damage states and associated repair-time parameters for benchmark building's damageable assemblies (Hecksher 2006).

Assembly Description	Unit	Damage State	Repair Effort	Repair Time Parameters	
				mean (hr)	90 th percentile (hr)
Ductile CIP RC beams	ea	light	epoxy	44.0	60.0
Ductile CIP RC beams	ea	moderate	jacket	190.0	240.0
Ductile CIP RC beams	ea	severe	replace	240.0	320.0
Ductile CIP RC beams	ea	collapse	replace	240.0	320.0
Ductile CIP RC columns	ea	light	epoxy	36.0	50.0
Ductile CIP RC columns	ea	moderate	jacket	150.0	200.0
Ductile CIP RC columns	ea	severe	replace	220.0	300.0
Ductile CIP RC columns	ea	collapse	replace	220.0	300.0
Column-slab connections	ea	light cracking	patch	2.3	2.5
Column-slab connections	ea	severe cracking	epoxy	12.0	15.0
Column-slab connections	ea	punching shear failure	replace	130.0	180.0
Drywall partition	64 ft ²	visible	patch	1.0	2.0
Drywall partition	64 ft ²	significant	replace	4.0	5.0
Drywall finish	64 ft ²	visible	patch	1.0	2.0
Drywall finish	64 ft ²	significant	replace	7.0	8.0
Exterior glazing	pane	crack	replace	11.5	15.0
Exterior glazing	pane	fallout	replace	11.5	15.0
Acoustical ceiling	250 ft ²	collapse	replace	0.2	0.4
Automatic sprinklers	12 ft	fracture	replace	15.0	18.0
Hydraulic elevators	ea	failure	repair	60.0	80.0

6.1.2 Irrational components of downtime

The previous section describes the process for calculating the repair times for each assembly group given their damage states. In addition, the total downtime of a building after a seismic event will include irrational components, such as the time accounting for

damage assessment, consultations with professional engineers, and the contractor bidding process before repairs can begin. This time delay caused by these irrational factors before construction begins is termed *mobilization time*. Because permit data does not include information about the purpose of earthquake-related repairs, it is difficult to distinguish between the mobilization time and the total building downtime caused by earthquake-related damage from available empirical data. Although constrained by the quality of available data, Comerio has performed various case-study efforts to help identify and quantify the various components of downtime (Comerio 2000, 2006; Blecher and Comerio 2007).

In a recent study, Comerio (2006) investigated the repair efforts at Stanford University after the Loma Prieta earthquake; after this earthquake, 25 buildings (of about 400 on the campus) were closed by building officials because they had excessive damage and a few others that were not damaged by the earthquake were also closed because they were made of unreinforced masonry. The repair times for the closed buildings on campus ranged from 0.4 to 2.6 years, and the total downtime for these ranged between 0.9 and 9.3 years. This gap between repair time and total downtime suggests that the irrational components of downtime require serious consideration. These results show that the building downtimes for the Stanford campus fall into three identified categories: the quickly repaired (40% of the closed buildings had a downtime of 3 years or less), the medium-term repaired (41% of the closed buildings had a downtime of 4-8 years), and the permanently closed (the remaining 19% of the closed buildings were permanently closed or demolished). The buildings requiring medium-term repair times were found to require this longer duration because of negotiations between the university and FEMA regarding the repair schemes for these buildings (Comerio 2006).

The anecdotal evidence from this study may be unique to a university campus setting where the relocation of occupants was alleviated by the large stock of buildings on the campus; this scenario allowed the university to prioritize the repair of some buildings over others, yielding the wide range of delay times before construction. This strategy for relocation and prioritizing of repairs may also be applied to buildings owners with large

stocks of commercial or residential buildings. However, one clear distinction should be made between the buildings on a university campus and those that are privately owned—an owner may not depend on government funding when making decisions about the repair effort of their damaged building(s). In fact, some commercial leases for high-end real estate include a clause that obliges the owner to repair damages to the building within a set period of time, e.g., 270 days is a typical period (Comerio 2006). If this amount of time is not feasible for the needed repairs of the earthquake damage, the owner is expected to promptly disclose this information to the leasee and terminate the lease agreement. This particular clause in a lease may motivate owners to quickly repair earthquake damage to their commercial buildings in order to avoid losing their current tenants. Keeping in mind the needs of commercial-building owners, the mobilization time for the high-priority buildings on the Stanford campus were used to inform the initial delay of construction for the benchmark building downtime estimates in the following section.

6.1.3 Methodology and example of downtime losses

The rational and irrational components of downtime, presented in Sections 6.1.1 and 6.1.2, respectively, have both been shown to be significant and must be considered in a realistic downtime estimate. The total downtime estimate is dependent on the repair scheme chosen by the building owner. The slow-track (components are repaired serially) and fast-track (components are repaired in parallel) repair schemes of Beck et al. (1999) were presented to a professional cost estimator as bounding cases for possible repair schemes; the fast-track repair method was deemed more realistic for current practice and is used in the following to estimate total building downtime. An example of the fast-track repair scheme for a 3-story steel frame building simulated in Beck et al. (1999) is shown in Figure 6.1.

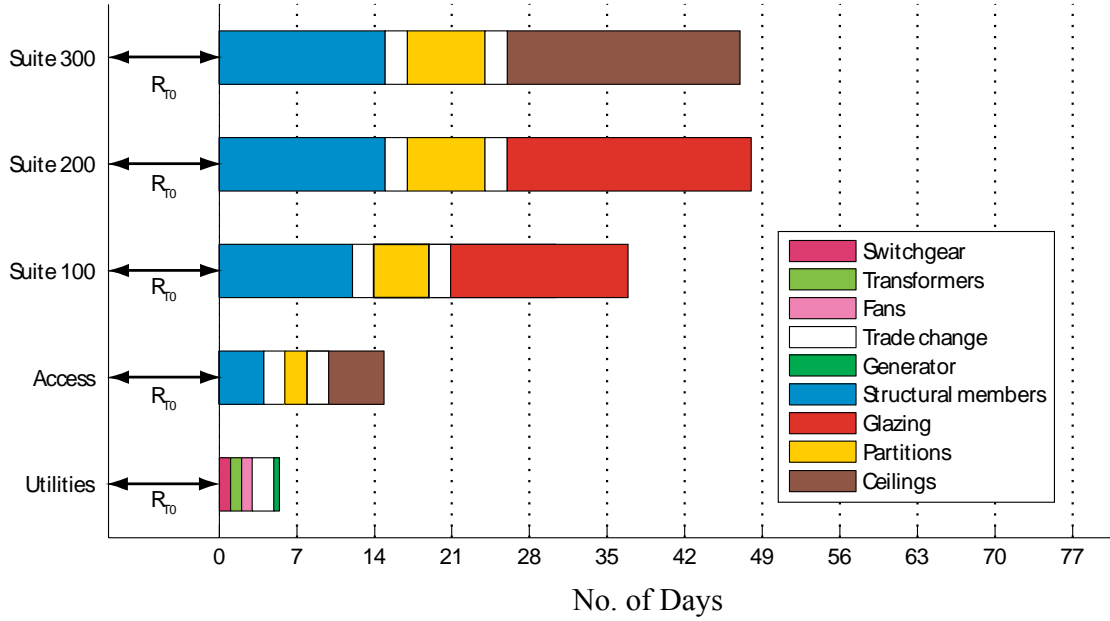


Figure 6.1 Gantt chart for fast-track repair scheme applied to an example 3-story steel frame building (reproduced from Beck et al. 1999).

For the benchmark building, each floor is considered as an operational unit. The mean total repair time conditioned on the structure not collapsing and on IM , $E[R_T | NC, im]$, is calculated by summing the downtime for each of the four operational units considered for the benchmark building, along with the change-of-trade delays and the initial mobilization delay:

$$E[R_T | NC, im] = \max\{E[R_U(m) | NC, im], m = 1, \dots, 4\},$$

$$E[R_U(m) | NC, im] = \max\{E[R_U^*(1) | NC, im], E[R_U^*(m) | NC, im]\} + E[R_{T0} | NC, im], \quad (6.3), (6.4), (6.5)$$

$$E[R_U^*(m) | NC, im] = \sum_{i=1}^{na(m)} E[R_i(m) | NC, im] + N_T(m) \cdot E[R_{COT}],$$

where $E[R_U(m) | NC, im]$ is the mean total downtime in days for operational unit $m \in \{1, \dots, 4\}$ (it is assumed that the ground floor must be operational for access to the upper stories); $E[R_U^*(m) | NC, im]$ is the mean repair time for operational unit m measured in calendar days from the date on which repair work is begun anywhere in the facility; $na(m)$

is the number of assembly groups in unit m ; $E[R_i(m) | NC, im]$ is as calculated in Equation (6.1); $N_T(m)$ is the number of changes of trade in repairing unit m ; R_{COT} is the change-of-trade delay (assumed to be the same for each trade, at least in the mean); and R_{T0} is the initial delay before construction begins (mobilization time). The change-of-trade delay depends on the complexity of the repair effort, the availability of labor, and the local economy. The estimates of the duration of this delay range from 2 days for the fast-track repair scheme to 2 weeks for the slow-track repair scheme (Beck et al. 1999); since the fast-track repair scheme is adopted for downtime estimation in this work, the 2-day duration is used as the expected value of the change-of-trade delay.

The expected value of mobilization time is not as straight forward to calculate as the other two components of building downtime. As described in Section 6.1.2, this initial time delay may include damage assessment, engineering inspections and preparation of drawings for repairs, and a possible bidding process for the construction work. Several methods for estimating mobilization times were considered. The one method that best exploits the results from the damage analysis and the available empirical data is a model for these mobilization delays conditioned on the results of the virtual inspector results (Section 4.1.2). If a building is green tagged, it is deemed safe to inhabit and will likely not require much mobilization time. For this scenario, the mobilization time is assumed to be equal to the time from the occurrence of the earthquake until a building is inspected, because building owners may not feel comfortable letting tenants back into a building until building officials deem the building safe to occupy. If a building is yellow tagged, the owner must take on the responsibility of hiring an engineer to perform a more detailed evaluation, as described in Section 4.1.1. The delay associated with waiting for the engineer to perform a detailed inspection will vary from owner to owner since it will depend on the owner's relationship with the engineer and their financial standing; this delay is highly variable and difficult to approximate from the available empirical data. If a building is red tagged, it is unsafe to inhabit the building and will likely require demolition or extensive repairs. The mobilization delay for those buildings that are red tagged and not demolished/replaced is substantial (Comerio 2006). The theorem of total probability is used to estimate the

expected total mobilization time conditioned on the building safety-tagging results of the virtual inspector:

$$\begin{aligned}
 E[R_{TO} | NC, im] &= E[R_{TO} | TAG_G] \cdot P(TAG_G | NC, im) \\
 &+ E[R_{TO} | TAG_Y] \cdot P(TAG_Y | NC, im) \\
 &+ E[R_{TO} | TAG_R] \cdot P(TAG_R | NC, im).
 \end{aligned} \tag{6.6}$$

The value of $E[R_{TO} | TAG_G]$ for the benchmark building is taken to be 10 days, which is estimated from inspection times of over 700 buildings inspected after the Loma Prieta earthquake; these data were made available by Blecher and Comerio, who are studying building-inspector survey data and assessor data collected by ABAG (2006).¹¹ Based on the estimate of a professional engineer with expertise in damage assessment and building inspection, the value of $E[R_{TO} | TAG_Y]$ is taken to be one month (Scawthorn 2006). The empirical data of the relevant closed buildings on the Stanford University campus described in Section 6.1.2 (that were a high priority to repair and not held back by lengthy negotiations with FEMA for government funding) were used to set the value of $E[R_{TO} | TAG_R]$ as equal to 6 months for the benchmark office building. The complete virtual inspector methodology for estimating the probabilities of a building being green, yellow, and red tagged for a given hazard level is presented in Section 4.1.2.

The mean total building downtime for a given hazard level is determined using downtime estimates for the collapsed and non-collapsed cases:

$$E[R_T | im] = E[R_T | NC, im] \cdot (1 - P[C | im]) + E[R_T | C, im] \cdot P[C | im], \tag{6.7}$$

where $E[R_T | NC, im]$ is the mean total repair time conditioned on no collapse and $IM=im$, including change-of-trade and initial mobilization delays, as computed in Equation (6.3), and $P[C | im]$ is the probability of collapse, which is estimated from the structural response

¹¹ ABAG stands for the Association of Bay Area Governments, a planning agency owned and operated by the City of San Francisco, which addresses problems related to housing, land use, and environmental quality (ABAG 2006).

simulated using the lumped-plasticity model described in Chapter 2. The mean downtime of a building that is demolished and replaced, $E[R_U | C, im]$, is estimated to be 38 months based on ABAG's data of the Northridge-earthquake building inspection forms (Blecher and Comerio 2006).¹²

The expected monetary loss due to downtime of the rented space in the building is calculated as the sum of the loss in rent revenue for all operational units, from the time of the earthquake until the time the rental unit repairs are complete. These operational units may correspond to rental units in the building or any type of floor-space division that is appropriate for the desired repair scheme (i.e., division that is least disruptive to occupants). As mentioned before, here each operational unit of the benchmark building is chosen to correspond to a single story and the expression for downtime loss at each hazard level is given by:

$$E[DTL | im] = E[DTL | C, im] \cdot P(C | im) + E[DTL | NC, im] \cdot [1 - P(C | im)], \quad (6.8)$$

$$E[DTL | NC, im] = \sum_{m=1}^4 E[U_U(m)] \cdot E[R_U(m) | NC, im],$$

where $E[DTL | C, im] = \$73,150/\text{month}$ (or $\$2440/\text{day}$), which is calculated by multiplying the average lease rate ($\$1.33/\text{ft}^2/\text{month}$) with the total leasable building area ($55,000 \text{ ft}^2$); $E[U_U(m)]$ is the mean rent per operational unit calculated from the average lease rate and the square footage of each unit. The mean downtime loss conditioned on no collapse and on the hazard level is calculated similarly for each operational unit, where the leasable square footages of the ground and upper stories equals $11,500 \text{ ft}^2$ and $14,500 \text{ ft}^2$, respectively. Note that the value of the lease rate was calculated for the benchmark building by averaging lease rates for twenty-five commercial buildings within a 15-mile radius of the benchmark site (LA Times 2006).

¹² The data set consists of 233 buildings in the cities of Los Angeles, Northridge, and Santa Monica that were demolished and rebuilt after the Northridge earthquake (Blecher and Comerio 2006).

The downtime vulnerability function of Equation (6.8) is combined with the hazard function to estimate the expected annual loss due to downtime:

$$EALD = \lambda_0 \int E[DTL | im] p(im | IM \geq im_0) d im, \quad (6.9)$$

where im_0 is taken as before to be 0.1g, λ_0 is the mean annual rate of events with $IM \geq im_0$; $E[DTL | im]$ is calculated as in Equation 6.8; and $p(im | IM \geq im_0)$ is the probability density function of damaging IM values. This equation is used to calculate the expected value of loss incurred by business interruption after an earthquake for the five designs of the benchmark building, and the results are presented in the next section.

6.1.4 Downtime loss results for benchmark building

The rational component of downtime, the repair time, is calculated at every hazard level using the fast-track repair scheme described above. The start and finish times of the sequential repairs of the damaged structural members, elevators, sprinklers, partitions, glazing, ceiling, and paint, in this order, are determined for each benchmark design. An example of these repair times including change-of-trade delays is shown graphically in Figure 6.2 as a Gantt chart, for the baseline perimeter-frame design (A, VID #1) for two hazard levels corresponding to 10%-in-5yr and 2%-in-50yr events. This figure shows that the repair times of floors two and three control the total downtime of the building. Also, the repair time for the structural members more than quadruples between $S_a=0.26g$ and $S_a=0.82g$. The repair times of the sprinklers, glazing, and ceiling are barely noticeable at the lower hazard level; these make a more significant contribution to the repair times at the higher hazard level. Additionally, the mobilization time ($R_{T0} = 10$ and 22 days, shown on the horizontal axis) has a considerably larger contribution to the total repair times of the units than most of the nonstructural components. Note that the repair time for the elevators is only considered in operational unit 1 because this unit was chosen to include the building accessibility components. Note further that building downtime is considered here as the

time required to repair all assembly groups; in an existing building, occupants may return during the repair effort, say for instance, while repair crews are painting. The method chosen here, although possibly conservative, is used consistently for all building designs so that their results may be fairly compared.

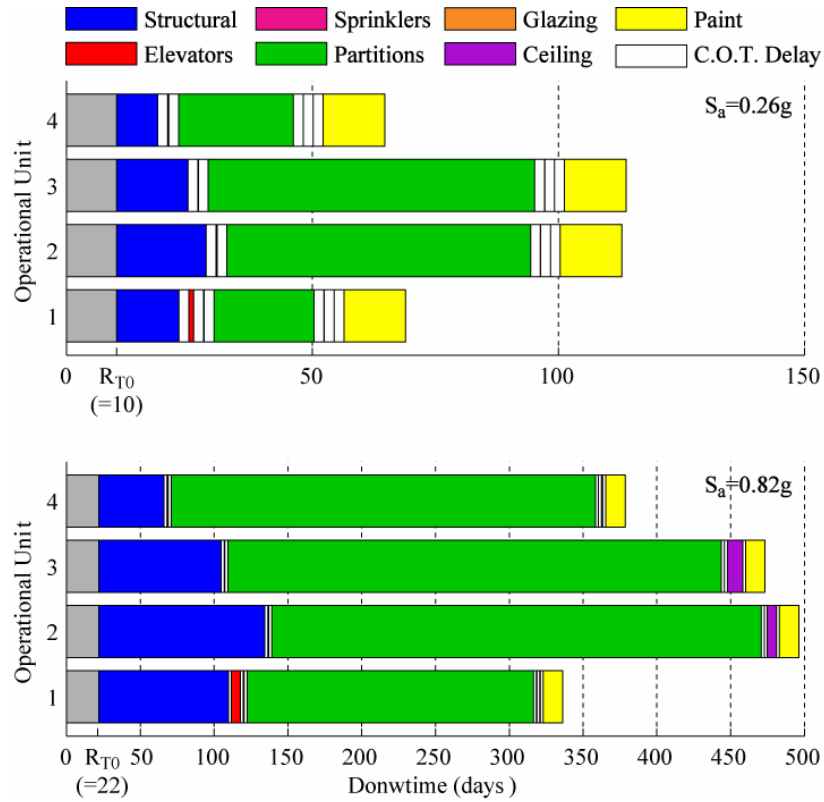


Figure 6.2 Gantt chart showing fast-track repair scheme at two hazard levels for Design A (VID #1).

Table 6.2 Design variant descriptions, corresponding downtime (irrational, rational and total downtimes) results at each hazard level, and EALD results.

Design (VID): description	Down-time Type	$S_a(T_1)$								EALD (\$USD)
		0.1	0.19	0.26	0.3	0.44	0.55	0.82	1.2	
A (VID #1): Baseline perimeter frame design.	Rational (days)	14	41	104	146	271	369	474	548	20,519
	Irrational (days)	10	10	10	10	12	14	22	41	
	Total (days)	24	52	114	157	284	388	518	655	
B (VID #3): Same as A, but with code-min strengths.	Rational (days)	18	79	210	227	348	407	501	545	28,362
	Irrational (days)	10	10	11	11	14	18	31	32	
	Total (days)	28	89	221	238	363	426	543	635	
C (VID #2): Same as A, but with uniform beam/column throughout.	Rational (days)	16	47	84	113	232	315	424	504	22,207
	Irrational (days)	10	10	10	10	13	16	35	53	
	Total (days)	26	57	94	124	245	335	485	642	
D (VID #9): Same as C, but no SCWB provision.	Rational (days)	20	83	203	216	317	369	444	508	32,726
	Irrational (days)	10	10	11	12	16	16	29	44	
	Total (days)	30	94	220	239	386	491	726	942	
E (VID #6): Baseline space frame design.	Rational (days)	16	32	75	108	206	317	535	858	19,517
	Irrational (days)	10	10	10	10	11	13	27	62	
	Total (days)	26	42	85	119	217	332	577	949	
Rational (repair) component of downtime = $E[R_T NC,im] - E[R_{TO} NC,im]$ (does not include collapse) Irrational (mobilization) component of downtime = $E[R_{TO} NC, im]$ Total downtime = $E[R_T im]$ (includes collapse)										

The total downtime results for five benchmark designs are given in Table 6.2 for each hazard level. The table lists the downtime due to the irrational component (the initial mobilization time, shown as the first block in the Gantt charts of Figure 6.2), the rational component of downtime (the repair time including change-of-trade delays), and the total downtime considering the probability of building collapse (Equation (6.7)). The irrational downtime ranges between 10 and 53 days for the perimeter-frame designs; the rational downtimes range between 14 and 548 days. This table also lists the expected annual loss due to downtime, EALD, for each design. These parameters are ideal to use in a simple comparison of the downtime results for all designs. Designs A (VID #1) and C (VID #2)

agree well with each other for all hazard levels and only differ in annualized losses of downtime by 8%. The design with code-minimum strengths (B, VID #3) and the one without the SCWB provision (D, VID #9) have similar downtimes to each other for hazard levels below $S_a=0.44g$. Above this hazard level, the downtime for design D (VID #9) increases rapidly, because of its higher probability of collapse resulting in almost an additional year of repair time for this design at the highest hazard level. The downtime of the space-frame design (E, VID #6) is considerably lower than for all the code-conforming perimeter-frame designs at hazard levels less than $S_a=0.55g$; beyond this point, the downtime for the space-frame design increases rapidly because of the additional number of moment-frame structural members, meeting the downtime value of 2.5 years of the non-code-conforming design D (VID #9) at $S_a=1.2g$. The comparison of irrational, rational, and total downtimes for the baseline perimeter-frame (A, VID#1) and baseline space-frame (E, VID#6) design are shown in Figure 6.3.

6.1.5 Comparison of downtime results with university studies

In an effort to study the impact of natural hazards on the UC Berkeley campus, Comerio (2000) proposed the estimates for building downtime as outlined in Table 6.3. The estimates of building downtime in this table were arrived at by accounting for an individual building's structural and nonstructural damage, mobilization time, event size, and location, the percentage of damaged building stock, and the economic conditions of the impacted area (Comerio 2006). In addition, these downtime estimates include the times it takes for damage assessment, for consultations with professional engineers, the bidding process, and the repair time. Although the method of Comerio's study is rather different from the loss estimation approach applied here to the benchmark building, the results of this previous

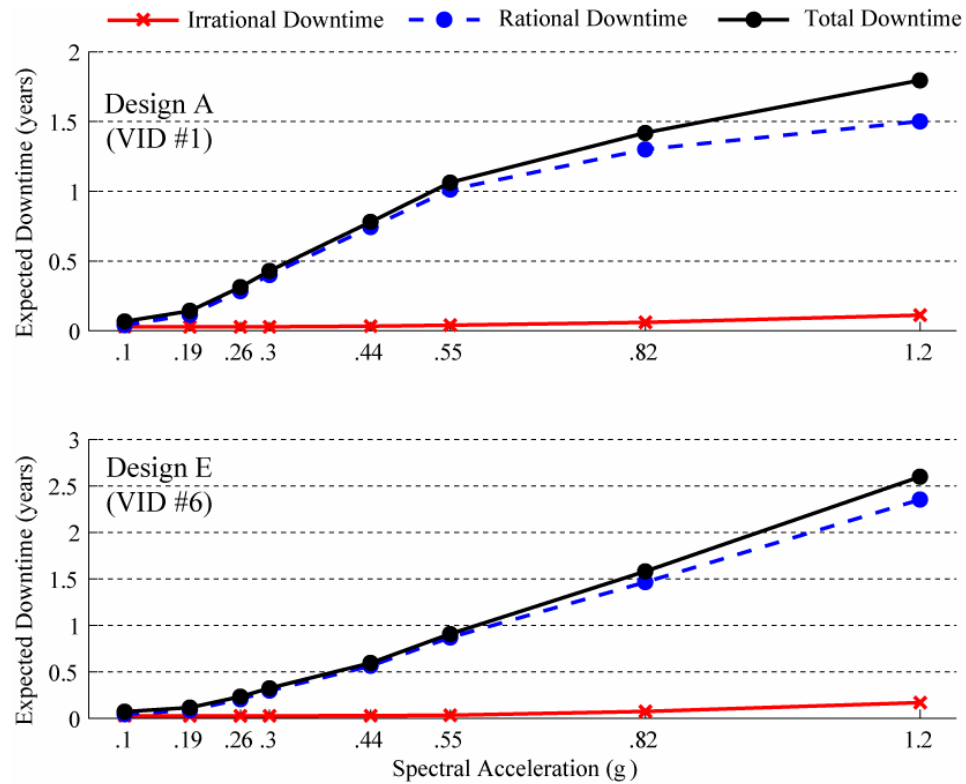


Figure 6.3 A comparison of the total downtime and the irrational and rational components of downtime for the baseline perimeter-frame (Design A, VID #1) and space-frame (Design E, VID #6) designs.

study provide an independent comparison of expected downtimes. Since the gross area of the benchmark building is >80,000 sf, this table estimates that it should have a downtime of 0-6 months when the building has minor or no damage and a downtime of 2-3.3 years for a building needing major repairs and/or replacement. The more conservative building designs, A (VID #1), C (VID #2), and E (VID #6) sustain no or light damage to their structural members and some slight damage to their nonstructural components for hazard levels up to and including $S_a=0.3g$ (shown in Figure 3.9, Figure 3.10, and Figure 3.12, respectively). In all of these cases, the corresponding downtimes are less than six months, which provides strong agreement with the results of the UC Berkeley campus study. Although none of the downtimes estimated for all designs of the benchmark building reach 3 years, the total downtimes for the two highest hazard levels, where higher damage states are reached (including collapse), fall within a range of 1.3-2.6 years. Further agreement with the downtime estimates of the benchmark designs is provided by the Stanford

University case study by Comerio (2006) introduced in Section 6.1.2, in which the repair times for closed buildings reach up to 2.6 years (downtimes reach up to 9.3 years). At the highest hazard level, the code-conforming benchmark designs have about 40% probability of being closed (or red tagged), and the non code-conforming has a 75% probability of closure. In these cases where closure probability is significant, the downtime due to repairs (rational contribution) ranges between 1.4 and 2.4 years. The correspondence of the benchmark-study total-downtime estimates with the Berkeley results, and the rational downtime estimates with the result of the Stanford study, provide strong support for the methodology presented here using estimates informed by empirical data and expert opinion.

Table 6.3 Expert-based estimates of downtime for the U.C. Berkeley campus based on building type and size, and extent of damage (reproduced from Comerio 2006).

Vision 2000 Structural Rating	Damage Description	Small	Large	Wood (All)
		<80,000 sf	>80,000 sf	
Time in Months				
9—10	Minimal Effort	0	0	0
7—8	Cleanup	0.25	0.5	0.25
6	Minor Repair	2	3	1
5	Minor/Major	4	6	3
4	Major Repair	20	24	6
1—3	Replacement	36	40	24

Note: Nonstructural ratings for each building were used in estimates made for specific buildings. This table is based on the collective experience of engineering and architectural practitioners, who have worked on earthquake repairs for public, private, and institutional clients.

6.2 Expected annual losses due to fatalities

Many people are uncomfortable with putting a price on human life, and the process is fraught with philosophical and economic challenges. However, public agencies routinely allocate scarce resources to improve life safety, and for the public good they must assess the value of competing activities, regulations, and policies that cost money but save lives (FHWA 1994). Typically, the “value of a statistical life,” or *VSL*, is used in benefit-cost analyses of competing policies (or building design, as in our case), where the main

objective is to reduce the number of human fatalities. A quantitative, meta-analysis approach that was used to estimate the value of a statistical life based on labor-market data shows that \$1.5-\$2.5 million (in 1998 dollars) is a plausible range for *VSL* (Mrozek and Taylor 2002). The obvious worth of human life suggests that it is inappropriate to neglect this value entirely in a comparison of economic benefits and costs.

6.2.1 Human loss results for benchmark building

The expected annual loss associated with fatalities (*EALF*) caused by building earthquake damage may be estimated by multiplying the expected annual number of fatalities (*EANF*) calculated in Section 4.2.2, with a reasonable *VSL*. The Federal Highway Administration (FHWA 1994) approved using \$2.6 million as an acceptable cost to assign to regulations or safety measures that avoid one future statistical death. The FHWA figure in 1998 dollars equals \$2.8 million, which is comparable to Mrozek and Taylor's suggested range of *VSL* (2002); a *VSL* of \$3.5 million (accounting for inflation) is used here. The values of *EALF* for the five benchmark designs compared in this work are given in Table 6.4. The results of this table show that the expected annual losses due to fatalities are low in comparison to the other annual losses due to repair cost and downtime. However, the value of *EALF*=\$79,800, estimated for the non-code-conforming design D (VID #9), particularly stands out.¹³

¹³ This figure corresponds to the loss of one human life over the lifetime of the building, taken as 50 years for this example.

Table 6.4 Design variant descriptions and corresponding expected annual number of fatalities (EANF) and the expected annual loss due to fatalities (EALF).

Design (VID): description	EANF (*10⁻³)	EALF (\$)
A (VID #1): Baseline perimeter frame design.	1.4	4,900
B (VID #3): Same as A, but with code-min strengths.	1.3	4,550
C (VID #2): Same as A, but with uniform beam/column throughout.	1.6	5,600
D (VID #9): Same as C, but no SCWB provision.	22.8	79,800
E (VID #6): Baseline space-frame design.	1.0	3,500

6.3 Total expected annual losses for benchmark building

The methodology and the results for estimating earthquake-related losses associated with repair cost, loss of human lives, and building downtime are given in Chapter 5 and this chapter. The results of the expected annual losses for each decision variable chosen for the benchmark building are summarized in Table 6.5, along with their totals. The results suggest that there is clearly one design that performs worse than all the others for all types of loss, which is, not surprisingly, the non-code-conforming design (design D, VID #9). Also, there is clearly one design that economically outperforms the others for the three types of loss, that is the space-frame design with moment-resisting frames on the exterior and interior of the building (design E, VID #6). The remaining three perimeter-frame designs fall somewhere in between these two extremes and interchange their ranks of economic performance for each decision variable. For example, the repairs of design A cause the least business interruption for the building in comparison to the other perimeter-frame designs; design B (VID #3) has the least number of expected fatalities of all the perimeter-frame designs; and design C (VID #2) costs less to repair than designs A and B (VIDs #1, #3). Therefore, if any one of these decision variables is taken alone as the performance metric used to select a building design, the result would be three different

answers. This finding clearly demonstrates the importance of considering the “3 Ds,” dollars, deaths, and downtime, in a complete seismic loss estimation of buildings.

The results of the benchmark study summarized in Table 6.5 form the basis for comparing the design options across the three decision variables. Several trade-offs are evident; as an example, the two primary designs previously compared in this work are emphasized. Although the mean repair costs are much higher for the space-frame (design E, VID #6) design than for the baseline perimeter-frame design (design A, VID #1) at the two highest levels of S_a (Table 5.1), the *EAL* and *EALF* for the space-frame design are approximately 30% less than for the perimeter-frame design. This can be attributed to the facts that mean repair costs of the space-frame design are lower for the more frequent events and that it has a lower probability of collapse. These types of comparisons, although informative, can be made even more useful to decision makers by conducting a benefit-cost analysis.

6.4 Illustrative benefit-cost analysis

The outputs of the loss analysis methodology presented in this work can be used to analyze trade-offs between the various building designs by using the benefit-cost analysis (BCA) framework. BCA is widely used at all levels of government, federal, state, and municipal, to account for the costs and benefits associated with various policy decisions. The decision variables considered in this loss analysis are the repair cost, downtime, and loss of human life; in decision theory these are said to correspond to three different *attributes*: called here cost, duration, and life safety performance.¹⁴ A major challenge in applying decision theory to this problem is to obtain a single reference attribute from these, which are typically measured using three different scales. Since the results of the benchmark study have been framed in terms of a single reference attribute, the expected annual losses, the various benchmark designs can be compared in a straightforward manner. The BCA framework used in the following is based on the proposed analysis from Zerbe and Falit-Baiamonte (2002) for decision making within PEER’s performance-based earthquake engineering

¹⁴ Decision theory is a rich field; a thorough introduction is provided by Berger (1985).

methodology. These authors explore the advantages of various evaluative criteria, including net present value (NPV), benefit-cost ratios (B/C), internal rate of return (IRR), payback period, and the wealth maximizing rate. Of these criteria, they rank NPV and B/C as preferable to the others.

The proposed PEER BCA framework includes the following minimum required steps (Zerbe and Falit-Baiamonte 2002):

- Define the client.
- Clearly state assumptions of the analysis.
- Clearly state and determine the benefits and costs.
- Choose an appropriate discount rate, accounting for inflation.
- Choose an appropriate evaluation criterion, such as NPV.
- Allow for uncertainty.
- Make a decision.
- Provide feedback.

Results of the benchmark study are used to as an example to demonstrate the utility of this BCA framework. The client (decision maker) is assumed to be the building owner who is comparing two designs for possible construction. The up-front costs (construction costs) are estimated for the baseline perimeter-frame and space-frame designs to be \$8.9 and \$9.0 million, respectively.¹⁵ The expected annual losses for repair costs, downtime, and fatalities are all considered as the “costs” for the BCA framework, and the lifetime of the building is taken to be 50 years. A discount rate was used to convert the repair costs and downtime losses over the lifetime of the building, into present day values. Several authors argue that discounting human lives is unethical (Revesz 1999, Zerbe and Falit-Baiamonte 2002), while others believe in using discount rates but cannot agree on a value (Farber 1993). However, because the expected annual losses due to fatalities are far smaller than the

annual losses from repair costs and downtime for all the code-conforming designs (all but design D, VID #9), the inclusion of a discount rate would have a negligible effect on the net costs. Therefore, a discount rate will not be used in estimating the losses due to human fatalities over the lifetime of the building. An equation for the mean of the present value of earthquake losses is given in Beck et al. (2002) and modified here to include discounting for repair costs and downtime but not for human fatalities:¹⁶

$$E[PVL(t)] = EALF \cdot t + \frac{(EAL + EALD)}{r} (1 - e^{-rt}), \quad (6.10)$$

where r is the discount rate. Zerbe and Falit-Baiamonte (2002) emphasize that the financial evaluation of a project is sensitive to the choice of this discount rate. The discount rate used in this example is 5%, the same used in Porter et al. (2004a), which falls within the recommended range of 2.5%-7%, given by Zerbe and Falit-Baiamonte (2002).

The benefits of the space-frame design over the perimeter frame design is calculated by using the results of the last column in Table 6.5 as $E_{perimeter}[PVL(t)] - E_{space}[PVL(t)]$, which equals \$403,500. Note that future income is not considered in these calculations because the rental space of all these designs is equal and therefore would not affect the cost-benefit trade-offs. The cost in the BCA is equal to the difference in costs of these designs, which is estimated to be \$100,000. The NPV, defined here as the difference between the present value of all benefits of a seismic design upgrade and the present value of the costs for this upgrade, equals \$303,500; the B/C ratio equals 4. These results would inform the owner that a space-frame design is the preferred choice based on the economic trade-offs. However, a study by Beck et al. (1999) showed that the decision maker's risk attitude is significant, and thus although a risk-neutral attitude is considered here, a risk-averse attitude should be considered in a future study to more accurately model an owner's

¹⁵ Up-front costs for the perimeter- and space-frame designs are estimated using the RSMMeans manual for construction cost data (2001).

¹⁶ "The present value of a given cash flow is just the sum of money that, if invested today at some relevant interest rate, will yield that cash flow" (Zerbe and Falit-Baiamonte 2002).

final decision. In this case, the variance and other higher central moments need to be calculated (Beck et al., 2002, Porter et al., 2004). Note that the estimates of the up-front construction costs, although crude, are used here to enable this simple comparative analysis. A future, more complete BCA implementation for the benchmark study would benefit from input by a professional cost estimator to determine more accurate up-front costs. It is the hope of the author that this short entrée into BCA demonstrates that the loss analysis methodology presented in this work provides the necessary inputs to a decision theoretic approach to PBEE design evaluation.

Table 6.5 Summary of expected annual losses for the three decision variables and five designs of the benchmark building.

Design (VID): description	EAL (\$)	EALD (\$)	EALF (\$)	EAL_{TOTAL} (\$)	E[PVL(50 yr)] (\$M)
A (VID #1): Baseline perimeter frame design.	66,585	20,519	4,900	92,004	1.84
B (VID #3): Same as A, but with code-min strengths.	95,656	28,362	4,550	128,568	2.50
C (VID #2): Same as A, but with uniform beam/column throughout.	51,933	22,207	5,600	79,740	1.64
D (VID #9): Same as C, but no SCWB provision.	112,930	32,726	79,800	225,456	6.66
E (VID #6): Baseline space frame design.	49,422	19,517	3,500	72,439	1.44

CHAPTER 7

Concluding Remarks

The previous four chapters document the significant results of the damage and loss analysis work conducted in pursuit of establishing a methodology for evaluating the performance of new reinforced-concrete buildings in response to seismic hazards. The implementation of the MATLAB Damage and Loss Analysis (MDLA) toolbox, described in Chapter 2, was necessary to apply PEER's PBEE framework to a building, as part of a benchmark study. The work presented, is to our knowledge, the most faithful attempt to estimate the main decision variables (termed the 3 *Ds*—dollars, deaths, and downtime), proposed by PEER and the ATC-58 Project for performance assessment of structures. The significant results and major contributions from each chapter are summarized below.

7.1 Significant results and major contributions

7.1.1 Chapter 2: Performance-based earthquake engineering framework

- The structural and nonstructural components included in the damage and loss estimation of the benchmark building were selected to closely agree with those deemed as necessary for a detailed-level performance assessment by the ATC-58 guidelines for next-generation performance-based seismic design.

- In order to perform a more complete loss assessment of the benchmark building, realistic nonstructural components were specified: exterior walls, interior partitions, conveying systems, automatic sprinklers, ceilings, and paint. In particular, these nonstructural components were designed to meet the specifications of the relevant current building codes.
- In contrast to previous studies, the damage analysis of the benchmark building accounts for three-dimensional effects in the performance of the structural and nonstructural building components. To implement this, the orthogonal building frames were modeled in a two-dimensional structural analysis, using the two horizontal components of the ground motion record. The geometric mean of the two horizontal components was considered for the selection of ground motion records.
- An analytical methodology for damage and loss estimation was implemented by the MATLAB Damage and Loss Analysis (MDLA) toolbox. The modular framework of PEER's PBEE methodology is reflected in the architecture of this toolbox, where the hazard, structural, damage and loss analyses are separate entities. Although targeted to the benchmark study, the MDLA toolbox provides a clearly defined interface for the results of the hazard and structural analyses and the models of damageable building components, enabling the application of the software package to future studies. As implemented, the toolbox generates statistical estimates of building safety tagging and the "3 Ds," and is capable of integrating these to inform decision-making in the design process.

7.1.2 Chapter 3: Damage estimation

- The MDLA toolbox was used to perform the damage analysis of ten variants (design and modeling) of the benchmark building. The damage visualization tool, presenting the average probability of reaching or exceeding the damage states of like components in each story, is useful for predicting locations of severe damage

and is an intermediate means for the performance comparison of the various designs.

- The most severe damage to the reinforced-concrete columns of the moment frames is found in the first story of all the building variants. The code-conforming designs resist structural damage at low levels of ground shaking, while the one design that does not enforce the SCWB provision has a significantly higher probability of suffering damage even at the lowest hazard levels.
- The damage results are used to make design comparisons, for instance the space-frame design is shown to resist nonstructural damage to a greater extent than the perimeter-frame designs—in general, the damage is less severe and the onset occurs at higher levels of ground shaking. These differences in damage across the building designs anticipate the repair losses subsequently determined.
- The damage results are also used to compare modeling choices, for example, ignoring the added strength and stiffness of the gravity frames in the structural model is demonstrated to be a reasonable approximation with respect to structural damage, while it leads to an exaggerated extent of nonstructural damage.

7.1.3 Chapter 4: Building and life safety

- The event-tree-based methodology for a *virtual inspector* is used to assess the safety of buildings, using ATC's existing damage assessment guidelines. The safety tagging procedure is encapsulated as an independent module that only requires the results of the damage analysis, yielding a quick safety evaluation. Although building-safety tagging may be considered a decision variable in its own right, and is therefore presented as an output of the MDLA toolbox, the results of this analytical module are subsequently used in estimating the downtime and fatality DVs.

- The results of virtual inspection reveal that, in general, the code-conforming designs exhibit similar safety tagging probabilities, in particular, the probabilities of red tagging are low at all but the highest hazard level. The tagging results for the non-code-conforming building show worse safety performance; the probabilities of red tagging are significantly higher at all hazard levels.
- An event-tree-based fatality model was developed that accounts for the factors affecting human injury identified in epidemiological studies of earthquake-related injuries. The model considers human fatalities due to the partial and global collapse of buildings, using probabilities of fatality based on relevant empirical data of human injuries in historic seismic events. The mean number of fatalities is determined using the probabilities of partial and global collapse, as provided by the virtual-inspector safety-tagging results.
- The results of the fatality estimation demonstrate that there is no imminent life safety risk in the code conforming building designs at all hazard levels; the expected number of fatalities over a 50 year lifetime of the building results does not exceed 0.08 for these designs. Although the fatality risk is considerably larger for the non-code-conforming design, the expected number of fatalities over a 50 year lifetime of this building is approximately 1.14, which is not alarming.

7.1.4 Chapter 5: Estimation of direct losses

- The MDLA toolbox was used to perform the loss analysis of ten variants (design and modeling) of the benchmark building. The mean total repair cost and the contribution of individual damageable building components to this cost are calculated across all hazard levels. Subsequently, these repair costs are used to determine the expected annual direct loss, which is one of several economic performance metrics useful for building design comparisons.
- The potential for financial loss is significant when considering that the expected annual losses from earthquakes are roughly equal to 1% of the replacement cost of

the building. The results show that the repair costs are highly sensitive to modeling choices; in particular, the choice of the initial stiffness of the structural elements significantly affects the expected annual loss. In addition, the findings of the loss analysis are consistent with those of previous chapters, the non-code-conforming design fares much worse than its code-conforming counterparts.

7.1.5 Chapter 6: Estimation of indirect losses and benefit-cost analysis

- A simplified methodology is presented for estimating the rational and irrational components of building downtime (accounting for building collapse) after seismic events. To best exploit the results of the damage analysis and the available empirical data, a model for the mobilization delay before construction begins is developed that is conditioned on the results of the virtual inspection. A realistic repair scheme is used to estimate the time to repair the building's earthquake damage. The MDLA toolbox generates downtime Gantt charts that have been used to compare the benchmark building designs and may be used for post-disaster planning and evaluating repair scheme options.
- The results of downtime estimation support a previous observation that delays before construction contribute significantly to total building downtime after a major event. Consistent with the findings in previous chapters, the expected downtime of the non-code-conforming design is the longest across all the hazard levels, and thus costliest overall. The correspondence of the benchmark-study total-downtime and total-repair-time estimates with previous empirical downtime studies provide strong support for the methodology presented here using estimates informed by empirical data and expert opinion.
- The results of the expected annual losses due to repair costs, downtime, and fatalities suggest that there is clearly one design (the non-code-conforming design) that performs worse than all the others and one (the space-frame design) that economically outperforms the others. The other three designs fall somewhere in between these two extremes and interchange their ranks of economic performance

for each decision variable. If any one of these decision variables is taken alone as the performance metric used to select a building design, the procedure would yield three different recommendations. This finding clearly demonstrates the importance of considering all three decision variables in a complete seismic loss estimation of buildings.

- An illustrative benefit-cost analysis is performed in which three disparate performance attributes—cost, downtime, and life safety—are combined into one economic performance metric based on the expected annual losses. Although crude up-front building costs were used, the result of the BCA clearly prefers the space-frame design over the perimeter-frame design based on future economic losses. This short entrée into BCA demonstrates that the loss analysis methodology presented in this work provides the necessary inputs to a decision theoretic approach to PBEE design evaluation.

7.2 Limitations of research

The goal of the presented body of work has been to develop and implement a complete methodology for damage and loss analysis and to apply this methodology as part of PEER's benchmark study. In pursuit of this goal, which necessitated the implementation of estimation procedures for the "3 Ds," several simplifications were taken, that although deemed reasonable for the present study, may be improved upon in future endeavors. These limiting simplifications are described:

- Some simplifications were taken in the site selection and hazard analysis. The site selected for the benchmark study is within 20km of 7 faults, but the site was selected so that no one fault produces near-fault motion that dominates the hazard. The results presented here should therefore be carefully interpreted when comparing to studies that focus on near-source effects (e.g., Hall et al., 1995). Additionally, this study, like most others, employs a Poisson occurrence model for seismic and damage events. This probability model is reasonable, for example, if

for design purposes, it is assumed that the building is restored to its initial condition after each damaging event. Considerations of damaging aftershocks (see Yeo (2005) for a framework for aftershock probabilistic seismic hazard analysis) should be considered, especially if the PBEE methodology presented here is used for emergency planning.

- The nonlinear dynamic structural analysis employed for the benchmark study was computationally expensive, which eliminated the possibility of using Monte Carlo approaches for propagating the uncertainties throughout the PBEE procedure. The computational effort for estimating the structural response also limited the loss evaluation of further design and model comparisons.
- A simplified damage analysis approach was used in this work to develop an analytical framework for building damage assessment. The damage analysis method assumes that each assembly group is composed of damageable components sensitive to the same *EDP*, and that their damage states are modeled as perfectly correlated and conditionally independent, given *EDP*, from all other assembly groups. Further reading on the effect of partial correlation between *EDPs* and damage states on future seismic losses can be found in Aslani (2005).
- Some simplifications were taken in the development of the downtime and casualty models. A single realistic repair scheme was used to estimate the rational component of downtime to compare total downtime of various building designs. Of course, such repair schemes will depend on the financial priorities of the property owner and on available resources and manpower after a damaging earthquake. This simplification is reasonable for the purpose of comparing designs, but optimal repair schemes should be explored in future studies that desire more realistic projection of economic and planning issues (Beck et al., 1999). Additionally, the mean building occupancy (instead of a complete probabilistic description of occupancy) is used to simplify the casualty estimation procedure for the purpose of comparing the life safety results for several designs. Finally, the presented methodology for the downtime and fatality modeling represents the best we can do

with the available data; we would have more confidence in the accuracy of the results if more empirical data relevant to U.S. seismic events and building practice were available. One way to remedy this is through the laborious cataloguing of earthquake reconnaissance data, such as the ongoing effort by Blecher and Comerio (2006) to estimate building downtime.

7.3 Future directions

- The results of damage and loss assessment for the designs of the benchmark building show that the one non-code-conforming design performs much worse than the other designs in virtually all cases. The MDLA toolbox, with its implementation of estimates of the “3 Ds,” provides the ability to extend this type of assessment to other designs of existing structures that deviate in different ways (beside the SCWB provision) from current building codes. Given that there are serious concerns for the seismic performance of existing structures in urban areas, this line of work can be used to inform a prioritization scheme for suggesting seismic retrofits and municipal emergency planning.
- The downtime methodology considered in this work focuses on the mobilization delays and the repair times. However, a building with no significant damage could also suffer downtime from secondary effects caused by an earthquake (i.e., fires, hazard spills, and utility interruption). For the design and emergency planning of building with special needs, such as those with large quantities of hazardous materials, specialized equipment, and critical facilities, it would be valuable to develop downtime models accounting for these secondary effects. With more realistic models, this work can be extended beyond the design process and used for emergency planning (i.e., evacuation plans and identifying building that are at higher risk).
- The illustrative benefit-cost analysis considers a risk-neutral attitude. However, previous work has shown that the decision maker’s risk attitude is significant; an interesting extension of the BCA presented here should consider the risk-averse

attitude that more accurately models the decision-making process. Also, a future, more complete BCA implementation for the benchmark study would benefit from input by a professional cost estimator to determine more accurate up-front costs.

- The damage and loss analysis methodology implemented in the MDLA toolbox parallels previous work on near-real-time loss estimation (Porter et al., 2004b, 2006a, 2006b). In fact, the methodology for the virtual inspector presented here is rooted in the rapid pre-inspection estimate of safety and operability developed as part of these earlier studies. As buildings become “smarter,” dense networks of inexpensive nodes of embedded sensing and computation will become the norm (Mitrani et al., 2002, Glaser 2004). An important future contribution will be to integrate these disparate streams of information into a continuously updating model for structural health monitoring. For example, it is conceivable that real-time information about building occupants and locations could be used in conjunction with rapid safety assessment to manage search-and-rescue efforts.

References

- ABAG, 2006. Association of Bay Area Governments, <http://www.abag.ca.gov>.
- (ACI) American Concrete Institute, 1990. *Design Handbook Volume 2: Columns* (ACI 340.2R-90). Detroit, MI.
- (ACI) American Concrete Institute, 2002. *Building Code Requirements for Structural Concrete (ACI 318-02) and Commentary (ACI 318R-02)*, Farmington Hills, MI.
- (ADAAG) ADA Act Accessibility Guidelines for Buildings and Facilities, 2002. The Access Board, <http://www.access-board.gov/adaag/html/adaag.htm>.
- Andrews, J. D. and A. Moss, 1993. *Reliability and Risk Assessment*, Essex, England: Longman Scientific and Technical.
- Ang, A. H-S. and W.H. Tang, 1975. *Probability Concepts in Engineering Planning and Design*, New York : John Wiley & Sons.
- (ANSI) American National Standards Institute, 2006. <http://www.ansi.org/>.
- (ASCE) American Society of Civil Engineers, 2002. *Minimum Design Loads for Buildings and Other Structures, ASCE-7-02*, Reston, VA.
- (ASCE) American Society of Civil Engineers, 2006. *Minimum Design Loads for Buildings and Other Structures, SEI/ASCE 7-05*. Reston, VA.
- (ASME) American Society of Mechanical Engineers, 2000. *Safety Code for Elevators and Escalators Standard A17.1-2000*. New York, NY.

- (ATC) Applied Technology Council. 1985. *ATC-13, Earthquake Damage Evaluation Data for California*. Redwood City, California.
- (ATC) Applied Technology Council. 1989. *ATC-20, Procedures for Postearthquake Safety Evaluation of Buildings*. Redwood City, California.
- (ATC) Applied Technology Council. 1995. *ATC 20-2, Addendum to the ATC-20 Postearthquake Building Safety Evaluation Procedures*. Redwood City, California.
- (ATC) Applied Technology Council. 1996a. *ATC 20-3, Case Studies in Rapid Postearthquake Safety Evaluation of Buildings*. Redwood City, California.
- (ATC) Applied Technology Council. 1996b. *ATC-40, Seismic Evaluation and Retrofit of Concrete Buildings*. Redwood City, California.
- (ATC) Applied Technology Council. 2005. *Guidelines for Seismic Performance Assessment of Buildings, 25% Complete Draft*. Redwood City, California.
- Aslani, H. and E. Miranda, 2004. Component-level and system-level sensitivity study for earthquake loss estimation. *Proceedings, Thirteenth World Conference on Earthquake Engineering*. Vancouver, B.C., Canada.
- Aslani, H., 2005. *Probabilistic earthquake loss estimation and loss disaggregation in buildings*, Doctoral Thesis, Stanford University Department of Civil and Environmental Engineering, Stanford, CA.
- Baker, J.W. and C.A. Cornell, 2003. Uncertainty specification and propagation for loss estimation using FOSM methods, *Proceedings, Ninth International Conference on Applications of Statistics and Probability in Civil Engineering (ICASP9)*. San Francisco, California.
- Baker J.W. and C.A. Cornell, 2005. A vector-valued ground motion intensity measure consisting of spectral acceleration and epsilon, *Earthquake Engineering and Structural Dynamics*, 34 (10), 1193-1217.

- Beck, J.L., K.A. Porter, R. Shaikhutdinov, S. K. Au, T. Moroi, Y. Tsukada, and M. Masuda, 2002. *Impact of Seismic Risk on Lifetime Property Values*, Final Report for CUREE-Kajima Phase IV Project, Consortium of Universities for Research in Earthquake Engineering, Richmond, CA.
- Beck, J.L., A. Kiremidjian, S. Wilkie, A. Mason, T. Salmo, J. Goltz, R. Olson, J. Workman, A. Irfanoglu, and K.A. Porter, 1999. *Decision Support Tools for Earthquake Recovery of Business*, Final Report for CUREE-Kajima Phase III Project, Consortium of Universities for Research in Earthquake Engineering, Richmond, CA.
- Behr, R.A., and C.L. Worrell, 1998. Limit States for Architectural Glass Under Simulated Seismic Loadings, *Proceedings, Seminar on Seismic Design, Retrofit, and Performance of Nonstructural Components*, ATC-29-1 January 22-23, 1998, San Francisco, Redwood City, CA: Applied Technology Council, pp. 229-240.
- Benjamin, J.R. and C.A. Cornell, 1970. *Probability, Statistics, and Decision for Civil Engineers*, New York: McGraw-Hill.
- Benuska, L., 1990. Loma Prieta Earthquake reconnaissance report. *Earthquake Spectra*, supplement to volume 6.
- Berger, J. O., 1985. *Statistical Decision Theory and Bayesian Analysis*, New York: Springer.
- Berry, M., M. Parrish, and M. Eberhard, 2004. *PEER Structural Performance Database User's Manual*, Pacific Engineering Research Center, University of California, Berkeley, California. <http://nisee.berkeley.edu/spd/>
- Blecher, H.E. and M.C. Comerio, 2007. Analysis of ABAG data (personal communication).
- Brown, P.C., and L.N. Lowes, 2007. Fragility functions for modern reinforced-concrete beam-column joints. *Earthquake Spectra* 23(2), Earthquake Engineering Research Institute, Oakland, CA: pp. 263-289.

- Choudhury, G.S., and N.P. Jones, 1996. Development and application of data collection for postearthquake surveys of structural damage and human casualties. *Natural Hazards* 13: pp. 17-38.
- Coburn, A.W., R.J.S. Spence, and A. Pomonis, 1992. Factors determining human casualty levels in earthquakes: mortality prediction in building collapse. *Proceedings of the Tenth World Conference on Earthquake Engineering*, Madrid, Spain: pp. 5969-5974.
- Comerio, M. C., 2000. *The Economic Benefits of a Disaster Resistant University*. WP 2000-02 plus three technical appendices, Institute of Urban and Regional Development, University of California, Berkeley, CA.
- Comerio, M.C., 2006. Estimating downtime in loss modeling. *Earthquake Spectra* 22 (2), Earthquake Engineering Research Institute, Oakland, CA: pp. 349-365.
- Cornell, C.A., 1968. Engineering seismic risk analysis, *Bulletin of Seismological Society of America* 58: pp. 1583-1606.
- Cornell, C.A., 1986. *Applicability of the Poisson Earthquake-Occurrence Model*, Electric Power Research Institute, Report EPRI NP-4770, Palo Alto, CA.
- Cornell, C.A., 1996. Calculating building seismic performance reliability: a basis for multi-level design norms, *Proceedings of the 11th World Conference on Earthquake Engineering*, Paper No. 2122, Acapulco, Mexico.
- Durkin, M.E., 1987. The San Salvador earthquake of October 10, 1986—casualties, search and rescue, and response of the health care system. *Earthquake Spectra* 3 (3), Earthquake Engineering Research Institute, Oakland, CA: pp. 621-634.
- Durkin, M.E., and C.C. Thiel, Jr., 1992. Improving measures to reduce earthquake casualties. *Earthquake Spectra* 8 (1), Earthquake Engineering Research Institute, Oakland, CA: pp. 95-113.

- Eberhart-Phillips, J.E., T.M. Saunders, A.L. Robinson, and D.L. Hatch, 1994. Profile of mortality from the 1989 Loma Prieta earthquake using coroner and medical examiner reports. *Disasters* 18 (2): pp. 160-710.
- Farber, D.A., and P.A. Hemmersbaugh. 1993. The shadow of the future: Discount rates, later generations, and the environment. *Vanderbilt Law Review*, 46: pp. 267-304.
- Fardis, M.N. and D.E. Biskinis, 2003. Deformation Capacity of RC members, as controlled by flexure or shear. *Otani Symposium*, Tokyo, Japan: pp. 511-530.
- (FEMA) Federal Emergency Management Agency, 1980. *An Assessment of the Consequences and Preparations for a Catastrophic California Earthquake: Findings and Actions Taken*. Washington, D.C.
- (FEMA) Federal Emergency Management Agency, 1997a. *FEMA 273, NEHRP Guidelines for Seismic Rehabilitation of Buildings*. Washington, D.C.
- (FEMA) Federal Emergency Management Agency, 1997b. *FEMA 274, NEHRP Commentary on the Guidelines for Seismic Rehabilitation of Buildings*. Washington, D.C.
- (FEMA) Federal Emergency Management Agency, 2000. *FEMA 356, Prestandard and Commentary for the Seismic Rehabilitation of Buildings*. Washington, D.C.
- (FHWA) Federal Highway Administration, 1994. *Technical Advisory: Motor Vehicle Accident Costs, Technical Advisory #7570.2*, U.S. Department of Transportation, Washington, D.C.
- Field, E. H., 2005. Probabilistic seismic hazard analysis (PSHA): A primer, http://www.relm.org/tutorial_materials/PSHA_Primer_v2.pdf.
- Finley, J., D. Anderson, and L. Kwon, 1996. *Report on the Northridge Earthquake Impacts to Hospital Elevators*. Contract No. 94-5122. California Office of Statewide Health Planning and Development (OSHPD), Sacramento, CA.

- Glaser, S.D., 2004. Some real-world applications of wireless sensor nodes. *SPIE Symposium on Smart Structures and Materials*. San Diego, CA.
- Glass, R.I., J.J. Urrutia, S. Sibony, H. Smith, B. Garcia, and L. Rizzo, 1977. Earthquake injuries related to housing in a Guatemalan village. *Science* 197 (4304): pp. 638-643.
- Goulet, C., C. Haselton, J. Mitrani-Reiser, J.P. Stewart, E. Taciroglu, and G. Deierlein, 2006. Evaluation of the seismic performance of a code-conforming reinforced-concrete frame building - Part I: Ground motion selection and structural collapse simulation. *Proceedings of Eighth U.S. National Conference on Earthquake Engineering*. San Francisco, California.
- Goulet, C., C. Haselton, J. Mitrani-Reiser, J.L. Beck., G.G. Deierlein, K.A. Porter, and J.P. Stewart, 2007. Evaluation of the seismic performance of a code-conforming reinforced-concrete frame building—from seismic hazard to collapse safety and economic losses. *Earthquake Engineering and Structural Dynamics*. (in press)
- Hall, J.F., 2003. Finite Element Analysis in Earthquake Engineering. In Lee, W.H.K., et al. editors, *International Handbook of Earthquake and Engineering Seismology*: pp. 1133-1158. Academic Press, United Kingdom.
- Hall, J.F., T.H. Heaton, M.W. Halling, and D.J. Wald, 1995. Near-source ground motion and its effects on flexible buildings. *Earthquake Spectra* 11(4), Earthquake Engineering Research Institute, Oakland, CA.
- Hamburger, R.O. and J.P. Moehle, 2000. State of performance-based engineering in the United States. *Proceedings of the Second US-Japan Workshop on Performance-Based Design Methodology for Reinforced Concrete Building Structures*. Sapporo, Japan.
- Haselton, C.B. and J.W. Baker, 2006. Ground motion intensity measures for collapse capacity prediction: Choice of optimal spectral period and effect of spectral shape. *Proceedings of Eighth U.S. National Conference on Earthquake Engineering*, San Francisco, California.

- Haselton, C. B., C. Goulet, J. Mitrani-Reiser, J.L. Beck, G.G. Deierlein, K.A. Porter, and J.P. Stewart, 2007. *An Assessment to Benchmark the Seismic Performance of a Code-Conforming Reinforced-Concrete Moment-Frame Building*, PEER Report 2006, University of California, Berkeley, California, (in preparation).
- HAZUS, 2002. *HAZUS99-SR2 Technical Manual*, Federal Emergency Management Agency, Washington, D.C.
- Hecksher, G., 2006. Component downtime estimates. (personal communication).
- Insurance Information Institute, 2006. *Earthquakes: Facts and Statistics*. <http://www.iii.org/media/facts/statsbyissue/earthquakes/>
- (ICC) International Code Council, 2003. *2003 International Building Code*, Falls Church, VA.
- Jones, N.P., F. Krimgold, E.K. Noji, and G.S. Smith, 1990. Considerations in the epidemiology of earthquake injuries. *Earthquake Spectra* 6(3), Earthquake Engineering Research Institute, Oakland, CA.
- Kang, T.H.K., J.W. Wallace, and K.J. Ellwood, 2006. Dynamic tests and modeling of RC and PT slab-column connections. *Proceedings of the 8th National Conference on Earthquake Engineering 8NCEE*, San Francisco, CA.
- Kennedy, R.P., and M.K. Ravindra, 1984. Seismic Fragilities for Nuclear Power Plant Risk Studies, *Nuclear Engineering and Design* 79, Philadelphia PA: Elsevier Science Publishers.
- Kramer, S.L., 1996. *Geotechnical Earthquake Engineering*, Upper Saddle River, NJ: Prentice Hall.
- Kunnath, S.K., A.M. Reinhorn, and R.F. Lobo, 1992. *IDARC Version 3.0: A Program for the Inelastic Damage Analysis of Reinforced Concrete Structures*. National Center for Earthquake Engineering Research, Technical Report NCEER-92-0022, Buffalo, NY.

- LA Times, 2006. An online resource for commercial real estate in the LA-area, powered by City Feet and sponsored by the LA Times. http://www.cityfeet.com/los_angeles/.
- Lilliefors, H.W., 1967. On the Kolmogorov-Smirnov Test for Normality with Mean and Variance Unknown. *Journal of the American Statistical Association* 62 (318): pp 399-402.
- Mahue-Giangreco, M., Mack, W., Seligson, H., and Bourque, L.B., 2001. Risk Factors Associated with Moderate and Serious Injuries Attributable to the 1994 Northridge Earthquake, Los Angeles, California. *Annals of Epidemiology* 11 (5): pp. 347-357.
- Massey, F.J., 1951. The Kolmogorov-Smirnov Test for Goodness of Fit. *Journal of the American Statistical Association* 46 (253): pp 68-78.
- Miller, L.H., 1956. Table of Percentage Points of Kolmogorov Statistics. *Journal of the American Statistical Association* 51 (273): pp 68-78.
- Moehle, J.P. and G.G. Deierlein, 2004. A Framework methodology for Performance-Based Earthquake Engineering. *International Workshop on Performance-Based Design*, Bled, Slovenia.
- Moehle, J.P., and Mahin, S.A., 1991. Observations on the Behavior of Reinforced Concrete Buildings during Earthquakes. In S.K. Ghosh, editor, *ACI SP-127 Earthquake-Resistant Concrete Structures--Inelastic Response and Design*: pp. 67-89. American Concrete Institute, Detroit, MI.
- Miranda, E. and H. Aslani, 2003. *Probabilistic Response Assessment for Building-Specific Loss Estimation*. PEER Technical Report. Berkeley, California.
- Mitrani, J., J. Goethals, and S.A. Glaser, 2002. *Field Testing of Wireless Interactive Sensor Nodes*. A report submitted to Japan's Port and Airport Research Institute (PARI), Yokosuka, Japan.
- Mitrani-Reiser, J., C. Haselton, C. Goulet, K.A. Porter, J.L. Beck, and G.G. Deierlein, 2006. Evaluation of the seismic performance of a code-conforming reinforced-concrete

- frame building - Part II: Loss estimation. *Proceedings of Eighth U.S. National Conference on Earthquake Engineering*. San Francisco, California.
- Mrozek, J.R., and L.O. Taylor, 2002. What determines the value of life? A meta-analysis. *Journal of Policy Analysis and Management* 21(2): pp. 253-270.
- Murakami, H.O., 1992. A simulation model to estimate human loss for occupants of collapsed buildings in an earthquake. *Proceedings of the Tenth World Conference on Earthquake Engineering*, Madrid, Spain: pp. 5969-5974.
- (NFPA) National Fire Protection Association, 2002. *Standard for the Installation of Sprinkler Systems*, NFPA-13, Quincy, MA.
- (NIST) National Institute of Standards and Technology, 2006. <http://www.nist.gov/>.
- (NOAA) National Oceanographic and Atmospheric Administration, 1972. *A Study of Earthquake Losses in the San Francisco Bay Area: Data and Analysis*. A Report for the Office of Emergency Preparedness. Washington, D.C.
- Ohta, Y., H. Ohashi, and H. Kagami, 1986. A semi-empirical equation for estimating occupant casualty in an earthquake. *Proceedings of the 8th European Conference on Earthquake Engineering*, Lisbon, Portugal.
- OpenSees, 2006. Open System for Earthquake Engineering Simulation, Pacific Earthquake Engineering Research Center, University of California, Berkeley, <http://opensees.berkeley.edu/>.
- Pardoen, G.C., R.P. Kazanjy, E. Freund, C.H. Hamilton, D. Larsen, N. Shah, and A. Smith, 2000. Results from the City of Los Angeles-UC Irvine shear wall test program, 6th *World Conference on Timber Engineering*.
- (PCBO) Pacific Coast Building Officials, 1927. *Uniform Building Code*, Whittier, California.

- Peek-Asa, C., Ramirez, M., Seligson, H. and K. Shoaf, 2003. Seismic, structural, and individual factors associated with earthquake related injury. *Injury Prevention* 9 (1): 62-66.
- PEER, 2005a. Pacific Earthquake Engineering Research Center: PEER Strong Motion Database, University of California, Berkeley, <http://peer.berkeley.edu/smcat/> (Sept. 15, 2005).
- PEER, 2005b. Pacific Earthquake Engineering Research Center: Structural Performance Database, University of California, Berkeley. <http://nisee.berkeley.edu/spd/>.
- Porter, K.A., 2000. *Assembly-based vulnerability of buildings and its uses in seismic performance evaluation and risk-management decision-making*, Doctoral Dissertation, Stanford University, Stanford, CA, published by ProQuest, Ann Arbor, MI..
- Porter, K.A., A.S. Kiremidjian, and J.S. LeGrue, 2001, Assembly-based vulnerability of buildings and its use in performance evaluation, *Earthquake Spectra* 17(2), Earthquake Engineering Research Institute, Oakland, CA.
- Porter, K.A., 2003. An overview of PEER's performance-based earthquake engineering methodology. *Proceedings of Ninth International Conference on Applications of Statistics and Probability in Civil Engineering*. San Francisco, California.
- Porter, K.A., J.L. Beck, R.V. Shaikhutdinov, S.K. Au, K. Mizukoshi, M. Miyamura, H. Ishida, T. Moroi, Y. Tsukada, and M. Masuda, 2004a. Effect of seismic risk on lifetime property value, *Earthquake Spectra* 20 (4): pp. 1211-1237.
- Porter, K.A., J.L. Beck, J.Y. Ching, J. Mitrani-Reiser, M. Miyamura, A. Kusaka, T. Kudo, K. Ikkatai, and Y. Hyodo, 2004b. *Real-Time Loss Estimation for Instrumented Buildings*, Report EERL 2004-08, California Institute of Technology, Pasadena, CA.
- Porter, K.A., J. Mitrani-Reiser, J.L. Beck, and J.Y. Ching, 2006a, Smarter structures: real-time loss estimation for instrumented buildings, paper NCEE-1236, *Proceedings, 8th National Conference on Earthquake Engineering*, San Francisco, CA.

- Porter, K.A., J. Mitrani-Reiser, and J.L. Beck, 2006b. Near-real-time loss estimation for instrumented buildings. *The Structural Design of Tall and Special Buildings*, 15 (1): pp. 3-20.
- Porter, K.A., 2007. Fragility of hydraulic elevators for use in performance-based earthquake engineering. *Earthquake Spectra* 23(2), Earthquake Engineering Research Institute, Oakland, CA: pp. 459-469.
- Revesz, R.L., 1999. *Environmental regulation, cost-benefit analysis, and the discounting of human lives*. Berkeley Program in Law and Economics, Working Paper Series, Paper 134.
- Rihal, S.S., 1982. Behavior of nonstructural building partitions during earthquakes. *Proceedings of the Seventh Symposium on Earthquake Engineering*, Department of Earthquake Engineering, University of Roorke, India, November 10-12, 1982, Delhi: Sarita Prakashan: pp. 267-277.
- (ROSRINE) Resolution of Site Response Issues from the Northridge Earthquake, 2005. Website by Earthquake Hazard Mitigation Program and Caltrans. <http://geoinfo.usc.edu/rosrine/>.
- RSMeans Corp., 2001, *Means Construction Cost Data*. Kingston, MA: RS Means Co.
- Samardjieva, E., and J. Badal, 2002. Estimation of the expected number of casualties caused by strong earthquakes. *Bulletin of the Seismological Society of America* 92(6): pp. 2310-2322.
- Scawthorn, C., 2006. Personal communication.
- Schiff, A.J., 2006. Personal communication via Keith A. Porter.
- Shoaf, K., H. Seligson, M. Ramirez, and M. Kano, 2005. *Fatality Model for Non-ductile Concrete Frame Structures Developed from Golcuk Population Survey Data*, PEER Report 2005/11, University of California, Berkeley, California.

- Sprinkler Fitters U.A. Local 483, 1989, untitled, San Carlos, CA.
- Stone, W.C. and A.W. Taylor, 1993. *Seismic Performance of Circular Bridge Columns Designed in Accordance with AASHTO/CALTRANS Standards*, National Institute of Standards and Technology, Washington, DC.
- (SEAOC) Structural Engineers Association of California. 1995. *Vision 2000, A Framework for Performance-Based Engineering*. Structural Engineers Association of California. Sacramento, California.
- Tierney, K.J., 1990. Developing Multivariate Models for Earthquake Casualty Estimation. *Workshop on Modeling Earthquake Casualties for Planning and Response*, Pacific Grove, CA.
- U.S. Census Bureau, 1980 census. Population and Housing Unit Counts: United States. Washington, DC. <http://www.census.gov/prod/cen1990/cph2/cph-2-1-1.pdf>.
- Vamvatsikos, D. and C.A. Cornell, 2002. Incremental dynamic analysis. *Earthquake Engineering and Structural Dynamic*, 31(3): pp. 491-514.
- Wagner, R.M., N.P. Jones, and G.S. Smith, 1994. Risk factors for casualty in earthquakes: The application of epidemiologic principles to structural engineering. *Journal of Structural Safety*, 13: pp. 177-200.
- Whittaker, A., Hamburger, R.O., Comartin, C., Mahoney, M., and Bachman, R. 2004. *Performance-Based Engineering of Buildings and Infrastructure for Extreme Loadings*. Technical paper submitted to the ATC-58 Project.
- Wikipedia, 2006. <http://wikipedia.org/>.
- Williams, M.S., and R.G. Sexsmith, 1997. Seismic assessment of concrete bridges using inelastic damage analysis. *Engineering Structures* 19 (3): pp. 208-216.

- Williams, M.S., I. Villemure, and R.G. Sexsmith, 1997. Evaluation of seismic damage indices for concrete elements loaded in combined shear and flexure, *ACI Structural Journal* 94 (3): pp. 315-322.
- Yeo, G.L. and C.A. Cornell, 2003. Building-specific seismic fatality estimation methodology, *Proceedings, Ninth International Conference on Applications of Statistics and Probability in Civil Engineering (ICASP9)*. San Francisco, California.
- Yeo, G.L., 2005. *Stochastic Characterization and Decision Bases Under Time-Dependent Aftershock Risk in Performance-Based Earthquake Engineering*, Doctoral Dissertation, Stanford University, Stanford, CA.
- Zerbe, R.O. and A. Falit-Baiamonte, 2002. *The Use of Benefit-Cost Analysis for Evaluation of Performance-Based Earthquake Engineering Decisions*. Pacific Engineering Research Center, PEER Report 2002/06, University of California, Berkeley, California.